UNIVERSITÉ DES SCIENCES ET TECHNIQUES DE LILLE

THESE

présentée à

L'UNIVERSITÉ DES SCIENCES
ET TECHNIQUES DE LILLE

pour obtenir le grade de

DOCTEUR ES SCIENCES PHYSIQUES

par

Claude DEVAUX

*

CONTRIBUTION A L'ETUDE DE LA COUVERTURE NUAGEUSE DE VENUS PAR L'ANALYSE DES MESURES PHOTOMETRIQUES ET DES PROFILS DE FLUX SOLAIRE TRANSMIS

*

Tome II

Soutenue le 25 Mai 1977 devant la Commission d'examen

Membres du Jury

M. SCHILTZ	Président
M. DOLLFUS, M. FYMAT, M. HERMAN	Rapporteurs
Mme LENOBLE, M. GEHRELS	Examinateurs

U. E. R. DE PHYSIQUE FONDAMENTALE

CHAPITRE III

ETUDE DE LA PHOTOMETRIE DETAILLEE SUR LE DISQUE DE VENUS

APPLICATION A L'ETUDE DE LA HAUTE ATMOSPHERE

Les paramètres disponibles pour l'étude de la lumière solaire rediffusée par Vénus sont la longueur d'onde λ du rayonnement, l'angle de phase V de la planète et le point M du disque observé. Les mesures les plus simples à analyser après l'albédo sphérique sont constituées par les courbes de phase $m_\lambda(V)$.

I - ANALYSE DES COURBES DE PHASE

L'analyse des courbes de phase a fait l'objet de nombreux travaux (Horak, 1950 ; Sobolev, 1964 ; Arking et Potter, 1968 ; Fymat,1972). Il apparait toutefois que ce type d'analyse est assez peu sensible aux propriétés diffusantes du milieu. A titre indicatif on a représenté (Fig III.1) les courbes de phase obtenues par Arking et Potter (1968) pour quatre types de fonctions de phase différentes (fig.III.2).

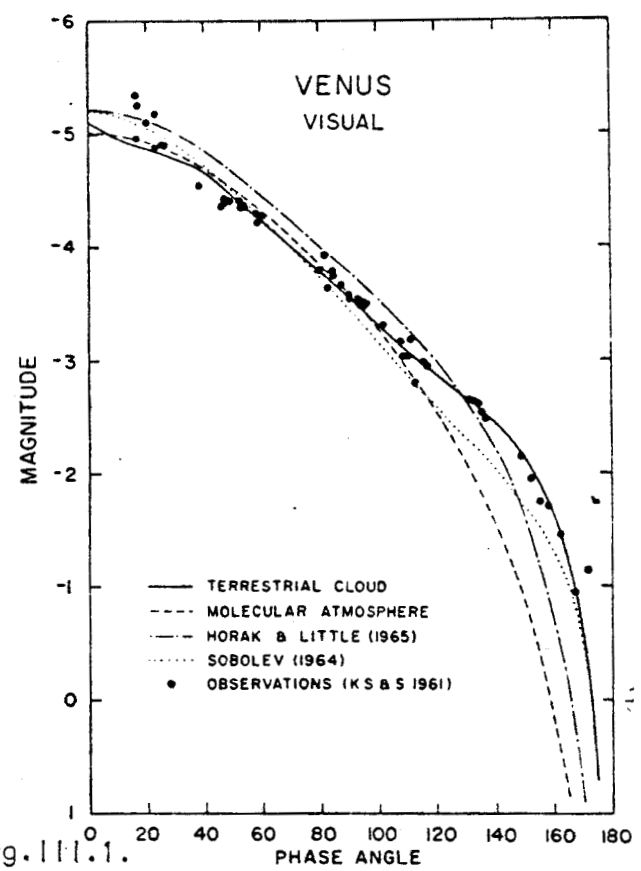

Fig.III.1.

FIG. 4. The luminosity of Venus in the visual spectrum vs phase angle. The luminosity is expressed in magnitudes after adjusting the Sun-Venus and Earth-Venus distances to the standard values, 0.723 and 1.0 AU, respectively. Four theoretical curves are compared with the observations of Knuckles *et al.* (1961).

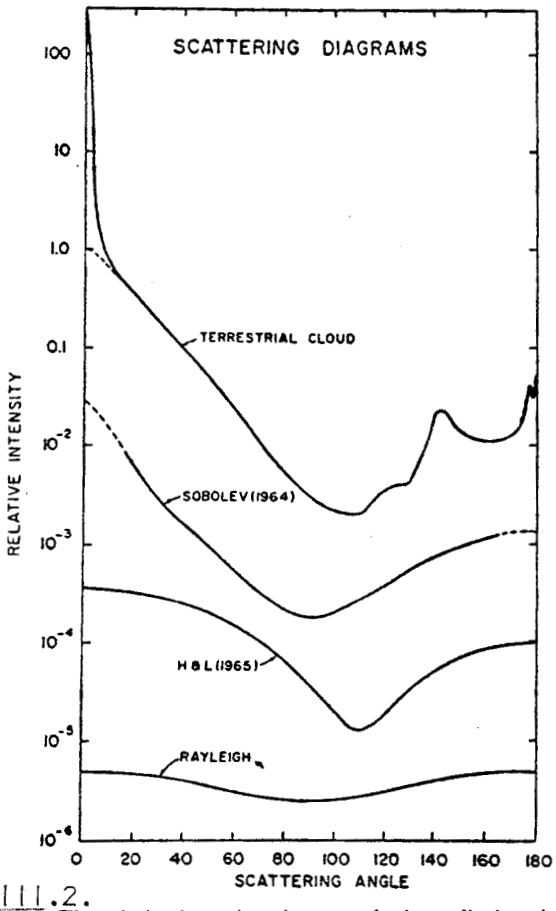

Fig.III.2.

. The relative intensity of scattered solar radiation, due to a single scattering, as a function of the scattering angle. Each curve is displaced along the ordinate by an arbitrary amount to separate them. The top curve represents the model of a terrestrial type cloud with particle size distribution shown in Fig. 2. The second curve is the scattering diagram derived by Sobolev (1964) by inversion of the observational data of Danjon (1949). The third curve is the scattering diagram used by Horak and Little (1965). The bottom curve is the Rayleigh scattering diagram, applicable to pure molecular scattering.

D'après Arking et Potter (1968).

Si l'on peut exclure une atmosphère purement moléculaire, l'accord déjà bon obtenu avec un modèle de nuage terrestre montre bien que le mécanisme de diffusion précis est vite sans grande influence sur le résultat. L'écart aux petits angles de phase est certainement significatif mais son interprétation nécessiterait des mesures très précises de la magnitude dans des conditions expérimentales très difficiles. Les meilleures conclusions étaient obtenues par Fymat et Kalaba (1972) qui par inversion des courbes de phase mettaient bien en évidence la nécessité de tenir compte de particules diffusantes, mais sans qu'il semble possible d'en déduire précisément l'indicatrice de diffusion.

A la suite des résultats obtenus par Hansen et Arking, nous avons repris cette étude en attribuant aux aérosols les caractéristiques déduites des mesures de polarisation. Les courbes de phase obtenues à diverses longueurs d'onde ont été comparées aux mesures d'Irvine (1968). L'albédo de diffusion simple a été ajusté pour redonner l'albédo sphérique A déduits de ces mesures. Les valeurs sont reportées dans le tableau III.1.

λ en Å	A	ω_o
3200	0,46	0,974293
3600	0,52	0,981236
4200	0,68	0,993146
4600	0,77	0,996726
5000	0,79	0,997215
6300	0,94	0,999776
7300	0,93	0,999672
10600	0,89	0,999255

TABLEAU III.1

Albédo sphérique monochromatique de Vénus
d'après Irvine (1968).

Comme on peut le constater sur la figure III.3 (a-h), l'accord est très satisfaisant. La variation spectrale de ces courbes de magnitude

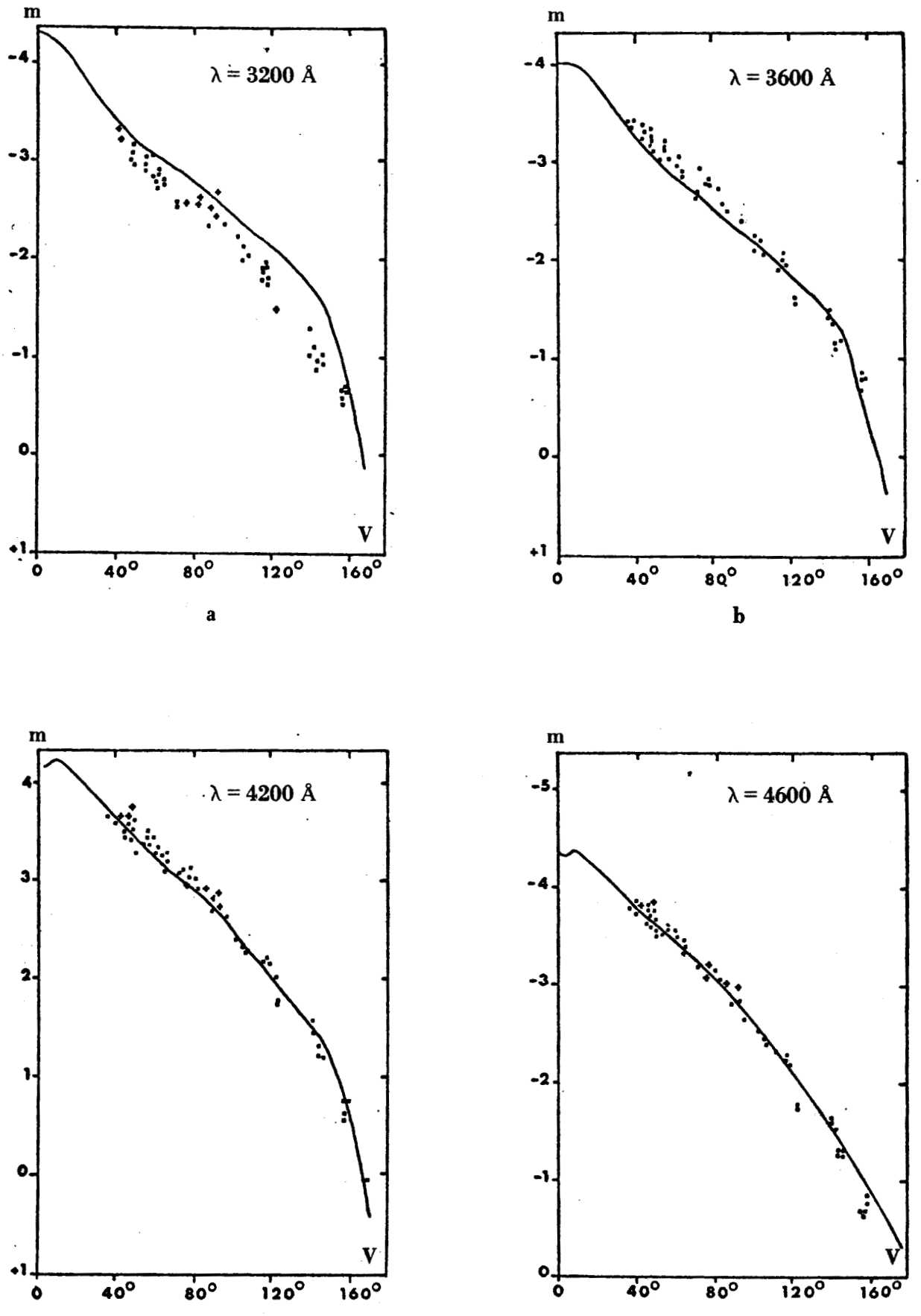

– Figure III-3 – Courbes de phase monochromatiques de Vénus.
Valeurs expérimentales (•, +) d'après Irvine (1968) ;
courbes théoriques (—) pour un modèle homogène.

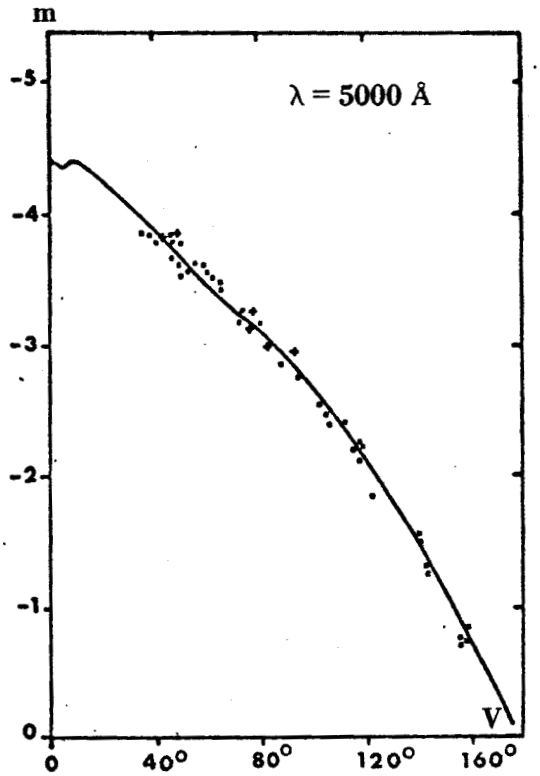

e

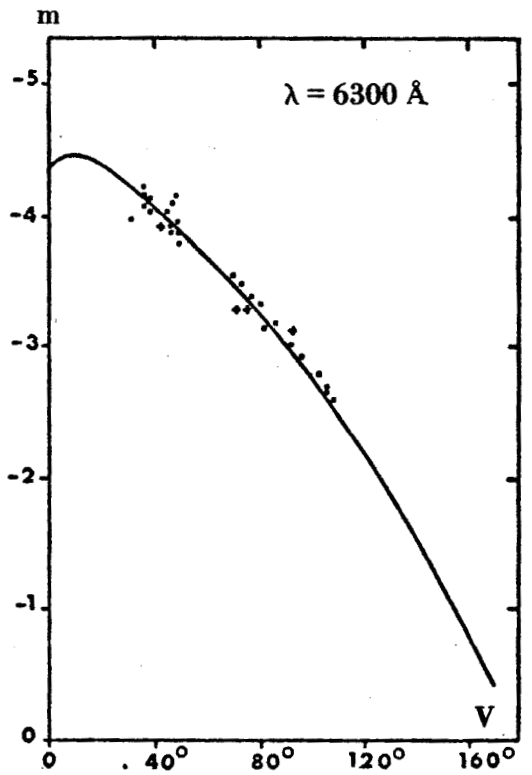

f

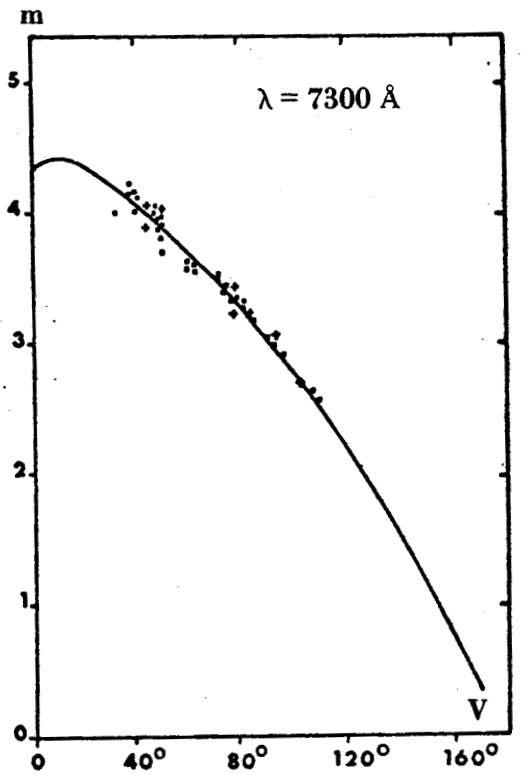

g

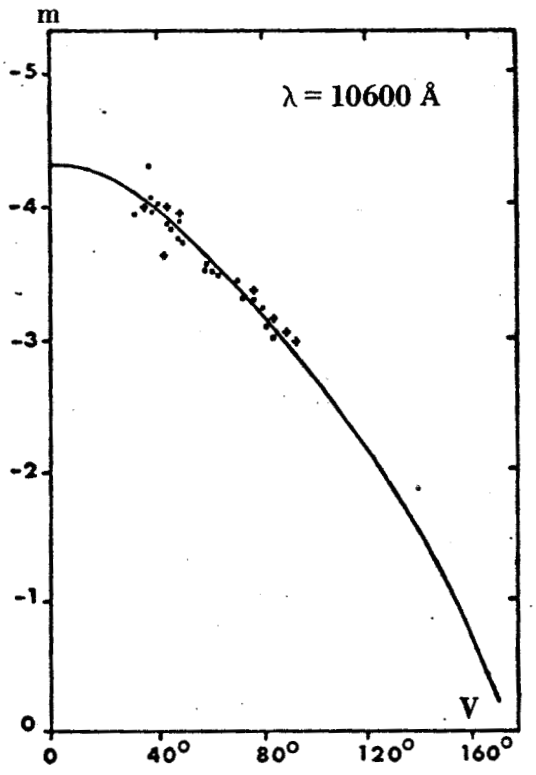

h

– Figure III-3 – (suite)

étant essentiellement commandée par l'absorption du milieu diffusant, la fonction de phase n'ayant qu'une influence secondaire, nous avons alors testé si ce type d'étude pouvait donner des informations sur la structure nuageuse de la planète. Compte tenu de l'absence d'absorption propre de $H_2 SO_4$ en U.V et de la faible réflectivité de Vénus en ultra violet, un problème intéressant est en effet de préciser à quel niveau de la couche nuageuse se fait l'absorption de ce rayonnement de plus courte longueur d'onde. Des modèles de nuages à deux couches ont donc été étudiés et on a repris l'analyse des courbes de phase pour de tels **modèles en** faisant varier le niveau de la localisation de l'absorption. L'effet éventuel devant être plus marqué si l'absorption est plus forte, les calculs ont été faits pour λ = 3270 Å qui correspond à une faible réflectivité de la planète Quelques uns des cas étudiés sont explicités ci dessous dans lesquels, la couche diffusante supérieure est conservative, ses aérosols ainsi que ceux de la couche inférieure ayant les caractéristiques de la polarisation.

$A^* = 0.47$	$A^* = 0.47$	$A^* = 0.47$
$\tau_1 = 4$, $\omega_0 = 1$, $P(\theta)$	$\tau_1 = 1$, $\omega_0 = 1$, $P(\theta)$	$\tau_1 = 1$, $\omega_0 = 1$, $P(\theta)$
$\tau_1 = 100$, $\omega_0 = 0.85726$, $P(\theta)$	$\tau_1 = 100$, $\omega_0 = 0.966565$, $P(\theta)$	$\rho = 0.416$, Loi de Lambert
a	b	c

Les résultats sont résumés sur la figure III.4 (a - b) ou les courbes de phase obtenues pour ces trois modèles sont comparées à celles du modèle homogène à un seul nuage. Compte tenu de la précision des mesures expérimentales, il est clair qu'une analyse plus poussée des courbes de phase semble actuellement assez peu prometteuse et n'aurait de réelles chances de succés qu'en portant sur des mesures absolues très raffinées, peut être envisageables à partir d'orbiters par exemple.

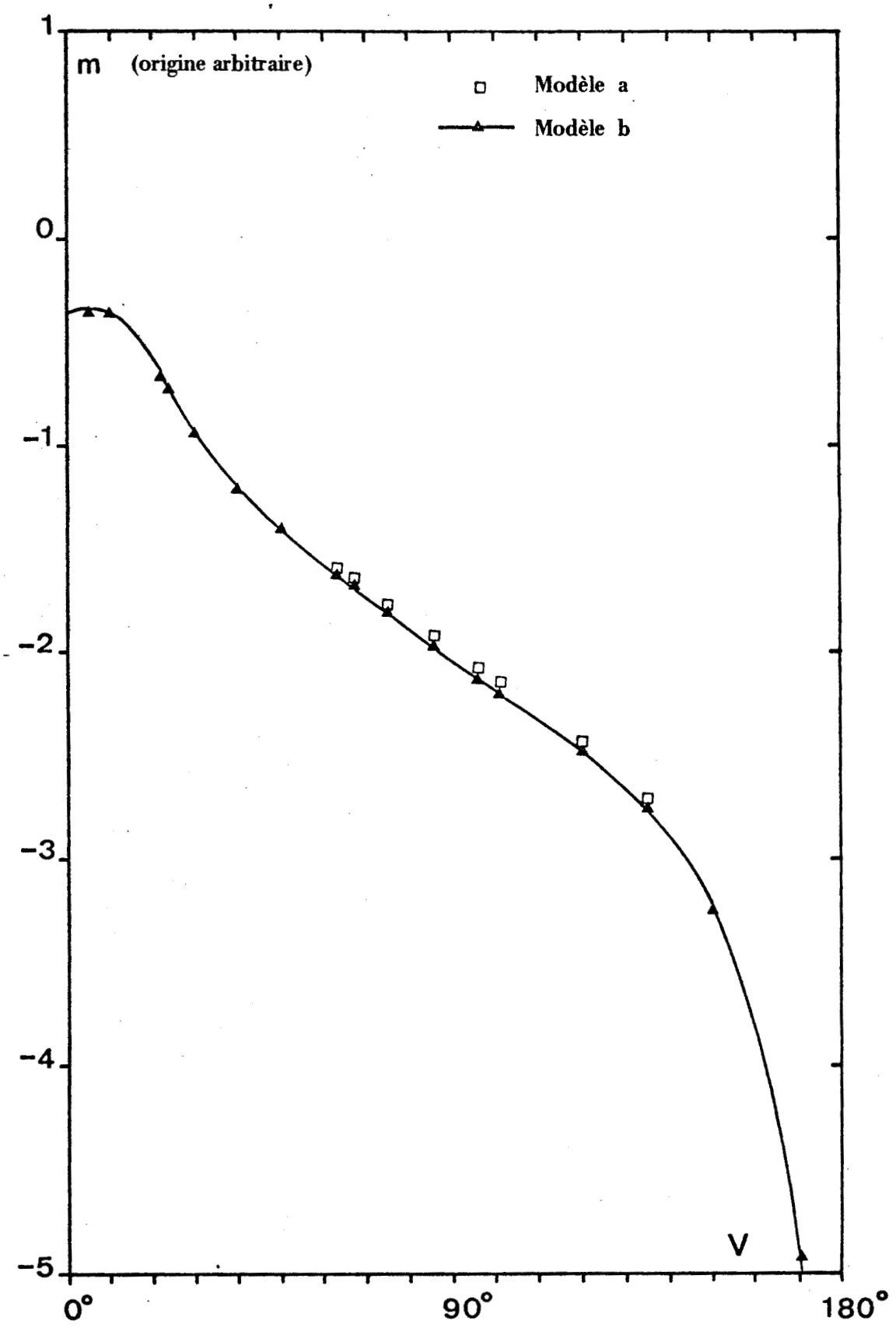

– Figure III-4.a – Courbe de phase de Vénus. ($\lambda = 3200$ Å)

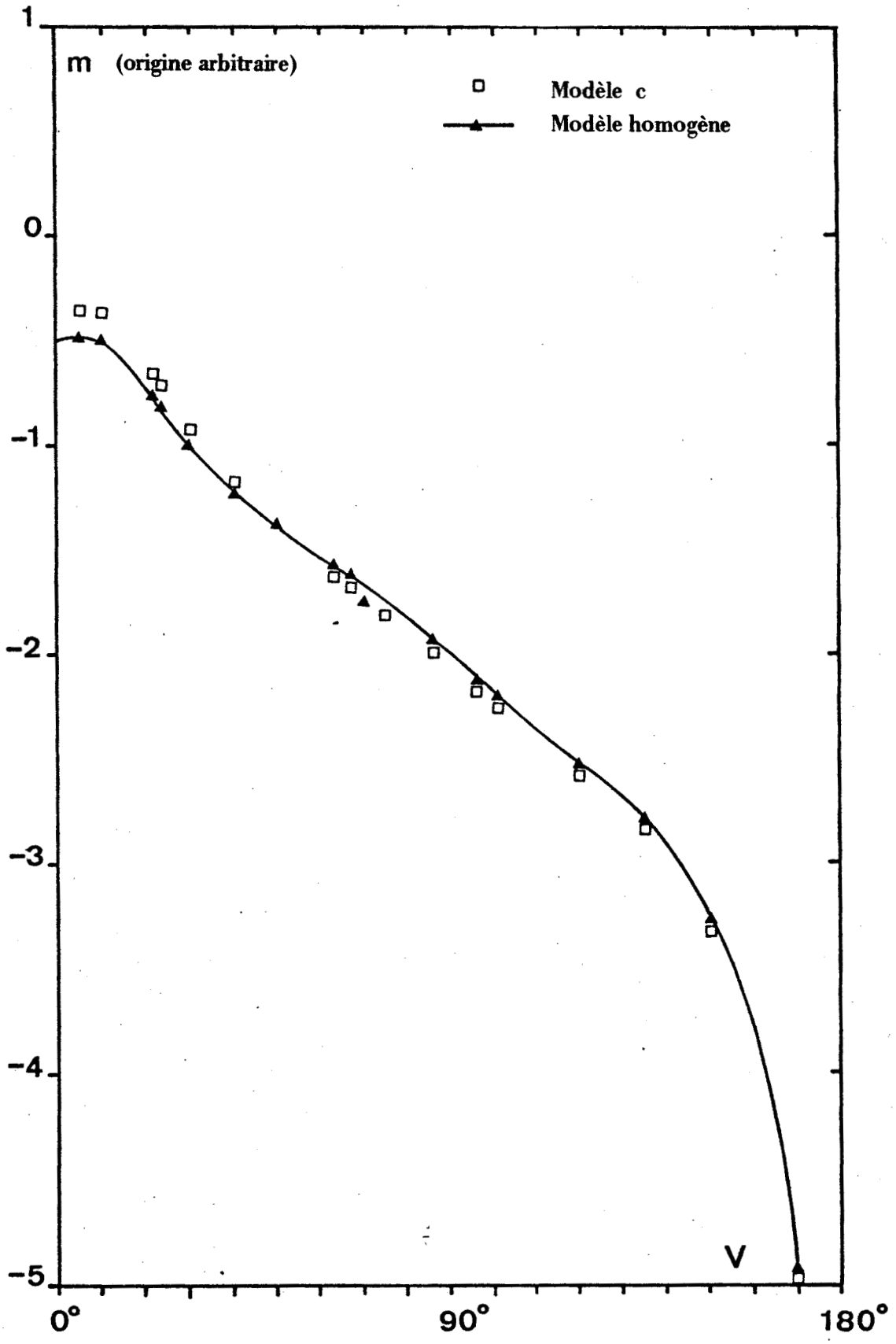

– Figure III-4.b – Courbe de phase de Vénus. ($\lambda = 3200$ Å)

II - ETUDE DES ISOPHOTES OBTENUES EN LUMIERE JAUNE

Une seconde étape a été d'entreprendre l'étude photométrique détaillée du disque de Vénus. Les mesures résolues de luminance I (M, V, λ) sont généralement présentées sous la forme de courbes d'égale luminances ou isophotes. Ces mesures plus fines devraient être plus riches en informations, particulièrement dans le proche U.V. où le phénomène essentiel est constitué par les taches sombres que présente Vénus, phénomène que les mesures intégrées ne prennent évidemment pas en compte. La figure III.5 présente quelques résultats expérimentaux extraits de Dollfus et al (1975), où apparaissent ces anomalies en U.V. et même certains jours en lumière visible.

Compte tenu de la lourdeur et de la complexité des problèmes posés, dans un premier temps, notre analyse a porté sur divers clichés obtenus en lumière jaune, et pour lesquels les isophotes présentaient une allure très régulière. Celle ci laissait espérer que dans ces conditions les plus fréquemment observées, Vénus présentait une structure nuageuse homogène horizontalement. Le problème était alors simplifié. Par ailleurs, dans ce domaine de longueurs d'onde, l'absorption et la diffusion sont presque exclusivement dues aux aérosols, la diffusion moléculaire contribuant de façon négligeable à la luminance. Si la nature des particules ne varie pas avec l'altitude, on peut donc également considérer le nuage comme homogène verticalement. On supposera de plus que la densité des particules est suffisante pour que la géométrie plane soit applicable en tout point. Il est possible que cette hypothèse soit en défaut au voisinage du limbe du terminateur et des pôles, et ces zones du disque seront exclues de notre analyse.

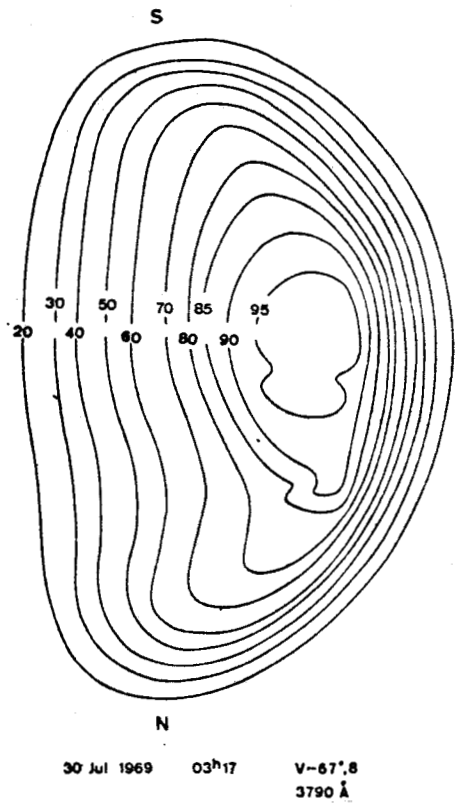

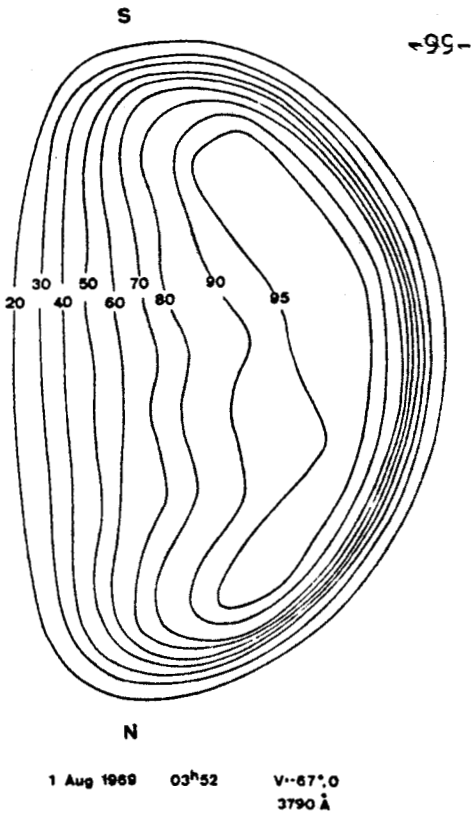

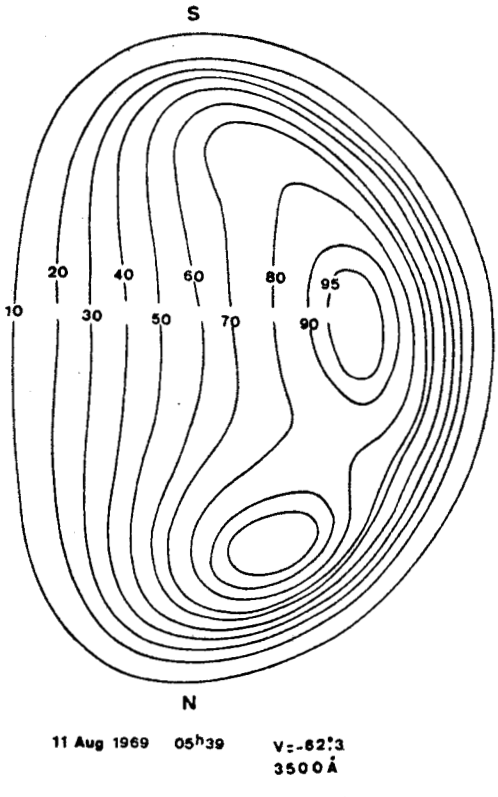

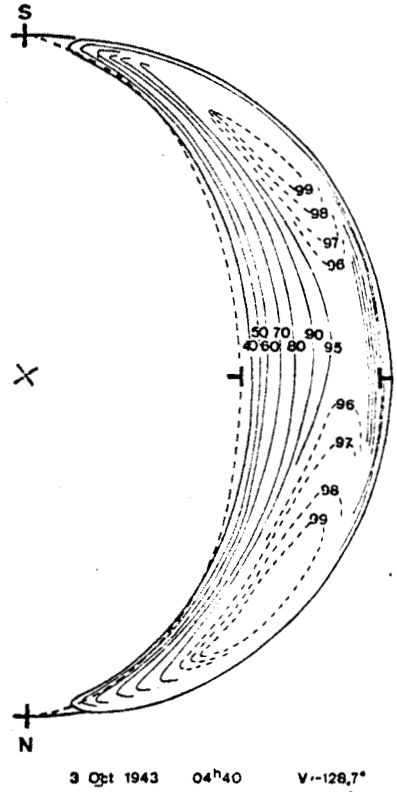

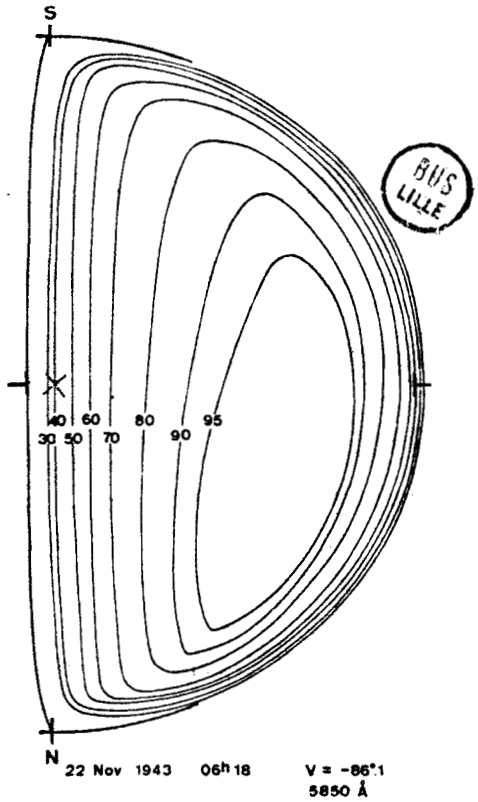

– Figure III-5 – Réseaux d'isophotes de Vénus d'après Dollfus et al. (1975) : anomalies visibles et ultra - violettes.

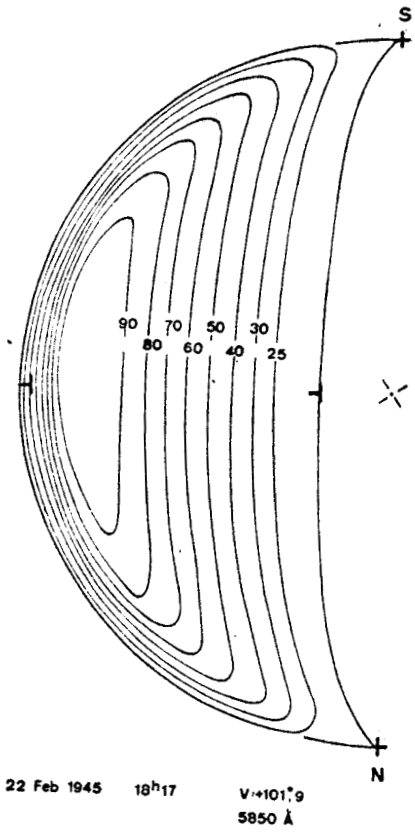

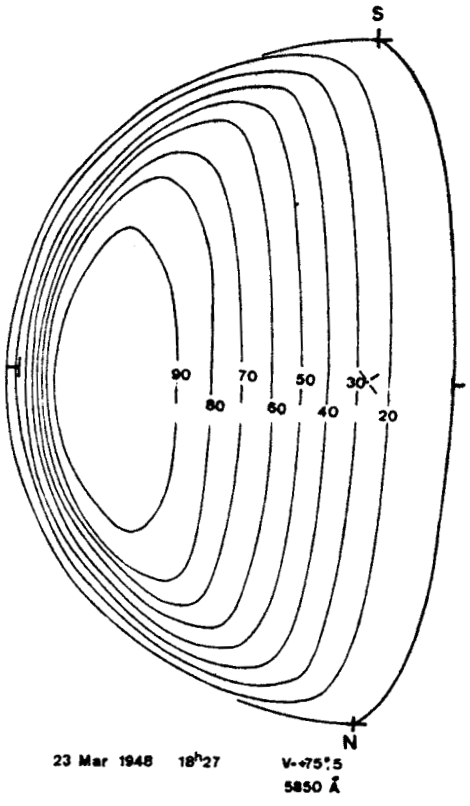

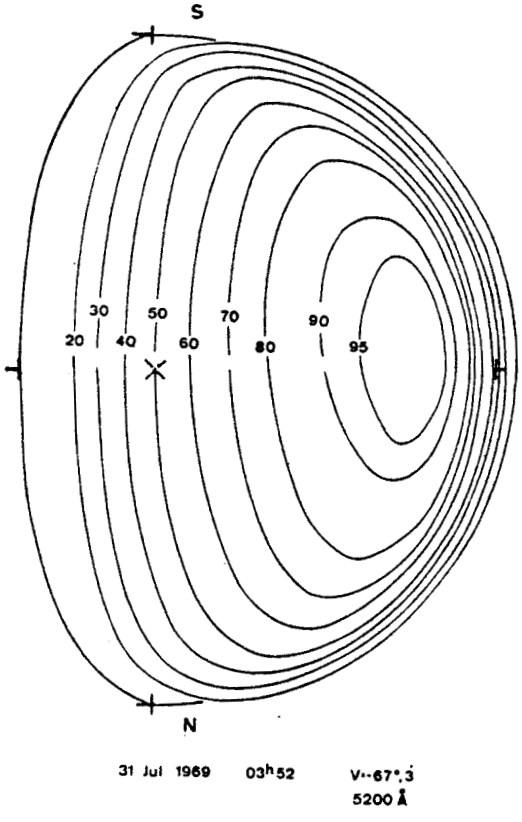

– Figure III-6 – Isophotes de Vénus ($\lambda = 5850$ Å) d'après Dollfus et al. (1975).

II - 1 - CAS D'UNE COUCHE HOMOGÈNE INFINIE

En première analyse nous devions donc tenter de comparer ces distributions expérimentales de luminance (Fig.III.6) aux résultats théoriques obtenus pour le modèle diffusant de Hansen et Arking puisque les particules qui y correspondent existent en altitude. Compte tenu des épaisseurs optiques déduites du sondage de Vénéra 8, nous avons considéré la couche nuageuse comme infinie. Le dernier paramètre à préciser est alors l'albédo de diffusion simple. Celui-ci influence essentiellement l'albédo sphérique A de la planète pour lequel on dispose des mesures d'Irvine (1968). On peut en déduire facilement ω_o à l'aide du noyau exponentiel. Sur la figure III.7 a extraite de l'article n°2 on voit que l'incertitude sur ω_o; résultant de l'imprécision de A n'a qu'une influence tout à fait négligeable sur la répartition de luminance théorique excepté aux petits angles de phase (dans ce cas les conditions d'observation sont difficiles) ou au voisinage du limbe (et dans ce cas la résolution limitée du télescope rend cette zone inexploitable). Cette incertitude sur ω_o est donc sans importance majeure sur les distributions relatives. On notera par contre que les mesures de Mariner 10 étant des mesures absolues, ce paramètre joue alors un rôle primordial comme le montre la figure III.7 b extraite de l'article n°3 ou l'on a tracé trois distributions équatoriales de luminance pour diverses valeurs de l'albédo sphérique.

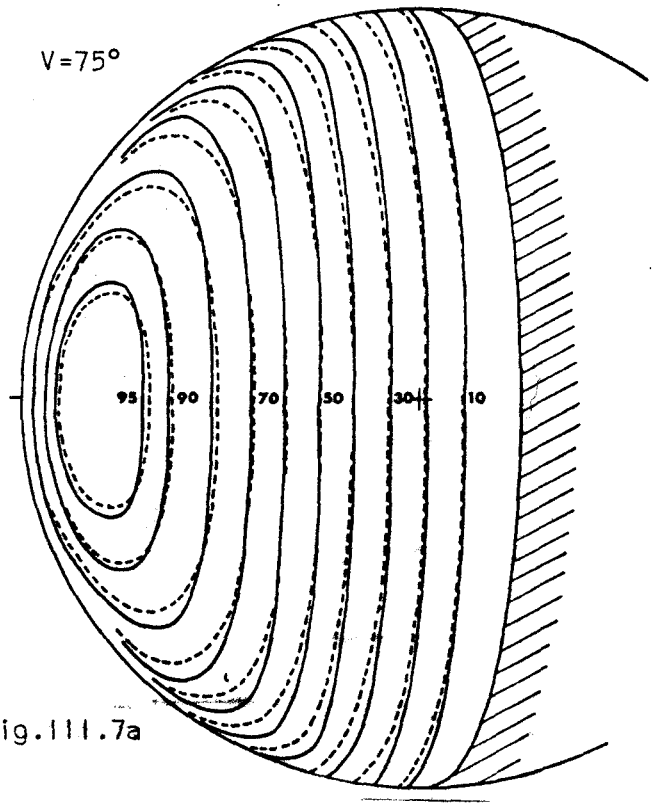

Fig.III.7a

Isophotes théoriques. A=1(---), A=0,8(——).

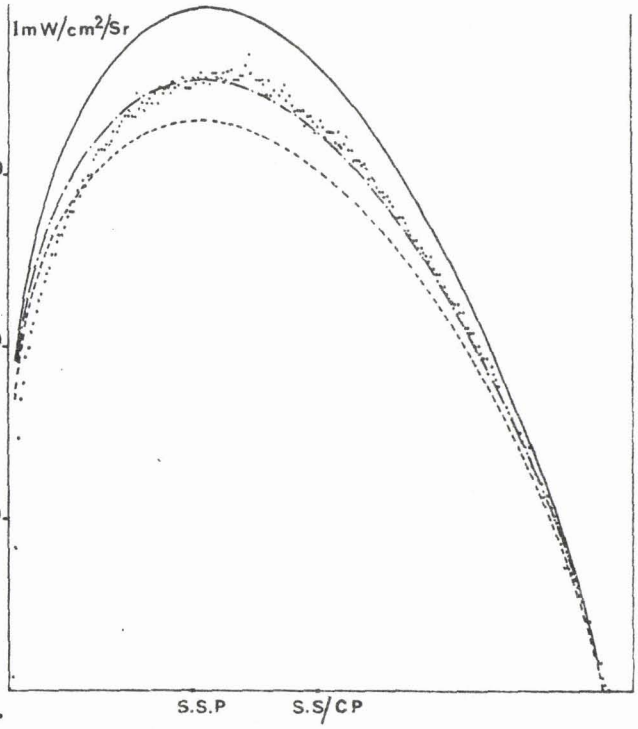

Fig.III.7b.

Equatorial radiance distribution for orange. Mariner 10 results (dots) and theoretical results for a homogeneous model: $A = 0.92$ (solid), $A = 0.843$ (dot-dashed), $A = 0.8$ (dashed).

Le problème essentiel pour comparer ces distributions théoriques aux observations disponibles est finalement celui de la superposition des deux réseaux. Les clichés expérimentaux n'étant pas déconvolués des effets d'appareil, on doit s'attendre à une dilatation apparente du disque (le limbe correspondant sensiblement à l'isophote 50). On a dans un premier temps essayé de suivre ce critère mais les désaccords obtenus nous ont amené à le vérifier plus soigneusement.

On a pour cela dégradé les réseaux de luminance théoriques à l'aide de fonctions d'appareils arbitraires et ajustables jusqu'à retrouver au voisinage du limbe les profils observés. Ces calculs approchés (traitement unidimensionel sur l'équateur), ont montré que quelque soit la fonction d'appareil choisie, il convenait de mettre le limbe sur l'isophote 52, 44 et 43,5 respectivement pour les angles de phase 101°, 67° et 75°. (Cf annexe 2 de l'article n° 4)et c'est ce critère qui a finalement été retenu. Sur les figures III.8 (a, b, c) les résultats expérimentaux sont comparés aux calculs. Il s'agit de résultats relatifs, les maxima ayant été arbitrairement ramenés à 100. Si la forme générale des courbes est qualitativement bien restituée, les valeurs relatives sont par contre assez mauvaises en général. A 75°, on pourrait améliorer l'accord mais au prix d'une légère incohérence avec les données du grandissement. A 67° et 101°, les divergences sont beaucoup plus nettes. Indépendamment des légers arbitraires de positionnement et de grandissement, on pourrait sans doute encore jouer sur le niveau zéro de la luminance (la correction sur les clichés du fond continu du ciel est en effet délicate et entraîne probablement une assez forte

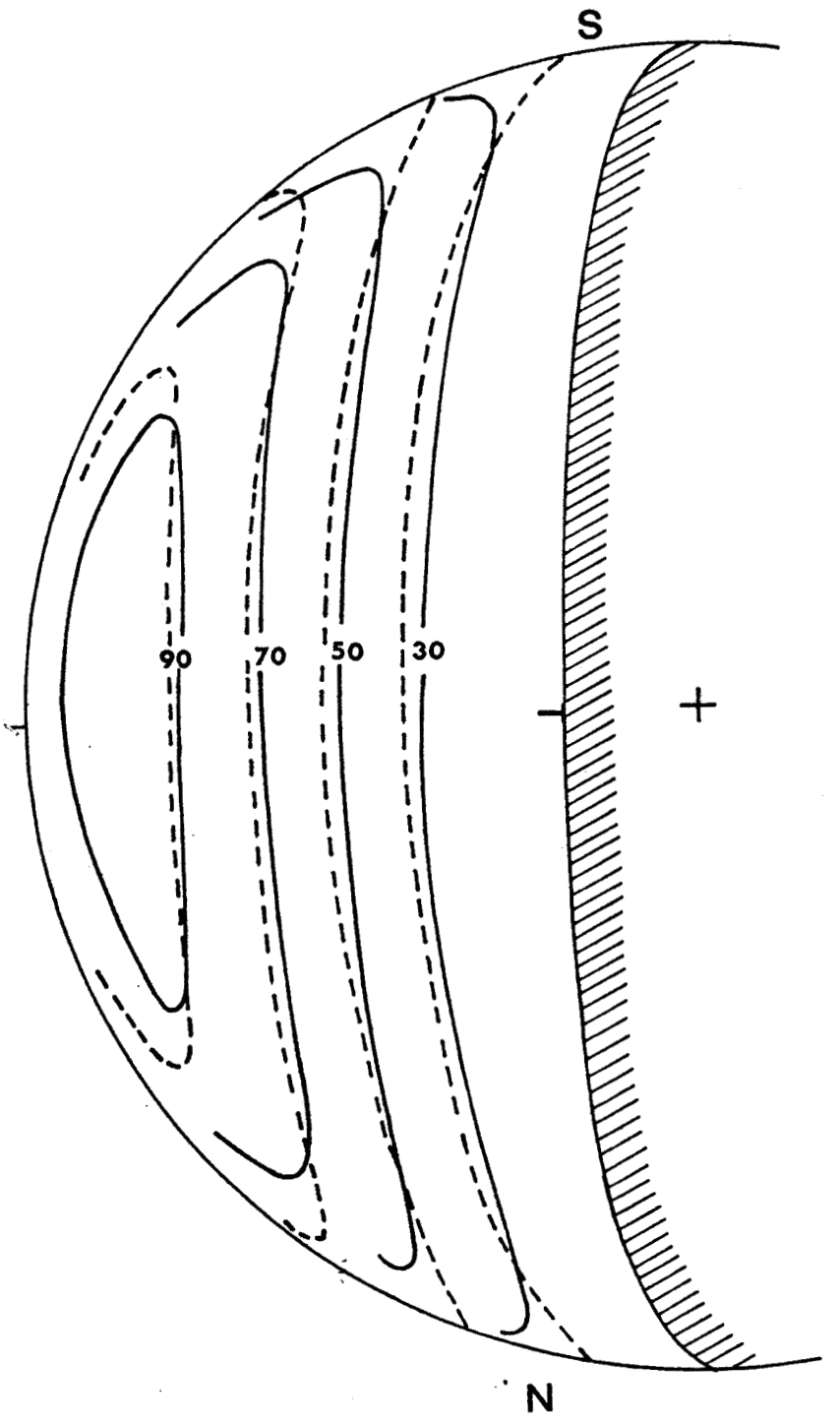

– Figure III-8.a – Comparaison des réseaux d'isophotes théoriques (- - -) et expérimentales (—) en lumière jaune. V = 101°

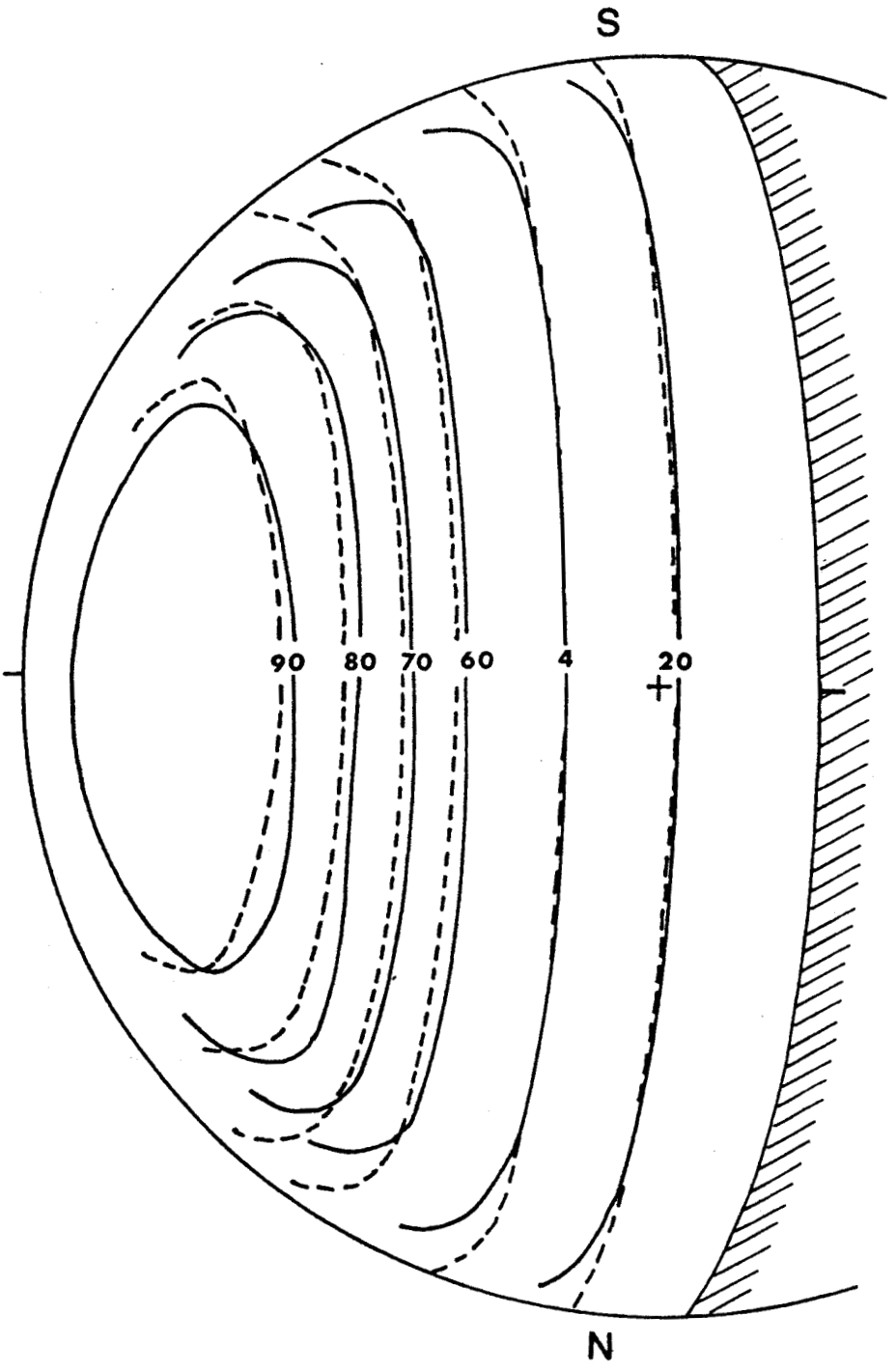

– Figure III-8.b – Comme pour la figure III-8.a.
V = 75°

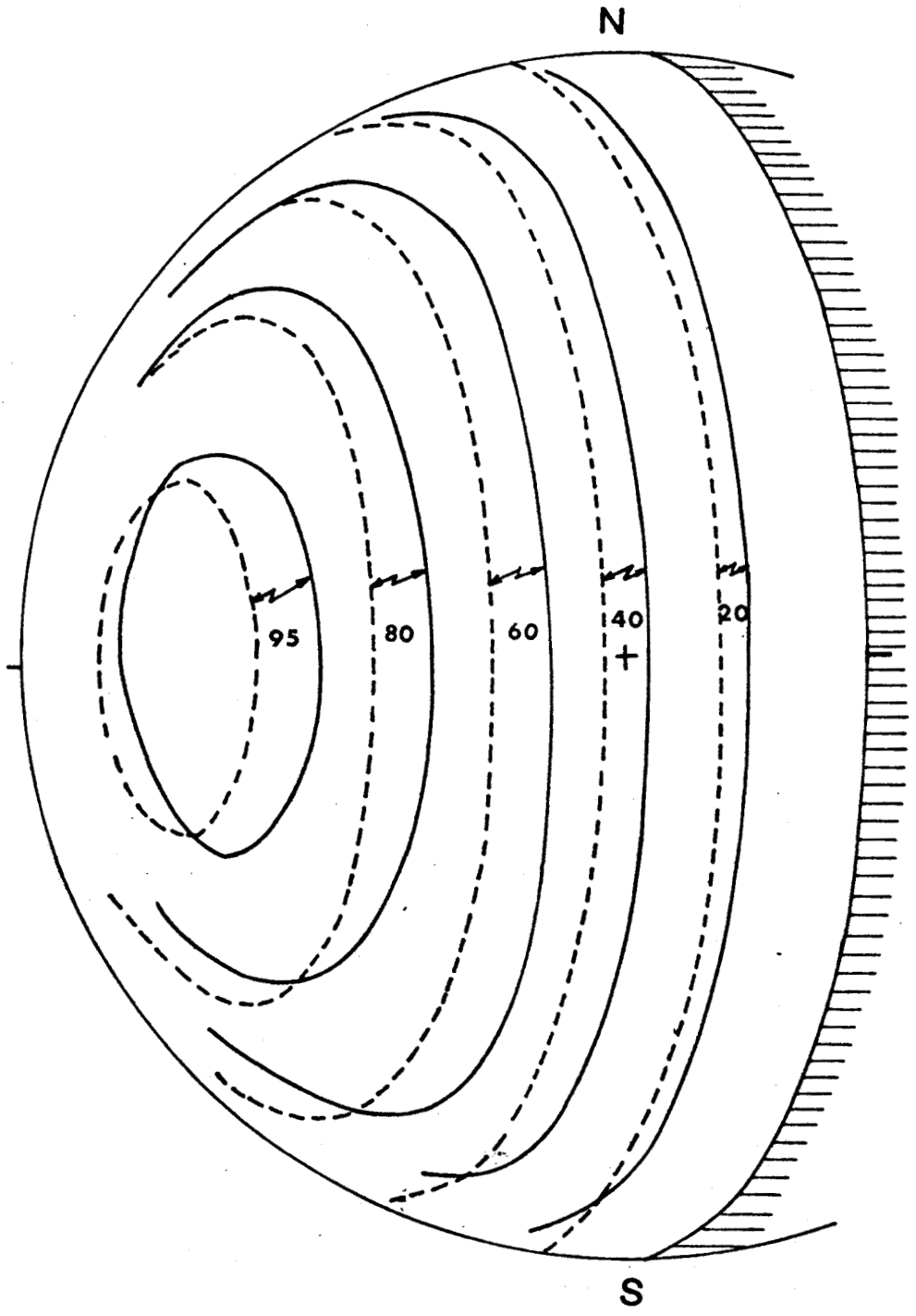

– Figure III-8.c – Comme pour la figure III-8.a.
V = - 67°

imprécision aux faibles niveaux). Mais il semble bien que le désaccord observé soit supérieur aux erreurs de mesures et que même les jours calmes un modèle homogène d'Hansen ne donne pas l'accord. Ce résultat n'est d'ailleurs pas trop surprenant. Il semble simplement montrer que les inhomogénéités observées parfois en lumière jaune sont plutôt un phénomène quasi permanent. Cette hypothèse se trouvait d'ailleurs vérifiée par l'application des principes de réciprocité aux distributions équatoriales de luminance obtenues à partir des clichés expérimentaux. La figure III.9 présente les résultats obtenus en appliquant ce principe aux mesures expérimentales pour un angle de phase de 67°, le limbe théorique étant placé sur l'isophote 40 et 50. Comme on peut le constater, ce principe est pris en défaut même si

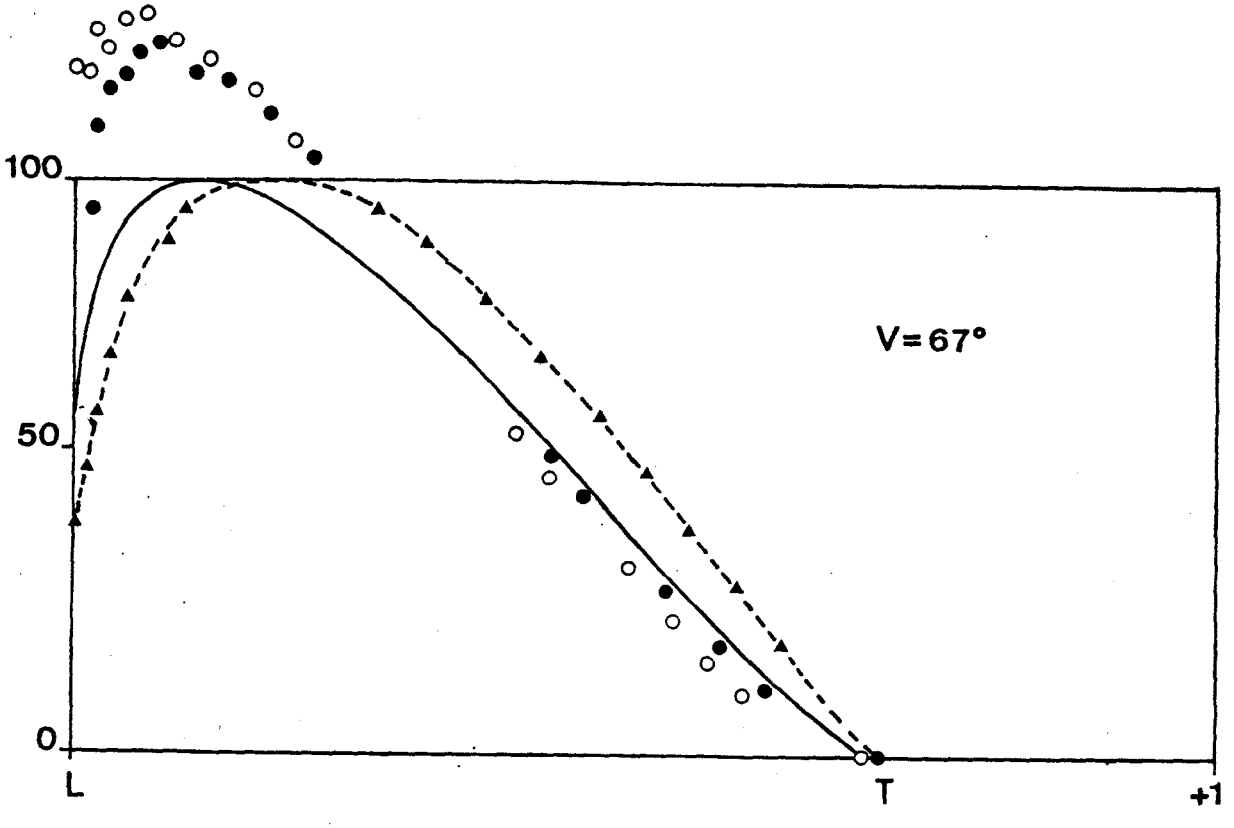

– Figure III-9 – Application des principes de réciprocité à une distribution équatoriale de luminance.

Limbe sur l'Isophote 40 (○), 50 (●)
Valeurs expérimentales (▲)
Distribution théorique (—)

l'on n'utilise pas les points expérimentaux proches du limbe, pour lesquels on sait que la mesure est perturbée, tout en déplaçant assez largement la

position présumée du limbre théorique. Le fait que les photos étudiées n'étaient pas déconvoluées des effets d'appareil laissait toutefois planer un doute sérieux sur ce premier résultat. Nous avons alors tenté d'analyser quelques clichés obtenus par Mariner 10 en Février 1974 grâce à un système de caméra-vidicon. Ici la difficulté provenait du grand nombre de points résolus sur le disque (plus de 50 000) et dans un premier temps nous avons limité notre analyse aux coupes équatoriales et polaires d'autant que les premières données dont nous disposions n'avaient pas encore été corrigées des effets de distorsion provenant à la fois du système optique et de l'électronique. Cette première analyse qu'on trouvera ici dans l'article n°3 montrait que, pour ces photos où la dégradation des images était d'une tout autre origine et où, compte tenu de la haute résolution spatiale, l'arbitraire du positionnement ne jouait ici pratiquement plus, la même analyse confirmait le désaccord constaté à partir des observations terrestres. Des mesures corrigées nous ayant été fournies par la suite, une comparaison a pu être effectuée entre les isophotes expérimentales (Fig.III.10 - a et b) et celles calculées avec ce premier modèle. L'écart constaté sur les figures III.11 (a et b) pouvait alors être considéré comme significatif. Ainsi donc, même en lumière jaune, lorsque Vénus semble présenter une très grande homogénéité, les clichés étudiés ne peuvent pas être interprés par un modèle a une couche homogène consistant avec les mesures en polarisation.

II - 2 - MODÈLE A DEUX COUCHES HORIZONTALEMENT HOMOGÈNES

La lumière polarisée étant essentiellement formée au sommet de la couche diffusante; elle ne donne d'informations que sur une faible partie de la couche nuageuse et on peut supposer que sous cette brume il existe une seconde couche constituée par d'autres aérosols. Une telle structure pourrait expliquer certaines anomalies observées et notre seconde approche a porté sur des modèles de ce type. Etant donné la multiplicité des paramètres, si l'on admet en plus de la structure stratifiée une inhomogénéité horizontale sur le disque, il sera toujours possible de bâtir des modèles qui donneront un bon accord. Plutôt que de rechercher une solution satis-

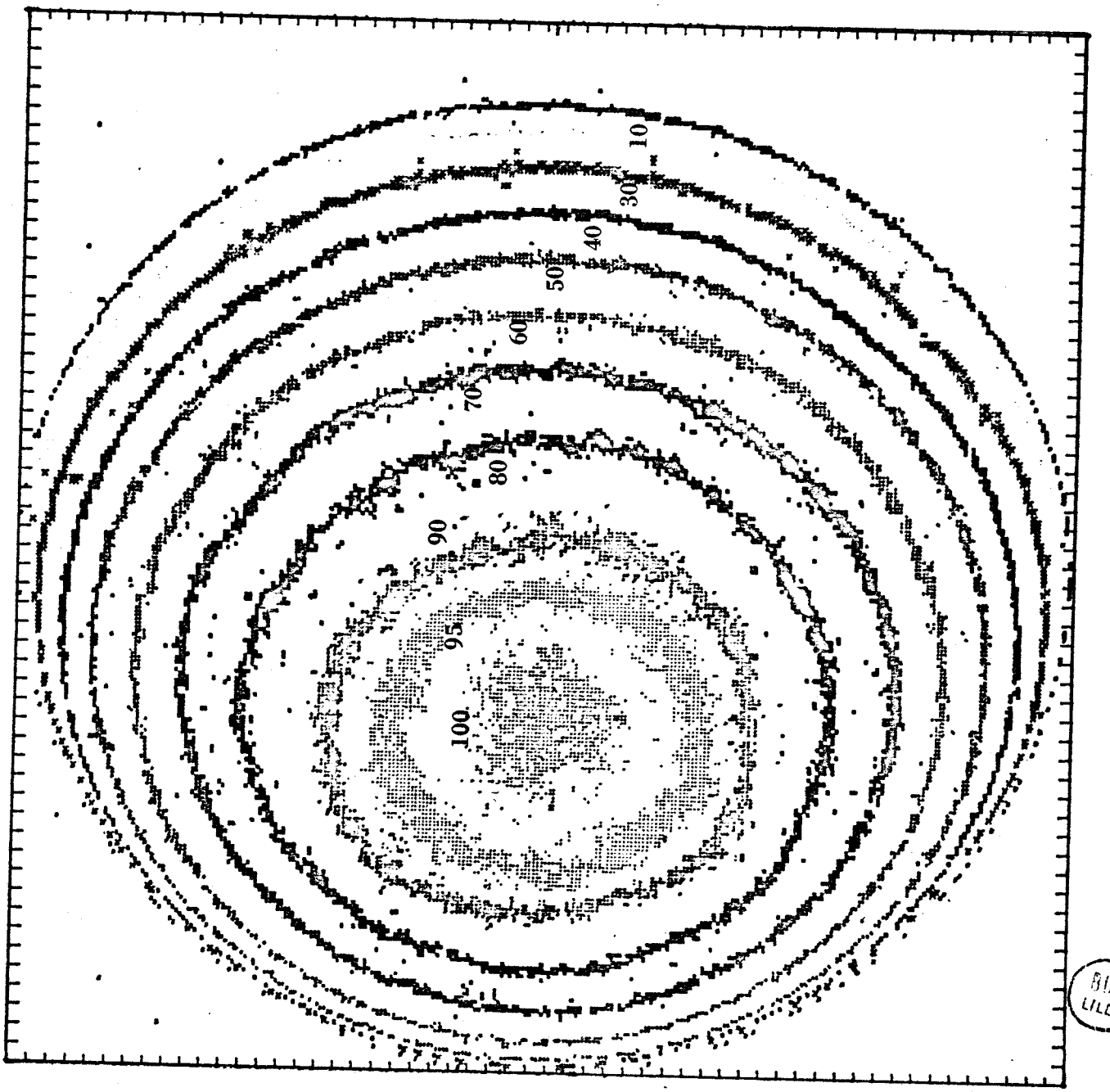

– Figure III-10.a – Isophotes expérimentales d'après Mariner 10.
$V = -23°35$; $\lambda = 0.58\ \mu m$

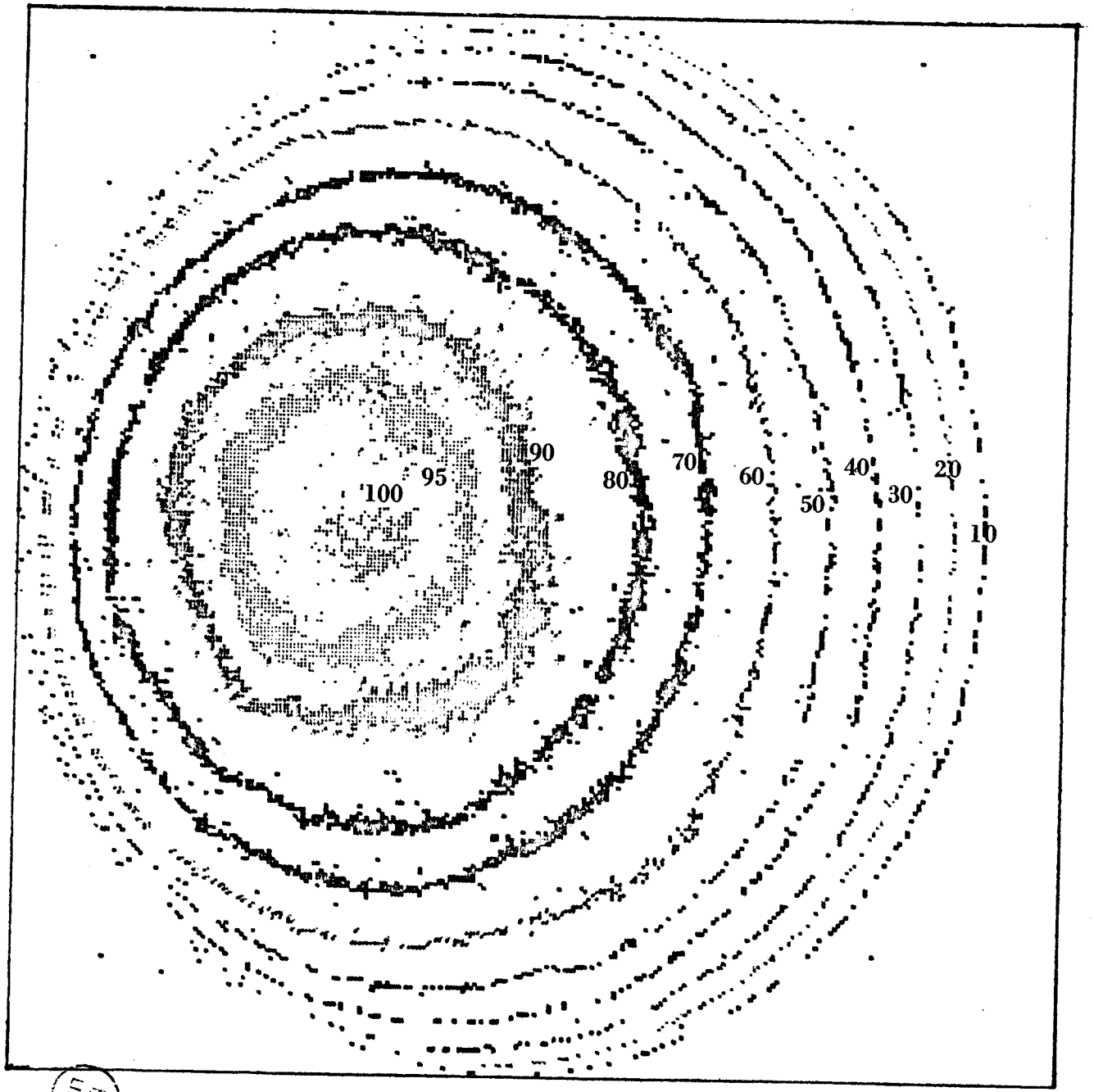

– Figure III-10.b – Isophotes expérimentales d'après Mariner 10.
V = - 23°35 ; λ = 0.46 μm

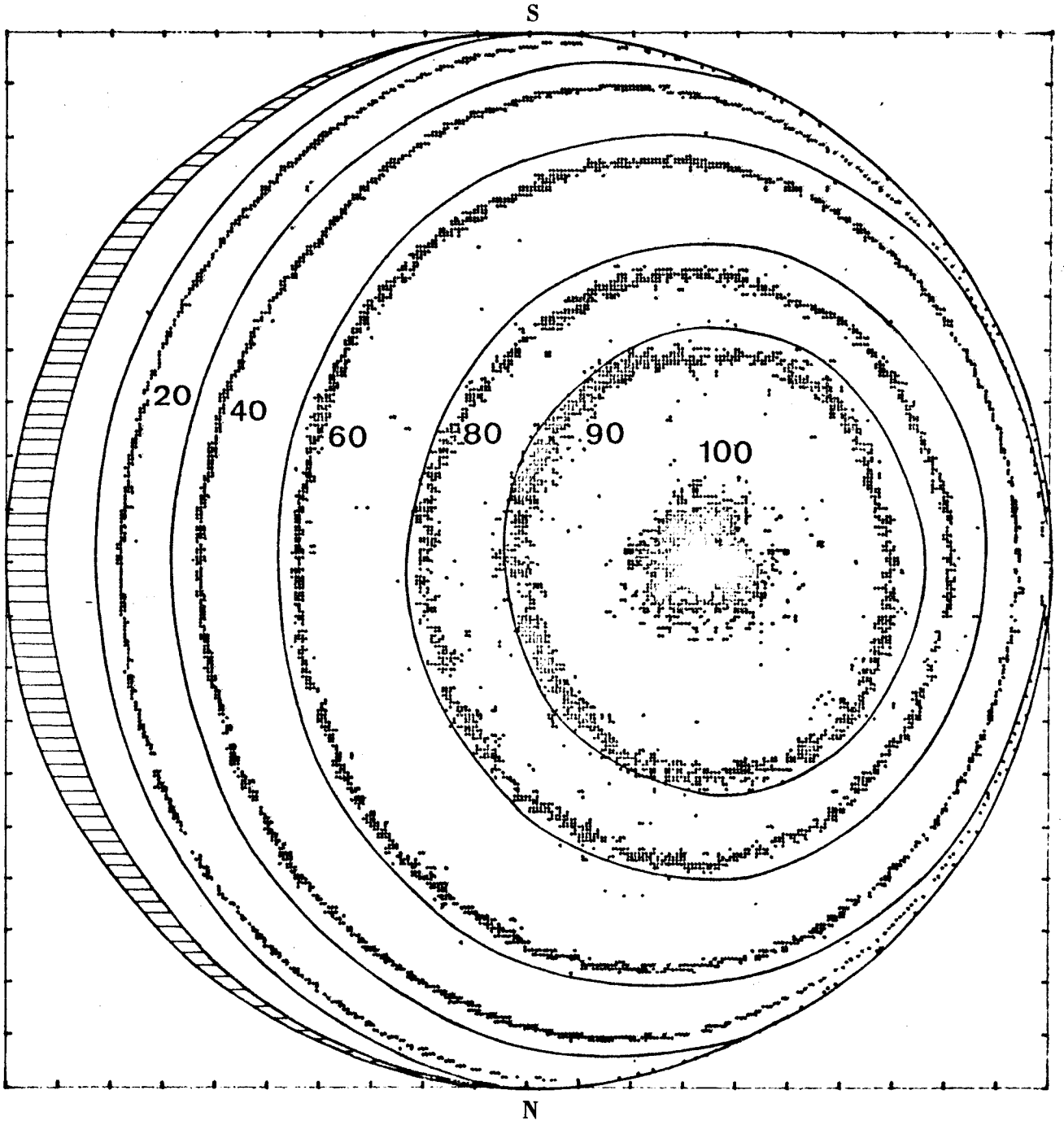

– Figure III-11.a – Comparaison des réseaux d'isophotes théoriques (—) à ceux de Mariner 10 (·). $V = -23°35$; $\lambda = 0.58\ \mu m$

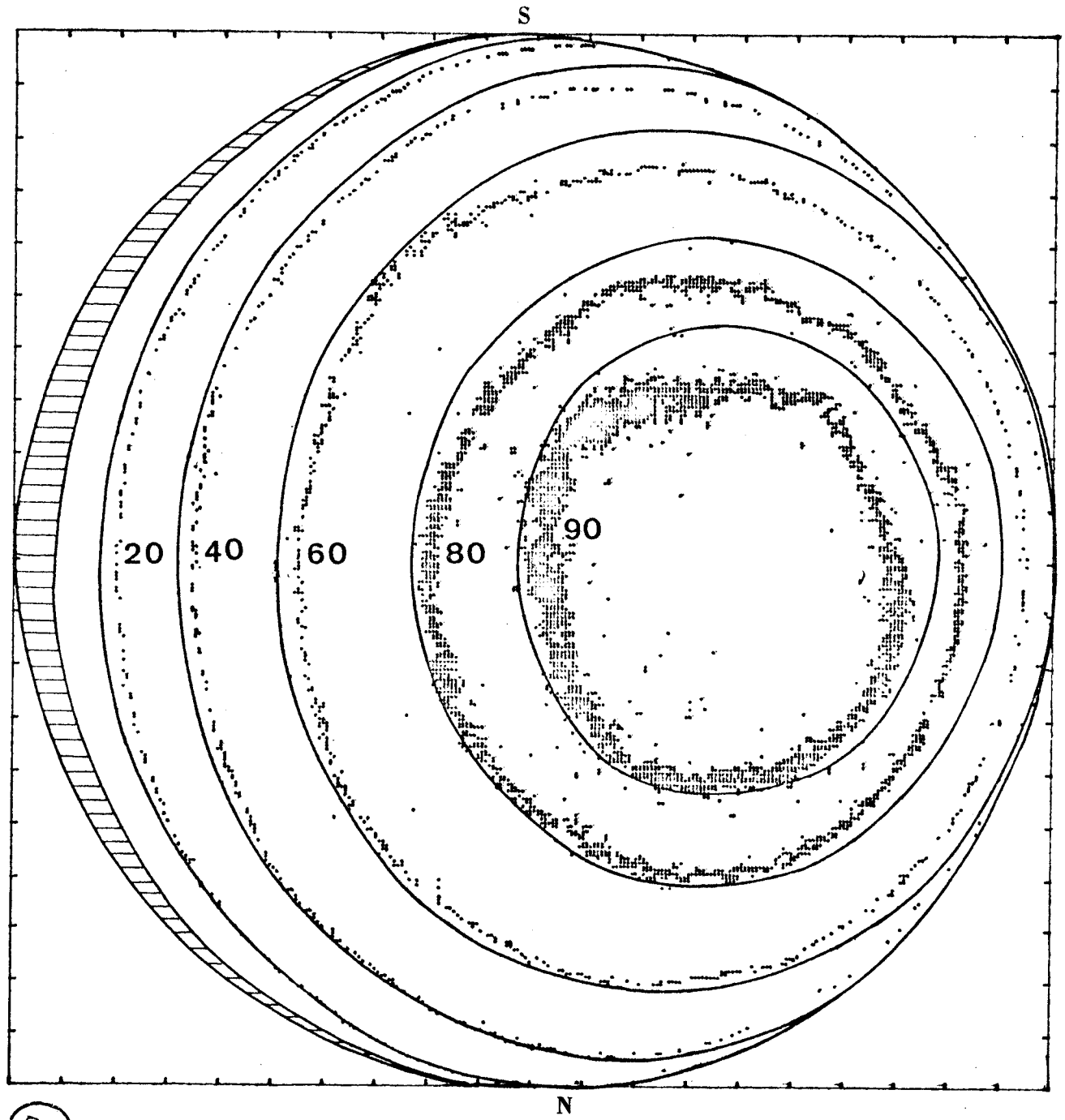

– Figure III-11.b – Comparaison des réseaux d'isophotes théoriques (—) à ceux de Mariner 10 (⁂).
V = - 23°35 ; λ = 0.46 μm

faisante, il semblait préférable d'étudier avant tout les possibilités de cette méthode d'analyse et d'en dégager les paramètres principaux. Nous avons tout d'abord considéré une couverture nuageuse à deux couches horizontalement homogènes. Les paramètres disponibles sont alors au nombre de six : la fonction de phase, l'albédo de diffusion simple et l'épaisseur optique pour chacune des deux couches considérées. Nous devons garder pour les aérosols supérieurs les caractéristiques déduites des mesures polarimétriques et une épaisseur optique totale des nuages assez grande. Afin que la couche nuageuse inférieure puisse influencer valablement les réseaux d'isophotes, l'épaisseur optique de la couche supérieure doit être assez faible (de l'ordre de quelques unités) par rapport à celle de la couche inférieure que l'on pourra considérer comme infinie. Ceci réduit à quatre les paramètres ajustables définis ci contre, compte tenu de la relation que τ_1^1, ω_o^1, ω_o^2 doivent satisfaire avec $P_1(\theta)$ et $P_2(\theta)$ pour respecter l'albédo sphérique.

L'influence de $P_2(\theta)$ étant d'autant plus grande que τ_1^1 est petit, on a étudié son influence dans le cas ou τ_1^1 est négligeable et calculé le champ de rayonnement pour des lois de diffusion très différentes dans le cas d'un nuage homogène infini. Ce travail résumé dans l'article n° 2 montre que l'influence de la fonction de phase sur le diagramme de luminance relative est en fait assez faible. A titre d'exemple, on en a extrait ci dessous, trois réseaux d'isophotes théoriques (Fig.III.12) obtenus pour trois fonctions de phase très différentes (Fig. III.13).

τ_1^1 ω_o^1 $P_1(\theta)$ {H.A} fixée
$\tau_1^2 \infty$ ω_o^2 $P_2(\theta)$

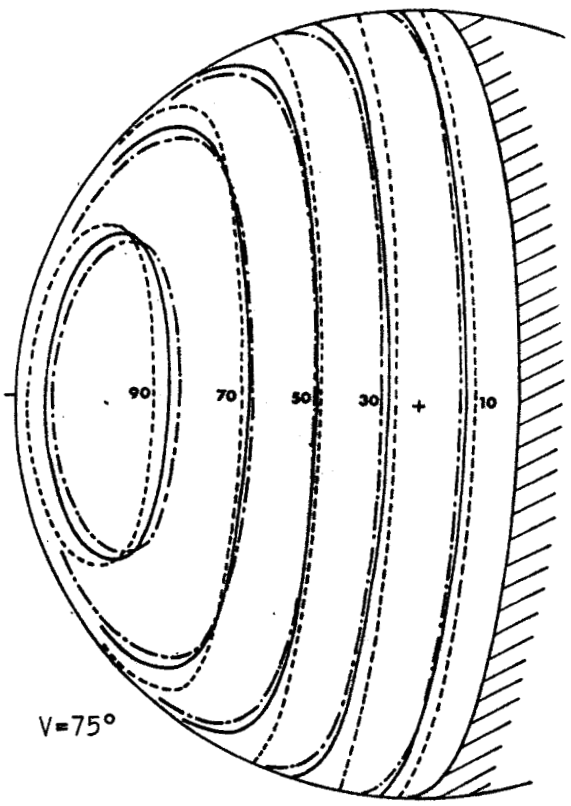

Fig.III.12. Rayleigh(---),
Cumulus(- -),{H.A}.

Fig.III.13.

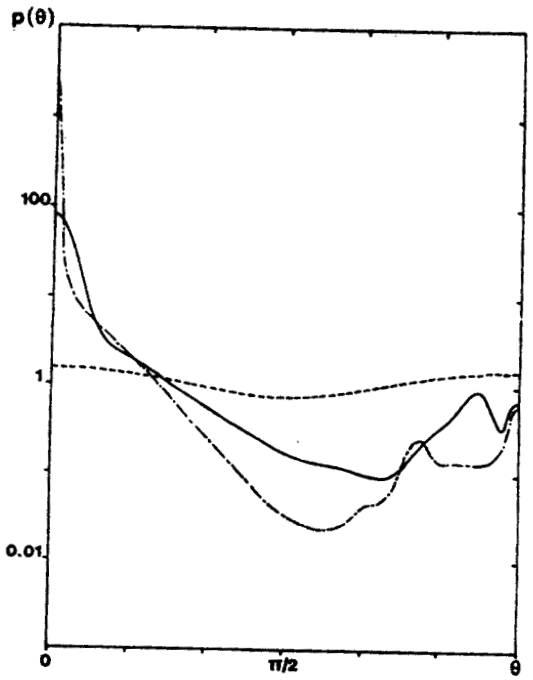

Phase functions at $\lambda = 0.58\,\mu$m for: Rayleigh scattering (---), a cumulus type cloud ($\bar{r} = 4\,\mu$m, $m = 1.33$) (—.—), the {A-H} model ($\bar{r}$=0.83 um, m=1.44) (——).

Mais de plus pour respecter les observations en polarisation, il faut au moins admettre une couche supérieure d'aérosols d'Hansen ayant une épaisseur optique minimum de l'ordre de 1. Dans ce cas, quelle que soit la fonction de diffusion P_2 (θ) des particules à priori inconnues du nuage inférieur , les résultats du modèle homogène sont restitués à mieux que 2% si les absorptions propres des deux nuages sont les mêmes. Ce résultat mis en évidence dans les articles 2 et 3 simplifie donc beaucoup l'analyse : on pourra substituer à ce nuage inférieur un milieu fictif, réfléchissant suivant une loi de Lambert à condition de lui attribuer une réflectivité égale à celle du nuage réel ainsi substitué.

Le seul problème à envisager est donc une éventuelle modification de la distribution de luminance qui proviendrait de la différence de réflectivité des deux couches nuageuses considérées. Cette étude a été faite pour une longueur d'onde moyenne de 0,46 µm; soit la longueur d'onde efficace du filtre bleu de Mariner 10. Celle ci correspond à un albédo

sphérique de 0,77 donc, à une absorption suffisamment forte pour qu'on puisse observer un effet possible mais à cette longueur d'onde, Vénus ne présente néanmoins pas encore les anomalies marquées observées en U.V et qui impliquent à l'évidence une inhomogénéité horizontale.

Deux cas extrêmes sont alors à considérer

- 1) un nuage supérieur conservatif ($\omega_o^1 = 1$), d'épaisseur optique τ_1^1 formés d'aérosols observés en polarisation. La reflectivité du nuage inférieur sera ajustée pour respecter l'albédo sphérique.

- 2) un nuage supérieur purement absorbant d'épaisseur optique τ_a, au dessus d'un nuage conservatif épais ($\rho = 1$).

Ces deux modèles sont schématisés ci dessous

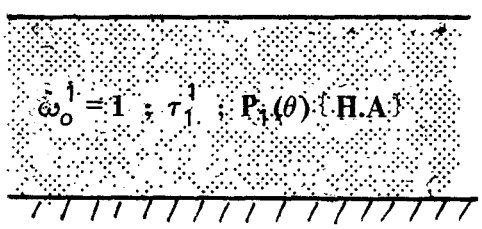

$\rho = 0.76$

1

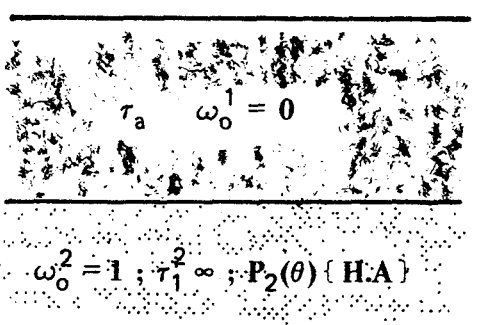

2

Quoique plus importants dans le modèle (2); les écarts observés par rapport au modèle de base sont encore essentiellement localisés près du limbe et du terminateur et restent faibles dans la partie centrale dù disque pour des angles de phase moyens comme on peut le constater sur les figures III.14 (a et b) extraites de l'article n°2 qui présentent les écarts des distributions équatoriales de luminance par rapport au modèle homogène de base.

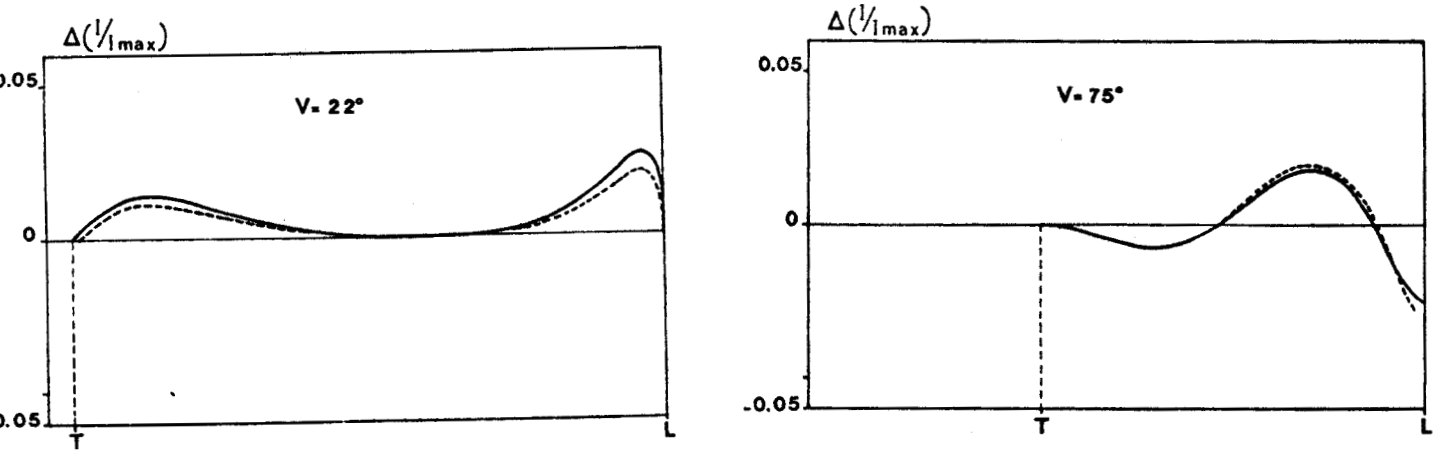

Fig.III.14a. Discrepancies $\Delta(I/I_{max})$ between the equatorial brightness distributions obtained with the homogeneous {A–H} model and a two layer one. $\lambda = 0.47\,\mu$m. Two-layer model (a) Upper cloud $\tau_1 = 0.5$, $\tilde{\omega}_0 = 0.9967$; lower cloud $\rho = 0.77$ (——). (b) Upper cloud $\tau_1 = 1$, $\tilde{\omega}_0 = 1$; lower cloud $\rho = 0.76$ (– – –). L = limb, T = terminator. Phase angle $V = 22°$.

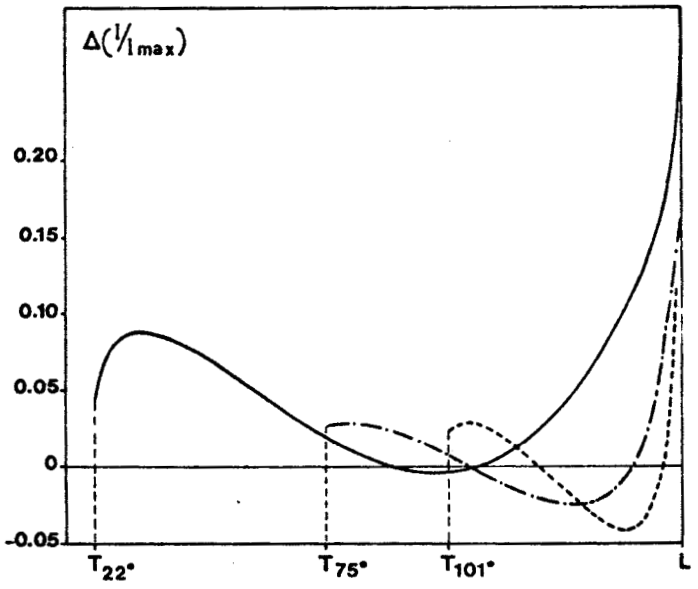

Fig.III.14b.

Discrepancies $\Delta(I/I_{max})$ between the equatorial brightness distributions obtained with the homogeneous {A–H} model and the two layer one: absorbing layer τ_a above a conservative {A–H} cloud. $V = 22°$, (——), $V = 75°$ (—·—), $V = 101°$ (– – –).

Les résultats de cette analyse montraient donc que l'aspect régulier des réseaux d'isophotes observé de façon quasi permanente en lumière jaune ne pouvait pas correspondre à une simple structure stratifiée couvrant de façon homogène l'ensemble du disque. Ceci rejoint d'ailleurs la forte inhomogénéité décelée par la mise en défaut des relations de réciprocité sur les clichés étudiés.

En revanche la simplification importante apportée par l'absence d'influence de P_2 (θ) sur les réseaux d'isophotes permettait d'envisager l'étude des contrastes et d'aborder des modèles inhomogènes horizontalement susceptibles de rendre compte des observations en U.V.

III- VARIATIONS HORIZONTALES DE LA STRUCTURE NUAGEUSE DE VENUS ANALYSE DES TACHES U.V.

On pouvait alors se poser la question de savoir si les inhomogénéités horizontales de la structure nuageuse, mises en évidence par cette analyse de quelques clichés en lumière jaune, et les taches sombres fréquemment observées en lumière ultra violette n'étaient pas corrélées. Nous avons donc cherché si un mécanisme d'absorption unique dont l'efficacité varierait avec la longueur d'onde pouvait expliquer l'ensemble de ces observations, et plus précisément s'il était possible d'en déduire une localisation grossière du niveau de la couche où l'absorption aurait lieu. Cette analyse porte sur une série de clichés obtenus quasi- simultanément à diverses longueurs d'onde. Les figures III.15 (a à f) extraites de Dollfus et al (1975) présentent ces observations polychromes de Vénus du 31 Juillet 1969 sous la forme de réseaux d'isophotes qui montrent de 0,58µm à 0,327 µm l'apparition des classiques taches ultra violettes.

III-1- MODÈLES DE NUAGES.

L'analyse de l'albédo sphérique de Vénus montre que l'absorption doit se produire en assez haute altitude pour le rayonnement U.V. (Cf Art. 4). Dans l'hypothèse d'un mécanisme d'absorption unique, on supposera donc l'influence du sol comme négligeable à toutes les longueurs d'onde. On considérera alors trois types extrêmes de répartition possibles de l'absorption par rapport à la couche diffusante d'où provient la lumière polarisée.

Dans le modèle I on considérera une couche conservative épaisse verticalement homogène ayant les caractéristiques diffusantes de la couche de référence sondée en polarisation surmontée d'un absorbant pur ayant une

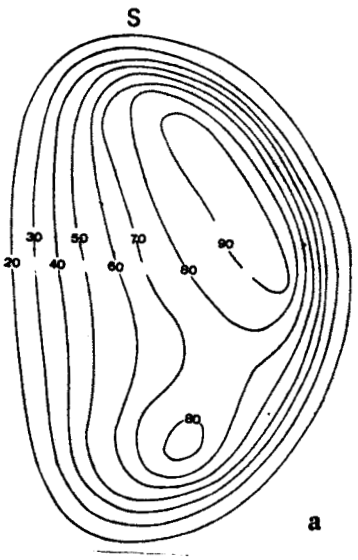

a

1 Jul 1969 04^h18 V=-67°3
3270 Å

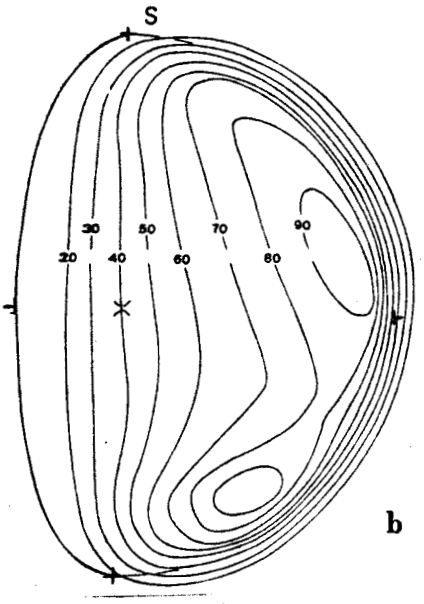

b

31 Jul 1969 04^h08 V=-67°3
3540 Å

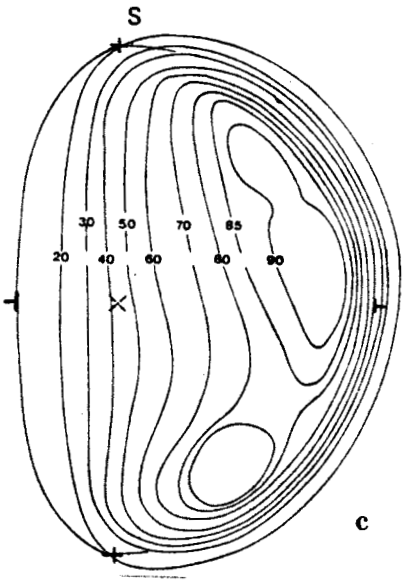

c

31 Jul 1969 04^h03 V=-67°3
3790 Å

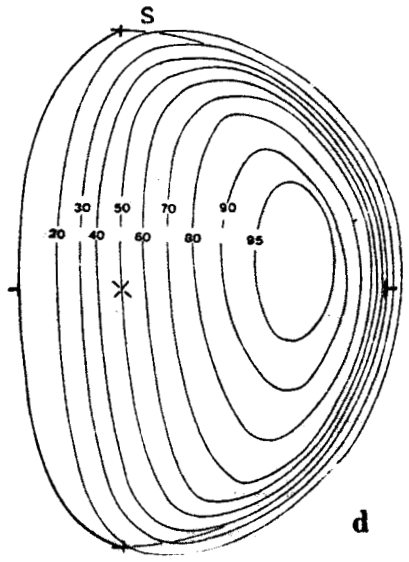

d

1 Aug 1969 03^h48 V=-67°0
4350 Å

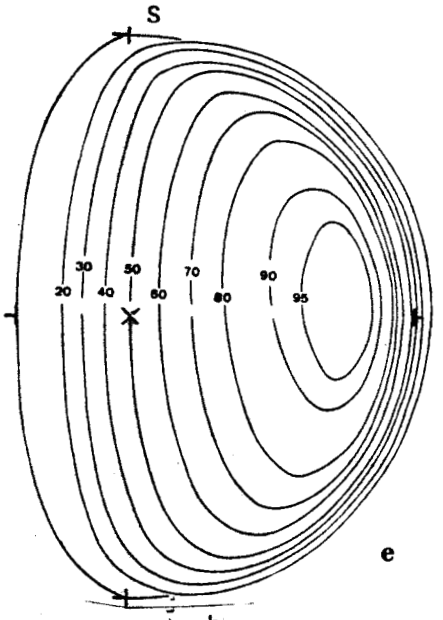

e

31 Jul 1969 03^h52 V=-67°3
5200 Å

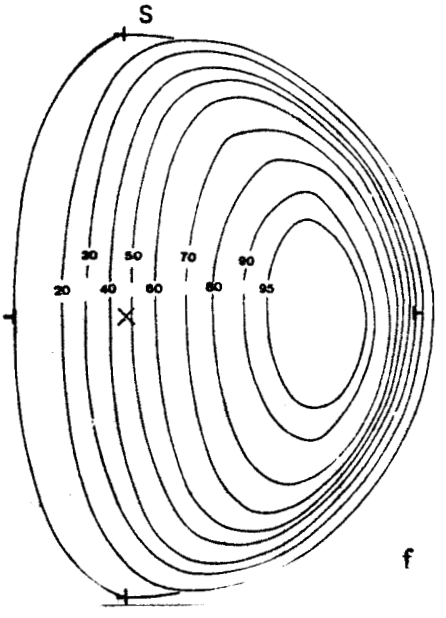

f

31 Jul 1969 03^h45 V=-67°3
5850 Å

– Figure III-15 – Isophotes de Vénus. Série polychromatique d'après Dollfus et al. (1975).

épaisseur optique τ_a variable où sera localisée toute l'absorption.

Dans le modèle II, on supposera au contraire que toute l'absorption a lieu sous la brume conservative de référence, d'épaisseur optique variable, dans une ou plusieurs couches nuageuses plus basses. Celles ci seront essentiellement caractérisées par une réflectivité globale ρ_λ en accord avec l'analyse précédente.

Enfin dans le modèle III, l'absorption sera répartie au sein même de la brume, verticalement homogène; on n'envisagera donc ici que des variations horizontales de l'albédo de diffusion simple $\omega_o(\lambda)$.

Ces différents modèles sont schématisés ci dessous

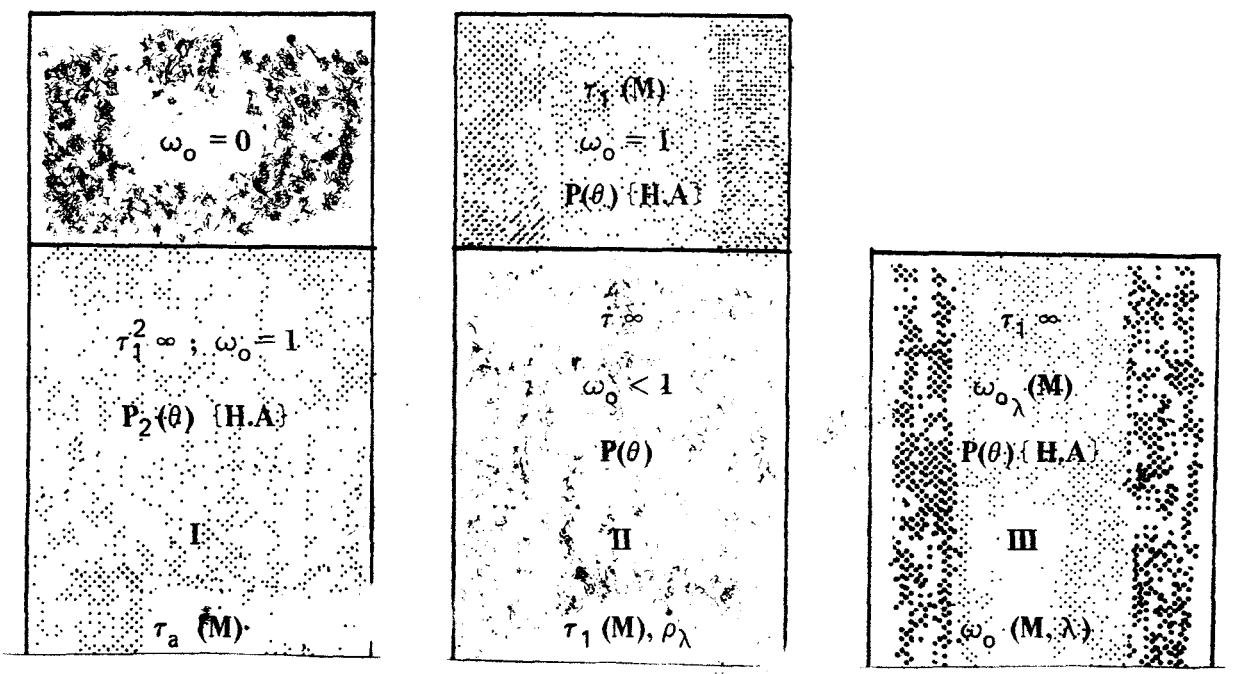

III - 2 - MÉTHODE D'ANALYSE

Pour une longueur d'onde de référence λ_o, on ajuste en tout point M du disque le paramètre ajustable à savoir τ_a (M), τ_1(M) pour ρ_{λ_o} fixé, ou ω_o (M, λ_o) de façon à retrouver la distribution de luminance observée à λ_o. On remarquera que dans le modèle II, à une luminance donnée correspond un intervalle de variation de ρ_{λ_o}, celui ci étant associé à une valeur appropriée de l'épaisseur optique τ_1(M). Nous ne retiendrons pour l'instant que les distributions extrêmes τ_1^{max}(M) et τ_1^{min}(M) qui correspondent respectivement aux réflectivités minimum $\rho_{\lambda_o}^{min}$ et maximum $\rho_{\lambda_o}^{max}$ permettant d'obtenir un accord en tous points

du disque. Puis partant de ces solutions initiales, on cherchera les distributions de luminance qui devraient en résulter aux autres longueurs d'onde. Les paramètres libres seront obtenus par les transformations simples suivantes :

Modèle I $$\tau_a (M, \lambda_1) = \tau_a (M, \lambda_o) \times A (\lambda_1)$$

Modèle II $$\rho_{\lambda_o} ; \tau_1 (M) \qquad \rho \lambda_1 ; \tau_1 (M)$$

Modèle III $$\frac{1 - \omega_o (M, \lambda_1)}{\omega_o (M, \lambda_1)} = \frac{1 - \omega_o (M, \lambda_o)}{\omega_o (M, \lambda_o)} \times B (\lambda_1)$$

Ces relations supposent que l'absorption provient d'un aérosol purement absorbant (dont l'efficacité varie avec λ , n'affectant donc pas la polarisation), la section efficace de diffusion des particules conservatives d'acide sulfurique calculée ne variant pratiquement pas sur l'intervalle spectral considéré. Pour chacun des trois modèles, on calcule alors les luminances absolues $I (M, \lambda_1)$ en fonction du seul paramètre libre ($A (\lambda_1)$, $\rho (\lambda_1)$, $B (\lambda_1)$) respectivement pour chacun des modèles I, II, et III que l'on fait varier jusqu'à retrouver les magnitudes $m (\lambda_1, V)$ déduites des courbes de phase d'Irvine (1968).

Les difficultés rencontrées au cours de cette analyse (localisation précise des points sur le disque, calcul des magnitudes) sont exposées dans l'article 4.

III - 3 - RÉSULTATS

Les distributions initiales $\tau_a (M, \lambda_o)$; $\tau_1 (M)$ et $\omega_o (M, \lambda_o)$ obtenues à 0,3790 µm ont été reportées sur les figures III.16, 17 et 18 respectivement. On s'est contenté de reporter sur la seconde la réparti-

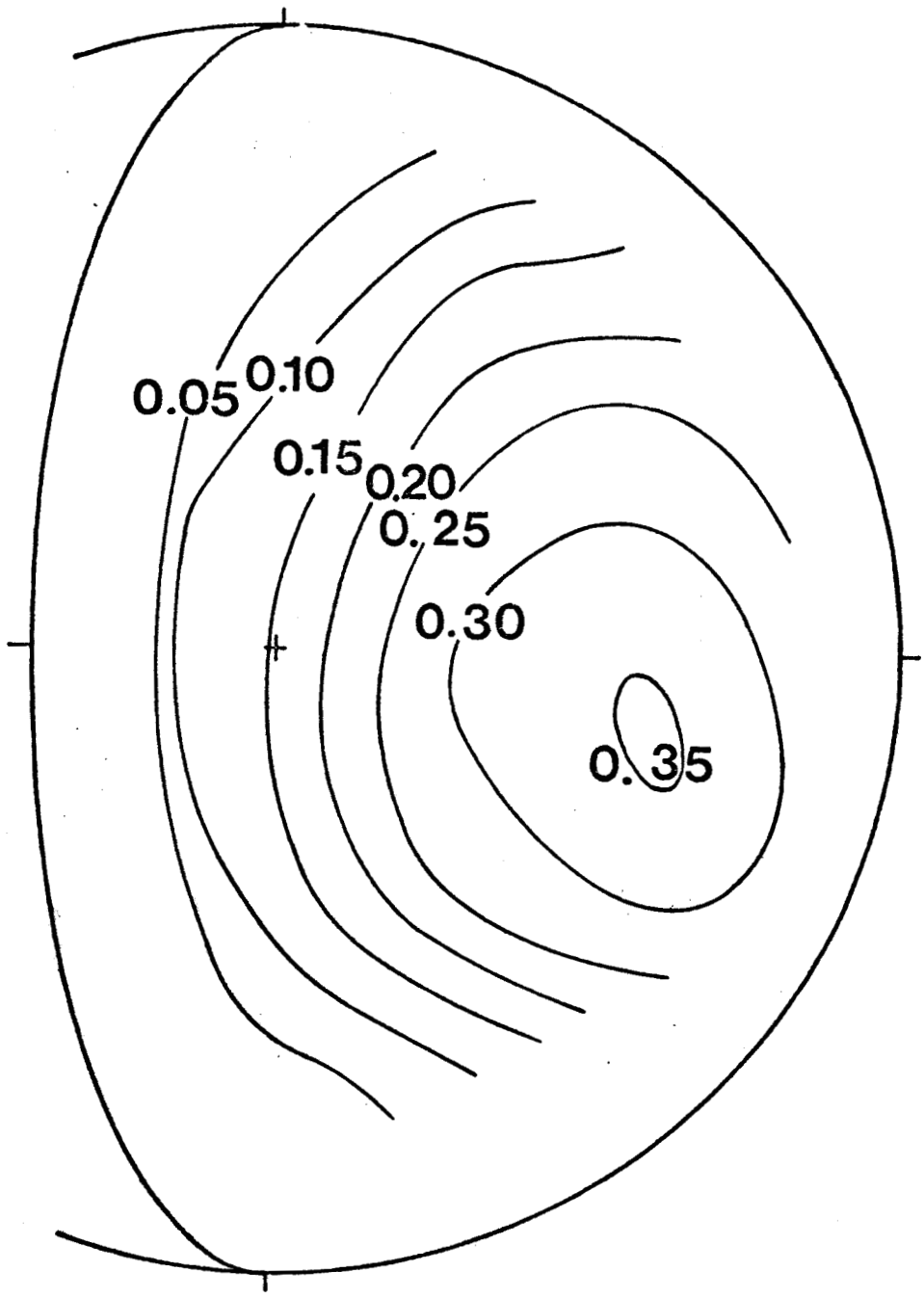

– Figure III-16 – Distribution de l'épaisseur optique $\tau_a(M)$ de l'absorbant pur. Modèle I ($\lambda_o = 3790$ Å ; $V = 67°$)

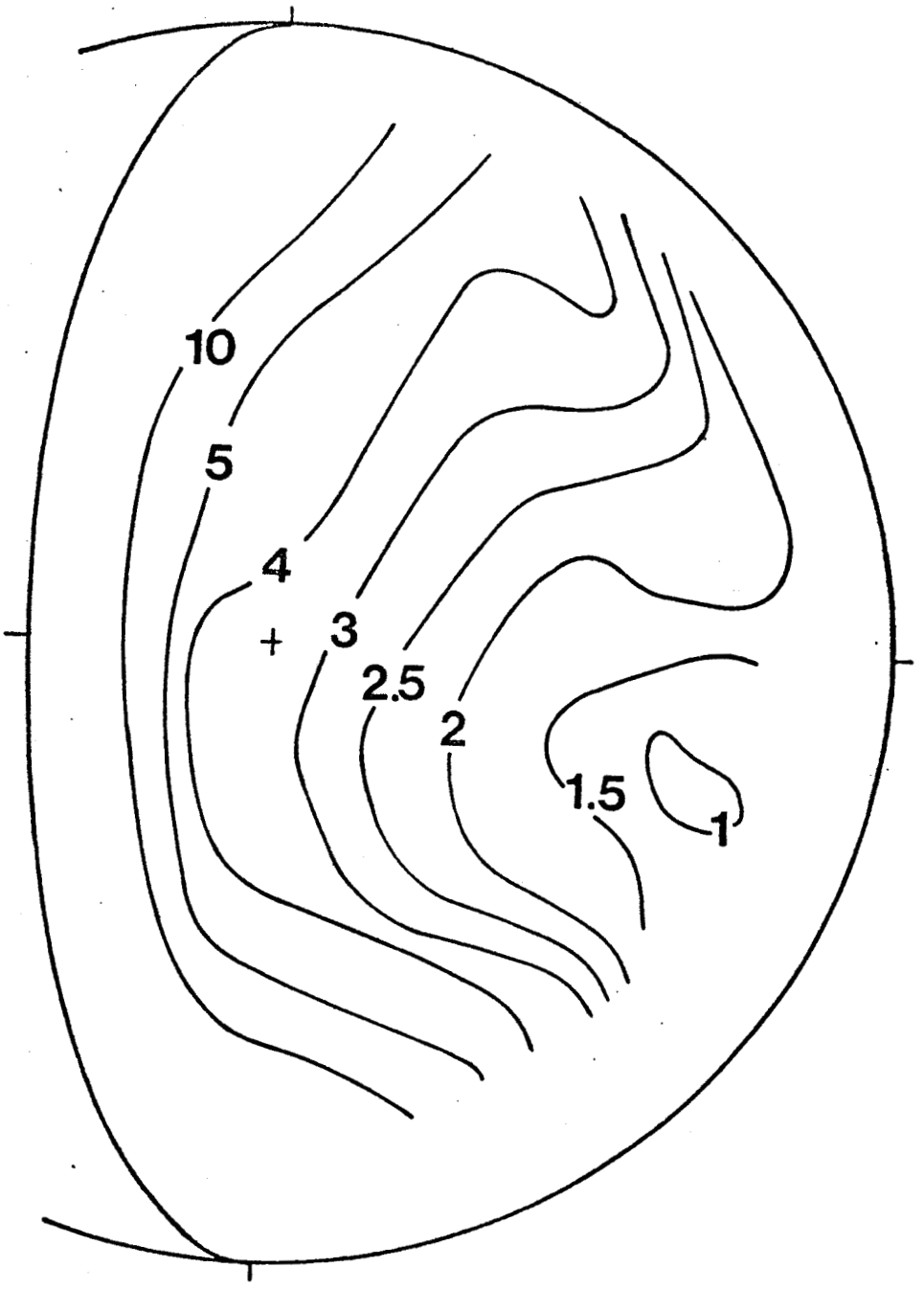

– Figure III-17 – Distribution de l'épaisseur optique $\tau_1(M)$ de la couche supérieure conservative.
Modèle II ($\lambda_o = 3790$ Å ; $V = 67°$)

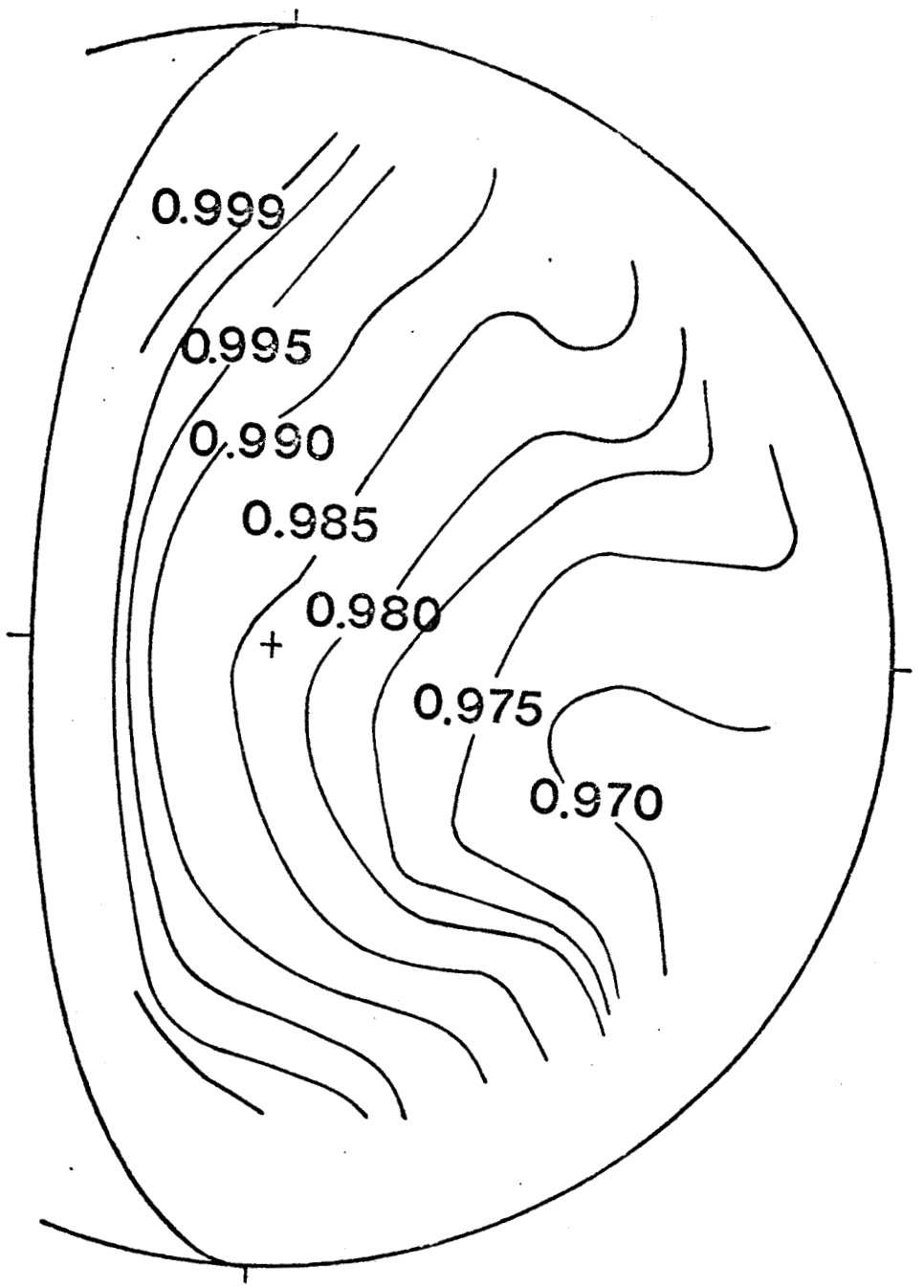

– Figure III-18 – Distribution de l'albédo de diffusion simple $\omega_o(M, \lambda_o)$ du nuage. Modèle III (λ_o = 3790 Å ; V = 67°)

tion τ_1 (M) correspondant à la solution moyenne obtenue. Il apparait en effet que les solutions extrèmes sont très voisines. Typiquement au centre du disque, l'épaisseur optique ne varie que de 2,5 à 3,5 environ; les épaisseurs plus fortes apparaissant au voisinage des pôles et du terminateur restant assez stables. Des épaisseurs plus fortes que τ_1^{max} impliqueraient une réflectivité de départ $\rho_{\lambda_o}^{min}$ si faible qu'il ne serait plus possible par la suite de retrouver la décroissance de magnitude pour les λ plus courtes. Pour des épaisseurs optiques plus faibles que τ_1^{min} nécessitant une réflectivité $\rho_{\lambda_o}^{max}$ plus élevée, on tend vers une distribution de luminance trop homogène et il devient impossible de restituer les dissymétries observées. On peut alors extrapoler des différents modèles vers les autres longueurs d'onde de la série.

III - 4 - Conclusions

Le calcul des différentes distributions théoriques I(M,λ) montre tout d'abord que dans l'intervalle spectral exploré les modèles I et III conduisent à des résultats pratiquement indiscernables dans la partie utilisable du disque et on ne comparera aux réseaux expérimentaux que les résultats confondus des modèles I et III d'une part et les résultats moyens du modèle II d'autre part. Les différents réseaux correspondant respectivement aux modèles I et III, aux mesures expérimentales et au modèle II, sont présentés sur les figures III.19,20 et 21 (a-f) extraites de l'article n°4. On constate d'abord que dans le domaine ultra violet, les observations semblent mieux restituées par les modèles où l'absorption a lieu au dessus ou au sein même de la brume. Dans la zone transitoire 0,39 µm - 0,43 µm où l'on ne dispose malheureusement pas d'observation, les réseaux théoriques se différencient à nouveau assez bien, les contrastes disparaissant plus rapidement dans le modèle II. Enfin dans le visible, les réseaux théoriques sont presque identiques, les

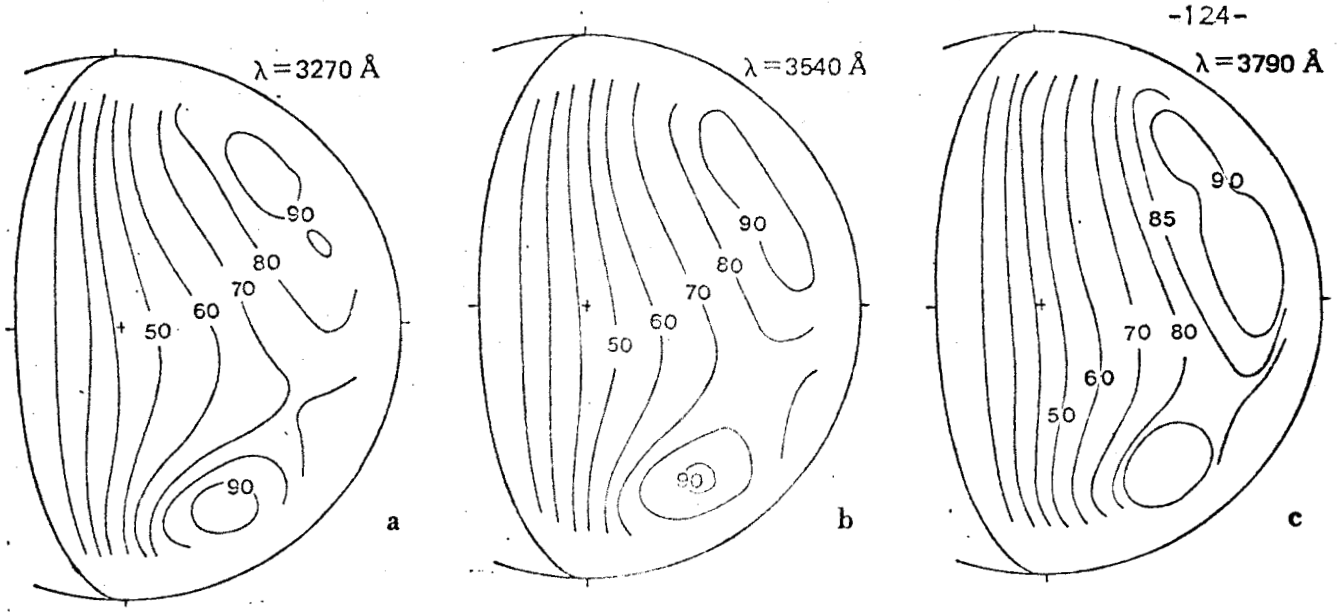

– Figure III-19 – Isophotes théoriques pour les modèles I et III.

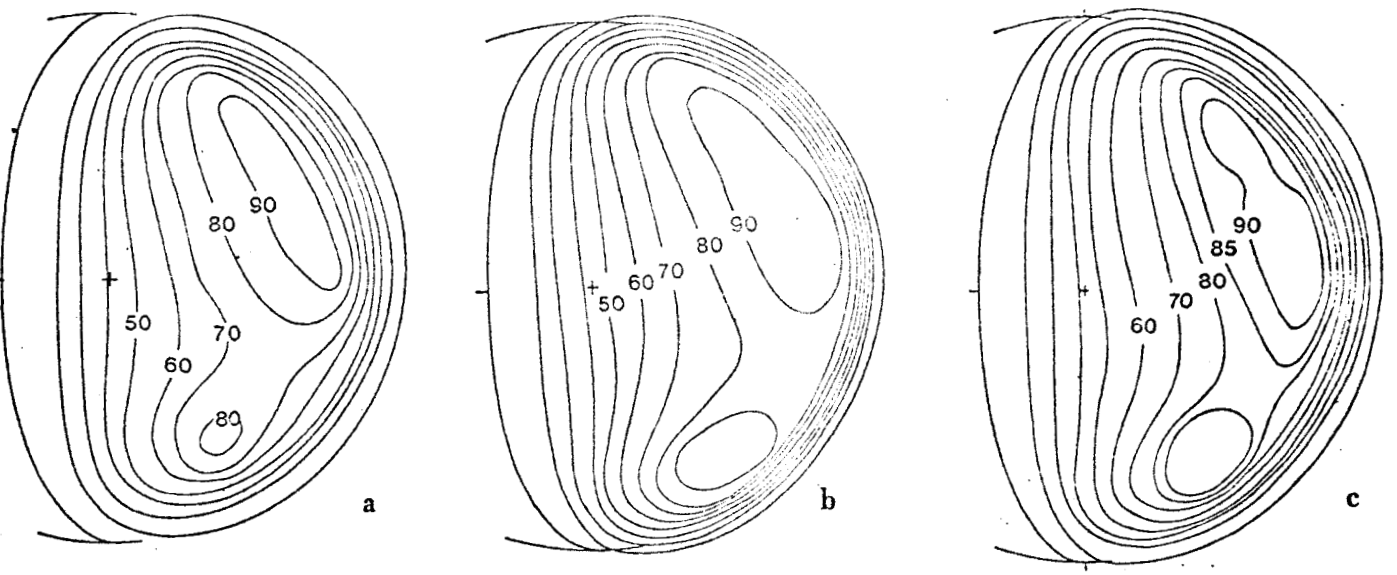

– Figure III-20 – Isophotes expérimentales d'après Dollfus et al. (1975).

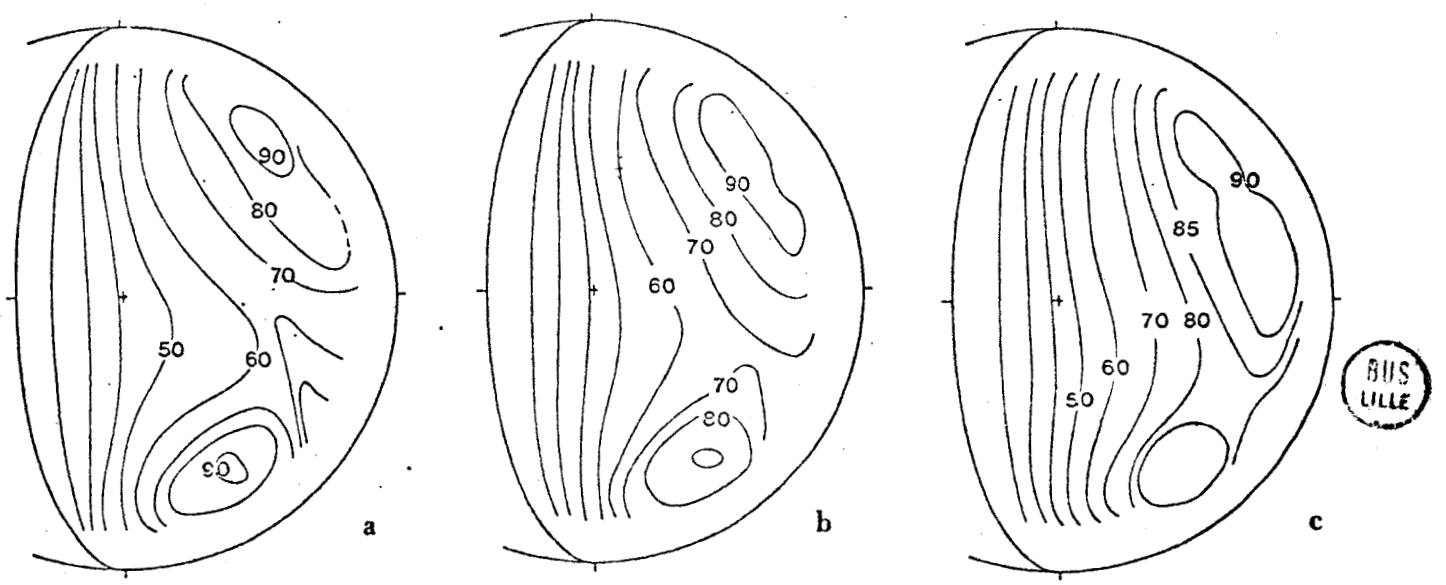

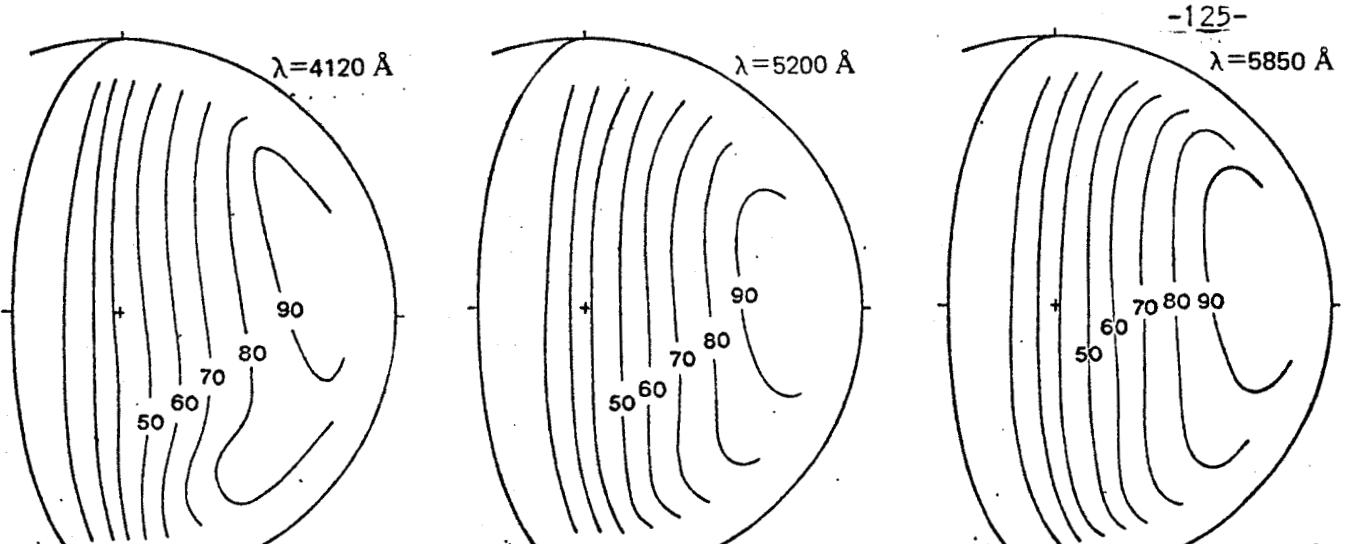

– Figure III-19 – Suite

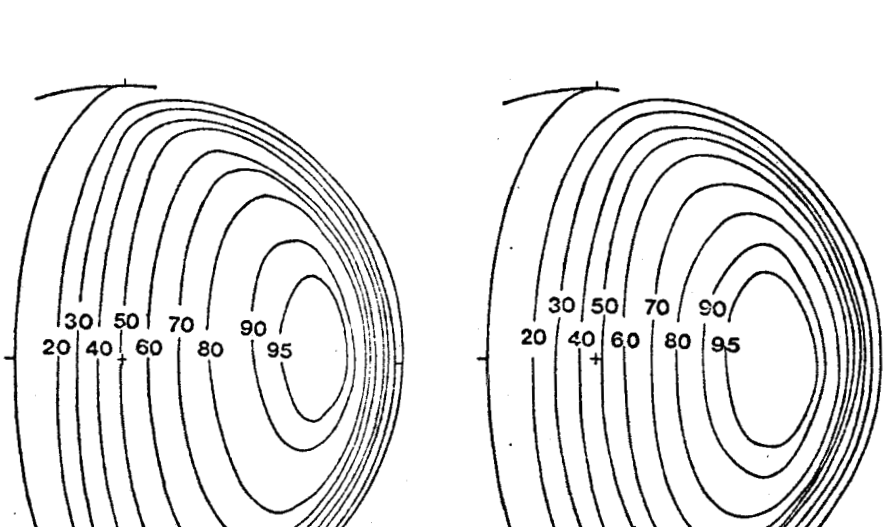

– Figure III-20 – Suite

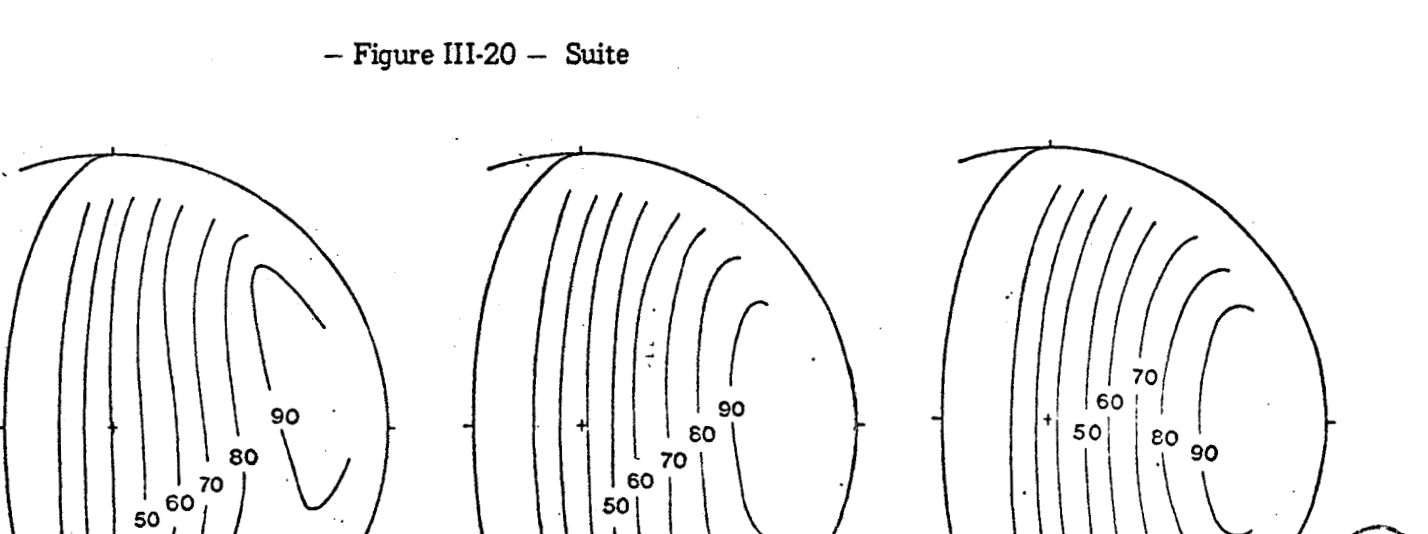

– Figure III-21 – Suite

dissymétries disparaissent, et les résultats théoriques se confondent pratiquement tous avec la distribution de luminance correspondant au modèle homogène infini déjà étudié et inconciliable avec les observations comme on l'a vu précédemment et il apparait donc impossible de corréler les observations visibles et ultra violettes dans l'hypothèse d'un mécanisme d'absorption unique. Dans le visible on relève en effet un déficit de lumière dans la région du point subsolaire. On peut alors envisager une influence du sol. Celle ci n'apparaitrait dans le visible qu'avec l'extinction de l'absorption propre du milieu et la décroissance rapide de la diffusion moléculaire, l'épaisseur optique totale des aérosols de l'atmosphère n'étant plus assez importante pour être considérée comme infinie dans cette région. Ceci semble d'ailleurs confirmé par les résultats préliminaires dès sondages plus récents effectués par Vénéra 9 et 10 (MAROV,1976), l'angle zénithal du soleil étant respectivement de 33° et 27°. Il faudrait admettre alors que l'épaisseur des nuages décroît régulièrement du terminateur au point subsolaire. Mais même en supposant la couche nuageuse conservative et très épaisse au terminateur, le déficit en luminance relative est tel que la magnitude correspondante serait trop faible.

ICARUS 26, 73–84 (1975)

ARTICLE N° 2.

Photometry of Venus

II. Theoretical Brightness Distribution over the Disk

C. BIGOURD, C. DEVAUX, M. HERMAN, AND J. LENOBLE

Laboratoire d'Optique Atmosphérique, Université des Sciences et Techniques de Lille, France

Received December 30, 1974; revised May, 5 1975

Theoretical brightness distributions over the Venus disk have been computed for homogeneous and multilayered cloud models. With homogeneous models, the relative brightness does not depend very much on the optical properties of the cloud, except near the limb or for small phase angles. For multilayered cloud structures, the relative brightness is nearly fixed by the structures and the relative brightness is nearly fixed by the scattering function of the uppermost cloud; the vertical distribution of the absorption is unimportant if the spherical albedo of the planet is given. If the horizontal inhomogeneities currently seen on Venus are due to a layered structure, with an optical thickness of the upper cloud varying from point to point, large simplifications seem possible, and measured contrasts at various wavelengths should permit a test of such a model.

I. Introduction

A large number of observations of the brightness distribution over the disk of Venus have been performed by Dollfus *et al.* (1974); these experimental results are described in Part I of this work on the photometry of Venus (Dollfus *et al.*, 1975).

Most of our present knowledge concerning the Venus clouds has been deduced from the polarization of the solar radiation reflected back to space by the clouds, because polarized light is particularly sensitive to the optical parameters of the particles (Hansen and Arking, 1971; Hansen and Hovenier, 1974). But polarized light can only give us information about the upper layer of the cloud (optical depth 2 or 3). The global scattered intensity is not so precise a source of information, but allows a deeper sounding of the cloud. The phase curve of Venus has already been studied by many authors (Sobolev, 1964; Arking and Potter, 1968; Fymat, 1972). Here we will investigate the distribution of the reflected sunlight upon the Venus disk. Such detailed measurements may contain more information than integrated ones. Only theoretical results will be given. Comparisons with the measurements reported previously (Part I) will be presented in Part III of this work.

II. Model of the Clouds: Computational Scheme

For intensity computations and for visible wavelengths, the molecular scattering of the Venus atmosphere is negligible. It will be assumed that the character of the scattering particles does not vary with altitude, so that we shall have homogeneous clouds. Later on we will consider clouds made up of several homogeneous layers.

It will further be assumed that the number density of the scattering particles is high enough to use plane geometry for any point on the disk. This last assumption may be wrong on the limb, but in any case the experimental data are also too inaccurate near the limb to allow a significant comparison.

As a basic model of the clouds we will use the results deduced from the polarization measurements (Hansen and Arking, 1971; Hansen and Hovenier, 1974); that is, spherical particles, with refractive index $m = 1.44$, effective radius $r_e = 1.1\,\mu$m, mean radius $\bar{r} = 0.83\,\mu$m, and number density

distribution given by

$$n(r) = n_0 r^p \exp(-qr);$$
$$p = 12; \qquad q = (12/0.83)\,\mu\text{m}^{-1}. \quad (1)$$

This model will be called the {A–H} model. Other scattering particles will be considered. They are always supposed to be spherical, so that their scattering phase function $p(\alpha)$ can be computed from Mie theory. The phase function will always be expanded in the form

$$p(\alpha) = \sum_{l=0}^{L} \beta_l P_l(\cos\alpha), \qquad \beta_0 = 1, \quad (2)$$

where the P_l are Legendre polynomials.

Given the law of scattering which is quite independent of the small absorption of the scattering particles at these wavelengths, the single scattering albedo $\tilde{\omega}_0$ will be deduced from the spherical (or Bond) albedo A of the planet, measured by Irvine (1968). For an infinite optical depth of the clouds, the exponential kernel approximation gives (Wang, 1972)

$$\frac{1+A}{1-A} = u(\tilde{\omega}_0, \beta_1),$$
$$u(\tilde{\omega}_0, \beta_1) = \left[\frac{(4-\tilde{\omega}_0)\,(3-\tilde{\omega}_0\beta_1)}{12(1-\tilde{\omega}_0)}\right]^{1/2}. \quad (3)$$

For a finite optical depth of the clouds, τ_1, above a ground (or another cloud) of reflectivity ρ, the same approximate method gives (Bigourd *et al.*, 1973)

$$\frac{1+A}{1-A} = u(\tilde{\omega}_0, \beta_1)\,\frac{1+\delta\tanh\gamma\tau_1}{\delta+\tanh\gamma\tau_1} \quad (4)$$

with

$$\delta = (1-\rho)\,u(\tilde{\omega}_0, \beta_1)/(1+\rho),$$
$$\gamma = (3-\tilde{\omega}_0\beta_1)/2u(\tilde{\omega}_0, \beta_1);$$

ρ, τ_1, $\tilde{\omega}_0$, β_l, and A are wavelength-dependent quantities.

Table I gives, at some wavelengths for which A is known, the single scattering albedo $\tilde{\omega}_0$ of the particles, assuming an infinite optical thickness and the {A–H} model.

Figure 1 gives the geometry of the problem. The center of Venus is O; S and E are the subsolar and the subterrestrial points; and M is the point of observation. Let ψ and ξ be the latitude and longitude

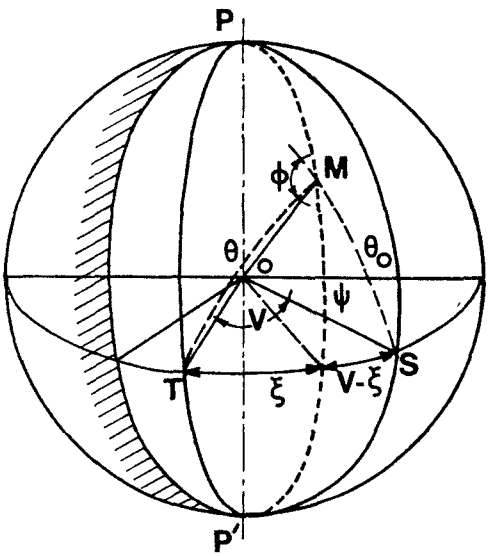

FIG. 1. Geometry of the problem.

TABLE I

λ	A	β_1	ω_0	β_1*	ω_0*	A_0
0.32	0.46	2.315	0.9740	1.911	0.9580	0.805
0.36	0.52	2.297	0.9820	1.914	0.9710	0.772
0.42	0.68	2.265	0.9935	1.9125	0.9900	0.708
0.46	0.77	2.241	p.9970	1.9325	0.9955	0.668
0.50	0.79	2.219	0.9965	1.9425	0.9963	0.600
0.63	0.94	2.134	0.9998			
0.73	0.93	2.076	0.9997			
0.86	0.89	2.038	0.9992			
1.00	0.89	2.040	0.9992			

of M, and V the phase angle of Venus; $\mu = \cos\theta$ and $\mu_0 = \cos\theta_0$, where θ_0 and θ are the angles with OM of the Venus–Sun and Venus–Earth directions. The scattered intensity $I(M, V)$ at M is then computed by the spherical harmonics method (Guillemot, 1967; Deuzé *et al.*, 1973), and obtained in the form

$$I(M, V) = \sum_{s=0}^{L} \cos s\phi \sum_{l=s}^{L} P_s^l(\mu) A_s^l, \quad (5)$$

where the coefficients A_s^l are functions of τ_1, ρ, $\tilde{\omega}_0$, μ_0, and β_l. Most of the computational work involved in obtaining the A_s^l is independent of the values of τ_1, ρ, and μ_0. Computations are made for $\mu_0 = 0.01$; 0.05 (0.05) 0.7; 0.7 (0.25) 0.975; 0.975 (0.05) 0.990 and 0.999. Even for small phase angles, there is a sufficient number of points to obtain an accurate distribution of the scattered light over the disk. For a given ellipse $\mu_0 = \cos\psi\cos(\xi - V) = \text{constant}$, projected upon the apparent Venus disk, $I(M, V)$ may be easily computed by (5) for as many points as necessary with

$$\mu = \cos\psi\cos\xi,$$

$$\cos\phi = -\frac{\cos V - \mu\mu_0}{[(1-\mu^2)(1-\mu_0^2)]^{1/2}}.$$

The final results will be given as curves of equal intensity, or isophotes, on the apparent disk of Venus; the maximum of $I(M)$ will be arbitrarily given the value 100.

For some of the investigated scattering functions (large particles), the exact expansion (2) was too long for computing purposes and we have used the truncation method tested by Hansen (1969) and Potter (1970). In the transfer equation, $\tilde{\omega}_0$ and $p(\alpha)$ are then replaced by the reduced quantities $\tilde{\omega}_0{}^*$ and $p^*(\alpha)$. If $p'(\alpha)$

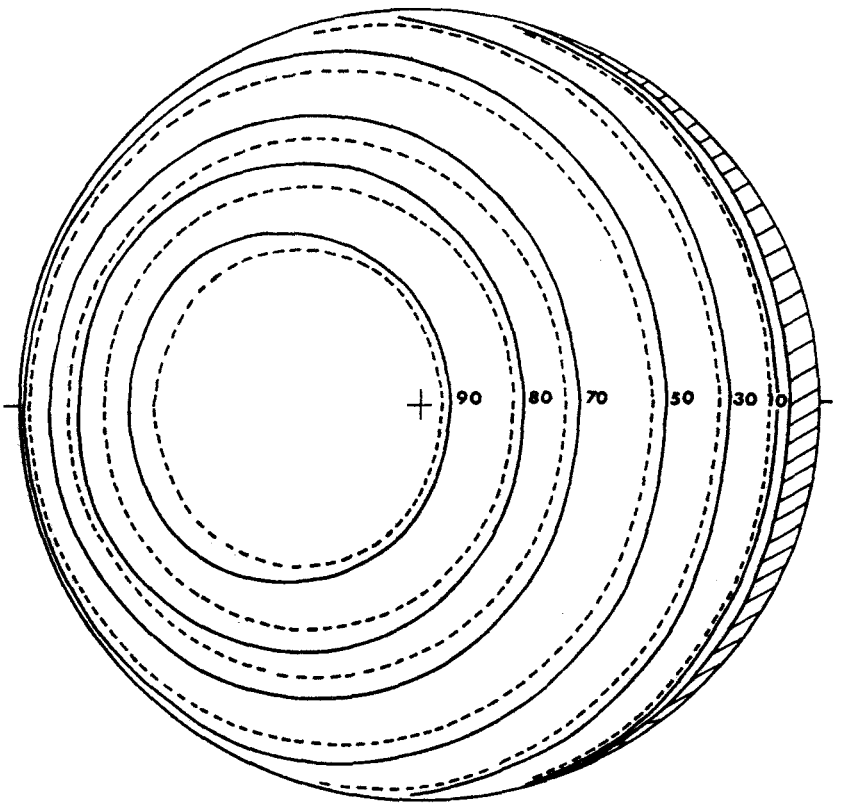

FIG. 2. Theoretical brightness distribution, for a homogeneous cloud {A–H} model at wavelength $\lambda = 0.58\,\mu$m. Spherical albedo $A = 1.0$ (---), $A = 0.8$ (——). Phase angle $V = 22°$.

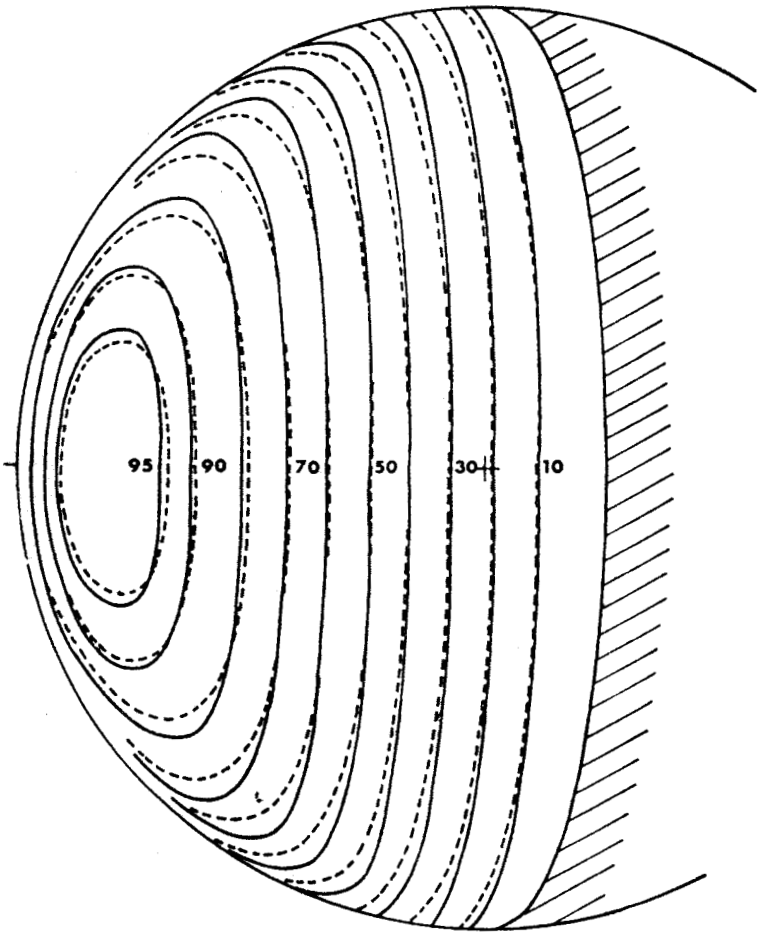

FIG. 3. Same as Fig. 2. $V = 75°$.

is the phase function $p(\alpha)$ truncated from its diffraction peak, with

$$A_0 = \int_{-\pi/2}^{+\pi/2} [p(\alpha) - p'(\alpha)]\, d(\cos\alpha),$$

we have

$$p^*(\alpha) = 2p'(\alpha)/(2 - A_0); \qquad (\beta_0{}^* = 1)$$
$$\omega_0{}^* = \tilde{\omega}_0(2 - A_0)/(2 - \tilde{\omega}_0 A_0). \qquad (6)$$

Except near inferior conjunction ($V > 120°$), or for points near the limb, this approximation is very good.

III. Results for the Basic Model

We first consider the brightness distribution over the Venus disk which would be obtained if the particles observed in polarized light have a sufficient optical thickness so that the major part of the reflected light comes from such scatterers. The accuracy of the polarization measurements is very good and, as will be shown later (Section IV), even large variations of the particles' refractive index and size distribution give small modifications of the isophote maps. Then the model is defined by $\tau_1 \sim \infty$ and the {A–H} phase function.

The single scattering albedo of the particles is deduced from the spherical albedo measurements which are rather inaccurate. Therefore we have carried out the numerical computations for different values of $\tilde{\omega}_0$ corresponding to different values of A. For the wavelength 0.58 μm, $\tilde{\omega}_0 = 0.99725$, 0.99961, and 1 give, respectively, $A = 0.8$, 0.92, and 1, so that the inaccuracy $\Delta A \sim 10\%$ (Irvine, 1968) is

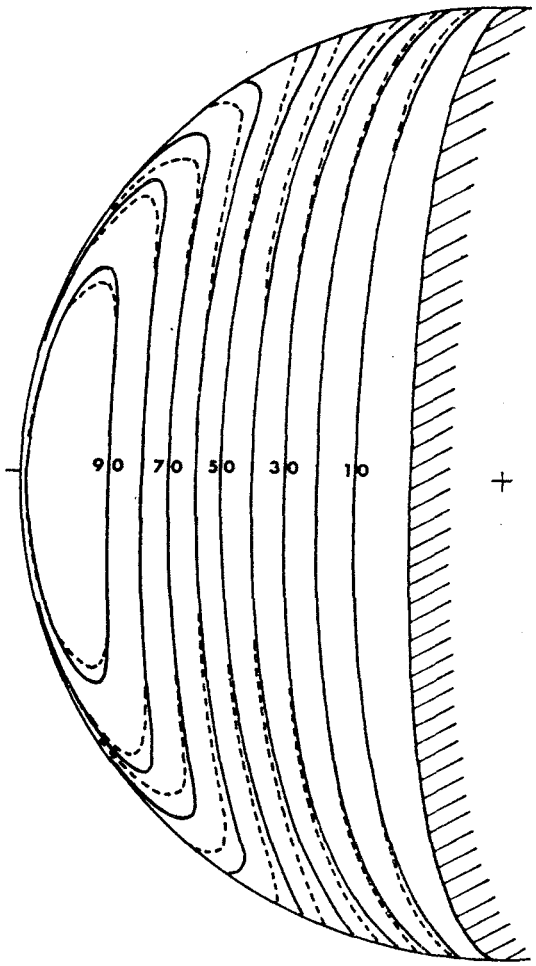

FIG. 4. Same as Fig. 2. $V = 101°$.

taken into account. The obtained isophote maps are given in Figs. 2, 3, and 4, corresponding to phase angles $V = 22°$, 75°, and 101°.

The variations of these maps are qualitatively clear, if we consider the reflected light as expanded in successive orders of scattering. Uesugi and Irvine (1969) have shown that the rate of convergence of the Neumann series

$$I(M, \omega_0) = \sum_{n=1}^{\infty} \tilde{\omega}_0{}^n R_n(M) \simeq A(M) \sum_{n=1}^{\infty} n^{-3/2} \tilde{\omega}_0{}^n \exp[-d(M)/n] \quad (7)$$

does not depend very much on $M[d(M) \cong$ constant], for elongated scattering functions, except near grazing emergence and incidence. So, the relative brightness is nearly independent of $\tilde{\omega}_0$ in the central part of the Venus disk. On the other hand near the limb the convergence of (7) is very rapid and only the few first orders of scattering, which are not very affected by absorption, contribute to the reflected light; then the relative brightness near the limb increases with the true absorption (when $\tilde{\omega}_0$ decreases). The larger the phase angle, the smaller the variation; for $V \geqslant 120°$, the brightness over the whole of each map corresponds to a few orders of scattering and becomes quite independent of $\tilde{\omega}_0$.

With the assumed homogeneous {A–H} model, the theoretical relative brightness is therefore well defined for not too small phase angles and can be compared with the observed relative brightness. The remaining uncertainties are not very important, since they are located in places where the experimental results are probably not very good, because of the limited resolution of the telescope. On the other hand, with the same hypothesis, accurate experimental isophote maps obtained near Venus superior conjunction would perhaps make it possible to fix a limit for the possible true absorption of the scattering particles. But for such phase angles ground-based measurements do not seem well suited.

IV. Two Cloud Models

Below the upper cloud, from which the polarized light comes, and which corresponds to the {A–H} model, there may be another kind of aerosol. Such a layered cloud structure could explain the inhomogeneities frequently seen as dark markings on the Venus disk. Let us see whether we can infer something about such an inhomogeneity from photometric measurements.

With a two-layer horizontally inhomogeneous model we have too many parameters, and we shall first analyze the general features of the problem with a horizontally homogeneous cloud cover, that is an assumed upper cloud with uniform optical thickness τ_1, above another lower layer. We then have four unknowns:

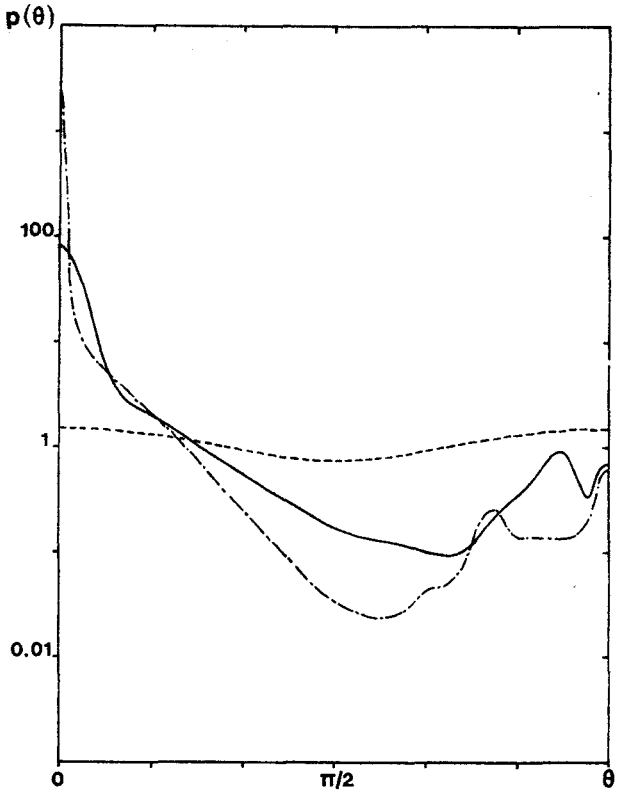

FIG. 5. Phase functions at $\lambda = 0.58\,\mu$m for: Rayleigh scattering (---), a cumulus type cloud ($\bar{r} = 4\,\mu$m, $m = 1.33$) (—.—), the {A-H} model ($\bar{r}$=0.83 um, m=1.44) (——).

τ_1 (we have to keep a large optical depth $\tau_1' \sim \infty$ for the lower cloud), the phase function $p'(\theta)$ for the lower cloud (we have to keep the {A–H} model for the upper one), and the single scattering albedos $\tilde{\omega}_0$ and $\tilde{\omega}_0'$ for the two layers. These unknowns, $\tilde{\omega}_0$, $\tilde{\omega}_0'$, $p'(\theta)$ and τ_1, have to obey the condition that the observed spherical albedo A of Venus is obtained.

For such a model the preceding basic results will be modified, owing to the modification of the upward radiation received at the bottom of the upper cloud. This change may qualitatively be analysed in two respects: (i) a modification of the spatial distribution of this upgoing radiation, and (ii) a modification of the upward flux (since the two clouds will generally have different absorptions and therefore different reflectivities).

To study the first effect, let us assume that the {A–H} layer is very thin and compute isophote maps, again for homogeneous models, but for other scattering laws than the {A–H} one. The discrepancies between such maps and those corresponding to the basic model will give the maximum possible perturbation due to $p'(\theta)$.

An exhaustive investigation of the various kinds of particles proposed for Venus is however impossible (in any case the number distributions and the shapes of these particles remain unknown), and we have only studied two examples of very different scattering media: Rayleigh scattering, and a cumulus type cloud ($\bar{r} = 4\,\mu$m, $m = 1.33$). The corresponding phase functions are given in Fig. 5 for wavelength $0.58\,\mu$m. These cases do not claim physical plausibility; they only correspond to large variations in backward and forward scattering.

Some comparisons of the corresponding brightness distributions are given in Figs.

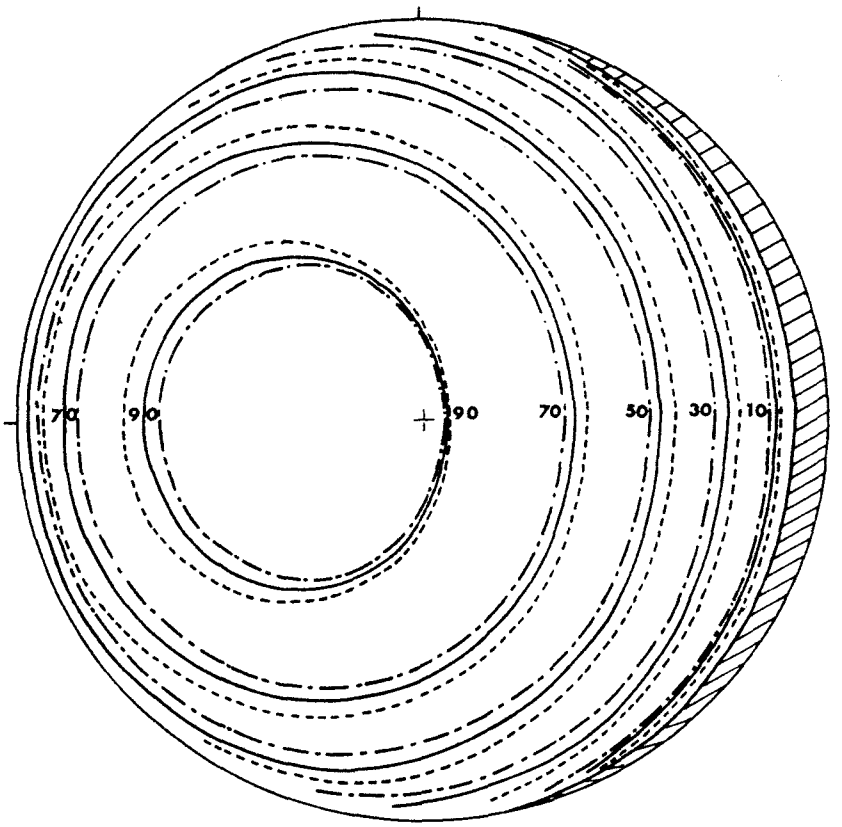

FIG. 6. Theoretical brightness distribution, for a homogeneous cloud at $\lambda = 0.58\mu$m. Spherical albedo $A = 0.92$. Phase function: Rayleigh scattering (– – –), cumulus type cloud (—·—), {A–H} model (——). Phase angle $V = 22°$.

6, 7, and 8. The single scattering albedo was always adjusted to obtain the same spherical albedo ($A = 0.92$). Here again, except for points near the limb or for phase angles near superior conjunction, the obtained variations are very small. The larger effect appears with Rayleigh scattering, but such discrepancies will certainly disappear when superimposing a thin but not negligible layer of the {A–H} model above these test clouds. To clarify this point, we have compared the basic results with the brightness distributions obtained with an upper {A–H} cloud of uniform optical thickness τ_1, above a fictitious lower cloud giving an isotropic upgoing radiation. The comparison has been made for $\lambda = 0.46\mu$m, $\tilde{\omega}_0 = 0.9967$ for the upper layer and $\rho = 0.77$ for the reflectivity of the lower one. Even for such an extreme variation of the upgoing radiation pattern received at the bottom of the upper cloud, the results of the basic model are practically retrieved within 2% for $\tau_1 = 1$. Figures 9, 10 and 11 give these relative discrepancies along the equator for three phase angles.

Actually we do not know the minimum optical thickness the upper {A–H} cloud must be given so that it can account for the observed polarized light, but $\tau_1 \sim 1$ seems good to order of magnitude. Moreover for plausible scattering laws $p'(\theta)$, an even smaller thickness τ_1 would certainly be sufficient to remove the small variations obtained in Figs. 6, 7, and 8. Consequently whatever particles there may be under the upper layer, it seems that their phase function is not at all an important parameter for our purpose, and so we can escape the difficult problem of having to choose a

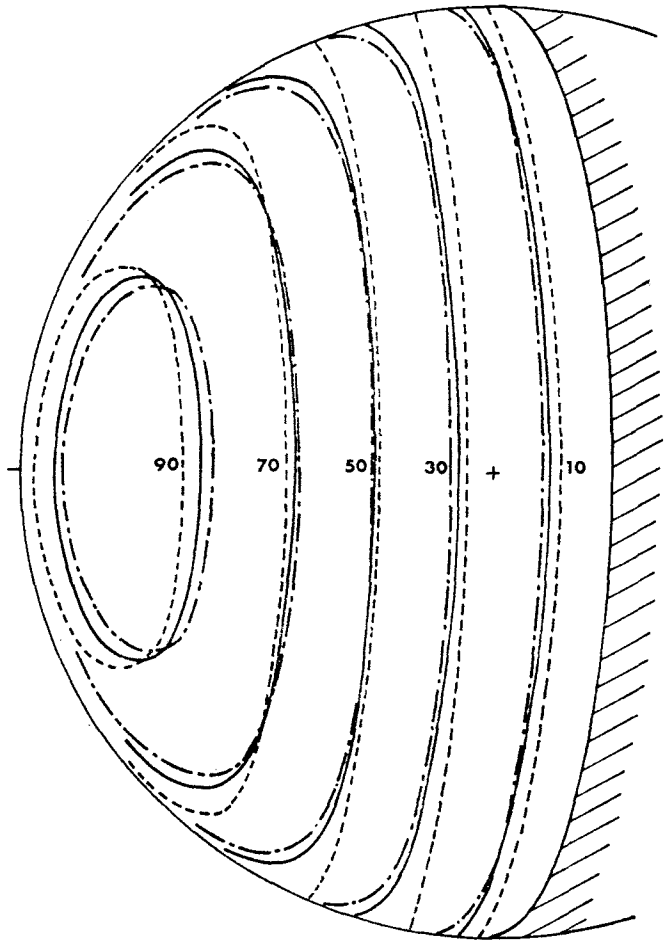

FIG. 7. Same as Fig. 6. $V = 75°$.

scattering model for the lower cloud; we shall merely substitute for it a fictitious scattering medium giving an isotropic upgoing radiance, with the reflectivity ρ of the real lower cloud. For further comparisons with experimental data, the validity of this simplification may have to be verified, and a more refined analysis undertaken only if too small values for τ_1 are obtained.

There now remains only to investigate the second possible effect, that is the variation of the brightness distribution due to the difference in the reflectivities of the two clouds. The larger this difference, the larger the effect, and for a first analysis it is sufficient to investigate the extreme cases of a perfectly conservative or purely absorbing upper layer.

Let us first consider a conservative {A–H} layer ($\tilde{\omega}_0 = 1$, optical thickness τ_1); the reflectivity ρ of the lower cloud will be deduced by (4) from the spherical albedo A. For wavelengths for which Venus has a high reflectivity, large effects cannot be expected, because the lower cloud itself will be nearly conservative: so we have made computations for $\lambda = 0.46\mu$m. The spherical albedo is then small ($A = 0.77$), so that there is a great difference between the reflectivities of the two layers, and the Rayleigh scattering remains negligible, so that a more refined model is certainly unnecessary. Figures 9, 10, 11 give, for

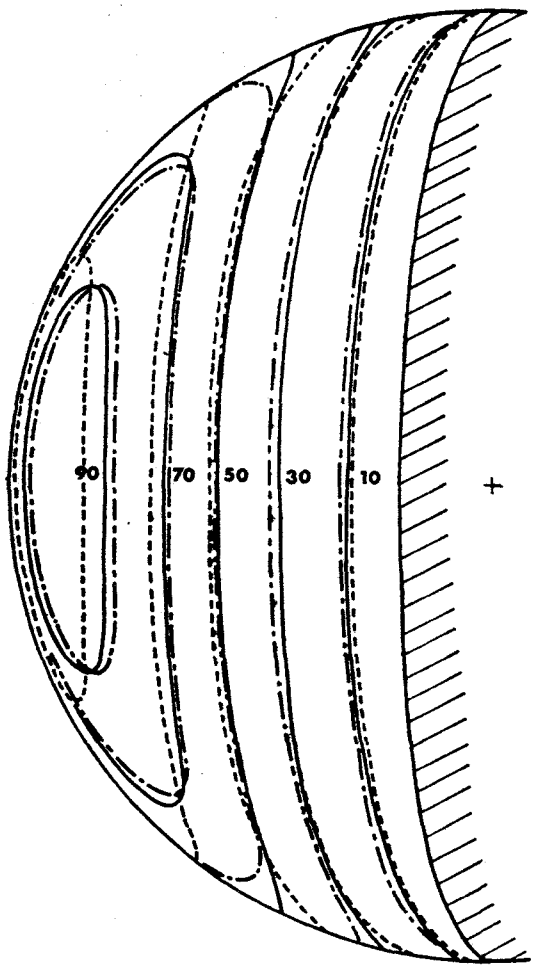

FIG. 8. Same as Fig. 6. $V = 101°$.

three phase angles, the differences between the equatorial brightness distributions obtained for this wavelength, with the basic model and with the two layer model just described ($\tau_1 = 1, \rho = 0.76$). The discrepancies are again very small and principally located near the limb.

The same is not true with the opposite hypothesis of an upper layer more absorbing than the lower cloud. With this model, the extreme case would correspond to a purely absorbing upper layer (optical thickness τ_a) above a conservative scattering cloud. Let $I(M)/I_{max}$ be the relative brightness obtained with this lower cloud alone, which is assumed to have the {A–H} model characteristics in order to explain the polarized features. With the absorbing cloud above, the observed brightness $I(M)$ will become $I(M)\exp[-\tau_a(1/\mu + 1/\mu_0)]$. To order of magnitude, $(1/\mu + 1/\mu_0) \simeq 4$ gives $A \simeq \exp(-4\tau_a)$, which fixes the value of τ_a. Let us put μ' and μ_0' for the point corresponding to I_{max}. The relative brightness distribution $I(M)/I_{max}$ obtained with the basic model will be multiplied by

$$A^{(1/\mu'+1/\mu_0'-1/\mu-1/\mu_0)/4}. \qquad (7)$$

For $\lambda = 0.46\mu$m, Fig. 12 gives the differences between the equatorial brightness distributions obtained with the basic model and with (7). The modifications are here greater than those obtained in the previous case, and perhaps such an ex-

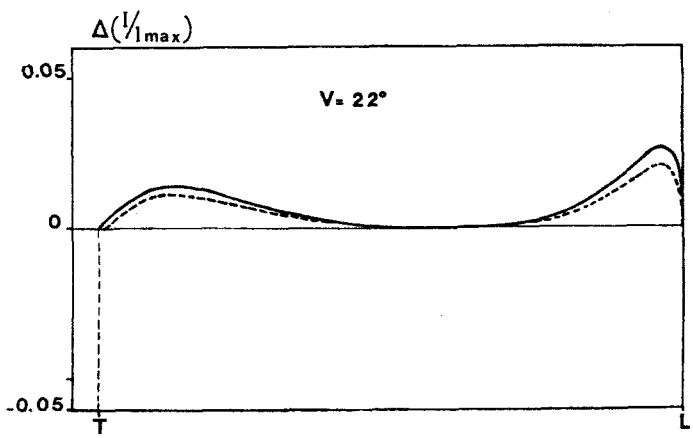

FIG. 9. Discrepancies $\Delta(I/I_{max})$ between the equatorial brightness distributions obtained with the homogeneous {A–H} model and a two layer one. $\lambda = 0.47\mu$m. Two-layer model (a) Upper cloud $\tau_1 = 0.5$, $\tilde{\omega}_0 = 0.9967$; lower cloud $\rho = 0.77$ (——). (b) Upper cloud $\tau_1 = 1$, $\tilde{\omega}_0 = 1$; lower cloud $\rho = 0.76$ (– – –). L = limb, T = terminator. Phase angle $V = 22°$.

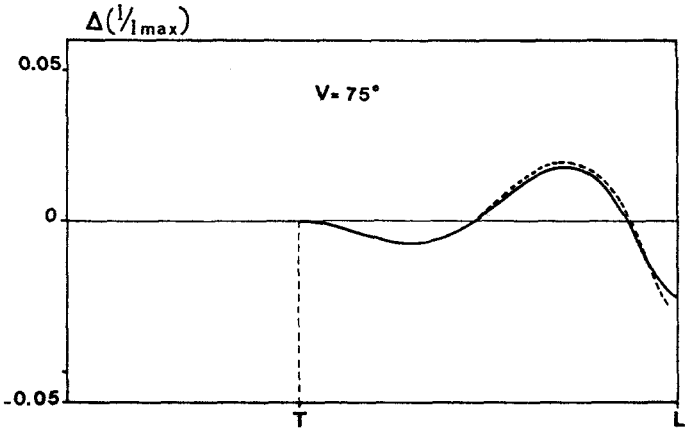

FIG. 10. Same as Fig. 9, $V = 75°$.

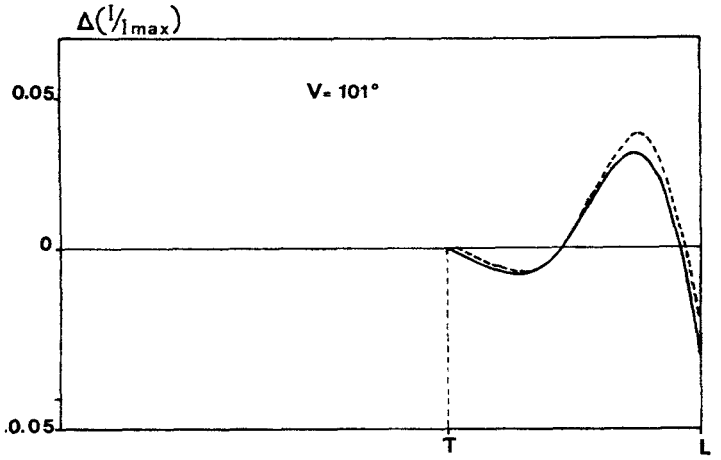

FIG. 11. Same as Fig. 9, V = 101°.

treme case could be detected from a detailed study of the experimental isophote maps. Nevertheless, for not too small phase angles, and for the central parts of the Venus disk, the mean features of the brightness distributions obtained with a two-layer horizontally homogeneous model do not depend very much either on the scattering function of the lower particles, or on the chosen values for ω_0, $\tilde{\omega}_0'$, and τ_1 which are supposed to give the observed spherical albedo A.

V. CONCLUSIONS

The above analysis has shown that accurate theoretical isophote maps can be computed, from the results obtained in polarized light, for an assumed horizontal homogeneity of the cloud pattern upon the Venus disk. Neither the inaccuracy for the true absorption, nor a vertical inhomogeneity of the cloud layer can greatly change these maps in their central parts.

Perhaps a two-layer cloud structure could be inferred from accurate photometric measurements, even for quiet days where Venus seems very homogeneous in visible light. Such a structure would be detected more easily with an upper cloud more absorbing than the lower cloud. But the characteristic features are then principally located near the limb, and are more prominent for small phase angles. High

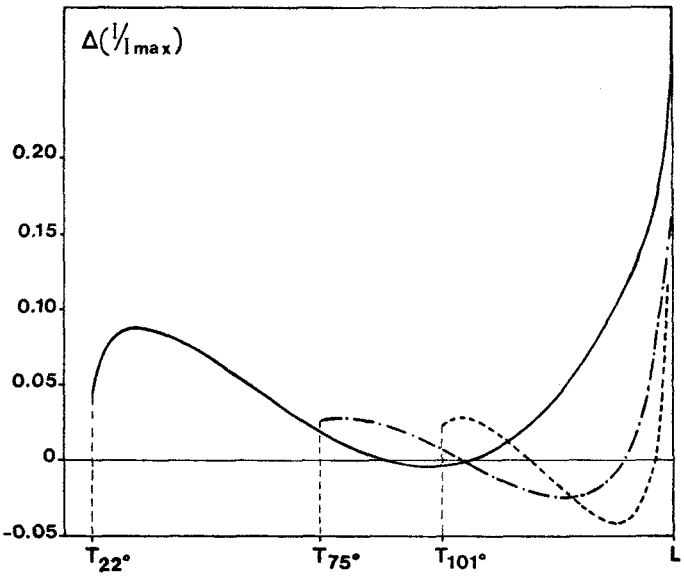

FIG. 12. Discrepancies $\Delta(I/I_{max})$ between the equatorial brightness distributions obtained with the homogeneous {A–H} model and the two layer one: absorbing layer τ_a above a conservative {A–H} cloud. $V = 22°$, (——), $V = 75°$ (—·—), $V = 101°$ (– – –).

resolution photometry would be necessary.

On the other hand, horizontal inhomogeneities, almost always seen on Venus in ultraviolet light and even sometimes observed at longer wavelengths (cf. Paper I) as dark markings, may be explained by a two-layer cloud structure, with the optical thickness of the upper layer varying from point to point. In such a case, the present study shows that large simplifications are possible, and the contrasts measured for various wavelengths should allow us to infer the variations of the optical thickness τ_1 of the upper layer and the location of the more absorbing cloud.

REFERENCES

ARKING, A., AND POTTER, J. (1968). The phase curve of Venus and the nature of its clouds. *J. Atm. Sci.* **25**, 617–628.

BIGOURD, C., DEVAUX, C., AND HERMAN, M. (1973). Albedos plan et spherique. Extension de la méthode de Wang (méthode du noyau exponentiel). Rapport Interne, Université des Sciences et Techniques de Lille.

DEUZE, J. L., DEVAUX, C., AND HERMAN, M. (1973). Utilisation de la méthode des harmoniques sphériques dans les calculs de transfert radiatif. Extension au cas de couches diffusantes d'absorption variable. *Nouv. Rev. d'Opt.* **4**, 307–314.

DOLLFUS, A., BOYER, C., CAMICHEL, H., AURIERE, M., BOWELL, E., AND NIKANDER, J. (1975). Photometry of Venus I: Observations of the brightness distribution over the disk. *Icarus* **26**, 53–72.

FYMAT, A. L. (1972). Inverse multiple scattering theory: Minimization search method of solution with application to the Venus atmosphere. Presented at the International Radiation Symposium of IAMAP. Sendaï Japan, 26 May–2 June 1972.

GUILLEMOT, J. C. (1967). Contribution à l'étude du transfert de rayonnement dans les nauges, par la méthode des harmoniques sphériques. *Rev. d'Opt.* **6**, 281–308.

HANSEN, J. E. (1969). Exact and approximate solutions for multiple scattering by cloudy and hazy planetary atmospheres. *J. Atm. Sci.* **26**, 478–487.

HANSEN, J. E. AND ARKING, A. (1971). Clouds of Venus: Evidence for their nature. *Science* **171**, 669–672.

HANSEN, J. E., AND HOVENIER, J. W. (1974). Interpretation of the polarization of Venus. *J. Atm. Sci.* **31**, 1137–1160.

IRVINE, W. M., (1968). Monochromatic phase curves and albedos for Venus. *J. Atm. Sci.* **25**, 610–616.

POTTER, J. (1970). The delta function approximation in radiative transfer theory. *J. Atm. Sci.* **27**, 943–949.

SOBOLEV, V. V. (1963). *A Treatise on Radiative Transfer*, pp. 283–288 D. van Nostrand, Princeton.

UESUGI, A. AND IRVINE, W. M. (1969). Computation of synthetic spectra for a semi-infinite atmosphere. *J. Atm. Sci.* **26**, 973–978.

WANG, L. (1972). Anisotropic nonconservative scattering in a semi-infinite medium. *Astrophys. J.* **174**, 671–678.

Reprinted from JOURNAL OF ATMOSPHERIC SCIENCES, Vol. 32, No. 6, June 1975, pp. 1177–1189
American Meteorological Society
Printed in U. S. A.

Article N° 3

Interpretation of the Photometric Measurements of Venus by Mariner 10[1]

C. DEVAUX, M. HERMAN AND J. LENOBLE

Laboratoire D'Optique Atmospherique, Université des Sciences et Techniques de Lille, Villeneuve D'Ascq, France

(Manuscript received 4 December 1974, in revised form 12 March 1975)

ABSTRACT

Observations by the television system on Mariner 10 of solar radiation reflected by Venus are analyzed by means of comparisons with theoretical computations. It is found that the distribution of radiance across the planetary disc in blue and orange light cannot be explained by a single homogeneous cloud consistent with polarization measurements.

Preliminary work has been done for analysis of the Mariner 10 data with a two-cloud model. It is anticipated that the data will allow the extraction of some knowledge of the variations of the optical thickness of the upper cloud, and of the relectivities of both layers.

1. Introduction

The purpose of this work is to deduce information on the structure of the Venus clouds from the radiance of the solar radiation scattered backward by the planet and observed at various points on the planetary disc by Mariner 10 (Devaux *et al.*, 1974).

This radiance depends on many parameters: the shape, size and refractive index of the particles; the albedo for single scattering; the optical thickness and vertical structure of the cloud; and possibly the ground reflection.

Most of our present knowledge of the Venus clouds has been deduced from polarization measurements, which are the most sensitive to the optical parameters of the particles (Hansen and Arking, 1971; Hansen and Hovenier, 1974). But the polarized light gives only information on the very upper part of the cloud, and we may expect radiance measurements to allow a deeper sounding of the cloud.

Assuming a first reasonable (according to our present knowledge) model of the Venus atmosphere, we will compute, by numerical resolution of the equation of transfer, theoretical values of the radiance to be compared to the experimental ones. Then we will modify the model until the best agreement is obtained. Such a method has been applied successfully to the ground-based measurements of the relative distribution of radiance over the Venus disc obtained by Dollfus *et al.* (in press); this work (Bigourd *et al.*, 1973; 1975) has shown that the radiance is more sensitive to the variation of the parameters near the limb than in the central part of the disc, but near the limb it is difficult to obtain good results with the limited resolution of the ground-based measurements.

The good quality and high resolution of the Mariner 10 pictures should allow a much more detailed and accurate interpretation, even considering the fact that they correspond to a small phase angle range and to only three wavelength intervals. Moreover, the radiances of Mariner 10 are given in absolute energies (W cm^{-2} sr^{-1}) and, knowing the incident solar flux, it will be possible to get comparisons on an absolute scale, which may constitute a useful check on the detector standardization.

2. Model of the Venus atmosphere

a. Basic model

We have chosen the simplest model of the Venus atmosphere which agrees with our present knowledge, that is, a homogeneous cloud layer between 70 and 32 km, above a pure scattering layer. This model has been shown to be compatible with the Venera 8 measurements of the downward flux (Devaux and Herman, 1975).

The scattering particles are assumed to have the characteristics deduced from the polarization measure-

[1] Presented at the Conference on the Atmosphere of Venus, Goddard Institute for Space Studies, 15–17 October 1974.

TABLE 1. Venus cloud characteristics.

λ (μm)	ω_0	τ_1	τ_R (inside cloud)	τ_R (above cloud)
0.36	0.9812	133	7.7	0.042
0.46	0.9967	132.9	2.9	0.015
0.58	0.9996	133.5	1.0	0.006

ments by Hansen and Hovenier (1974):

refractive index $m=1.44$

mode radius $r_m=0.83\ \mu$m

effective radius $r_e=1.1\ \mu$m

size distribution $n(r)=n_0 r^{12}\exp(-12r/r_m)$.

We will use for the optical thickness τ_1 and the albedo for single scattering ω_0 at the wavelength $\lambda=0.7$ μm the values deduced for a homogeneous cloud from the Venera 8 measurements (Devaux and Herman, 1975):

$$\tau_1^{0.7}=135,\quad \omega_0^{0.7}=0.9998.$$

The albedo for single scattering which has been found to be nearly independent of τ_1, if τ_1 is large enough, can be deduced for all wavelengths from the measurements of the spherical albedo A of the planet performed by Irvine (1968).

The scattering cross section K_λ and the phase function $p_\lambda(0)$ are computed for the chosen model of the particles and for the necessary wavelengths from Mie theory. The optical thickness for other wavelengths is deduced from $\tau_1^{0.7}$ by

$$\tau_1^\lambda=\tau_1^{0.7}\frac{\omega_0^{0.7}}{\omega_0^\lambda}\frac{K_\lambda}{K_{0.7}},$$

which simply expresses the fact that the number of scattering particles is the same for all wavelengths.

The values of τ_1 and ω_0 are given in Table 1 for the effective wavelengths of the three filters used on Mariner 10; the Rayleigh optical thickness τ_R above the cloud and inside the cloud (for the whole layer 32–70 km) has also been given.

It may be seen that the optical thickness of the cloud is large enough to completely neglect Rayleigh scattering at least in the orange and the blue. In the ultraviolet it may appear necessary to take it into account for refined comparisons.

Moreover, the outgoing radiation is the same as for a semi-infinite layer, which solves the problem of choosing a boundary condition at ground level and reduces the computation time.

The polarization measurements are very accurate and the possible small deviations from the accepted values would have a negligible effect on the radiance computations. But the spherical albedo values are given by Irvine (1968) with an imprecision of about 10% and we may have to vary ω_0 in the corresponding range to compare the theoretical results with the measurements.

b. Two-layer model

As mentioned above the particles deduced from the polarization measurements correspond to the upper layer of the cloud and we may assume a thin layer of such particles above a cloud with different particles, that is, with a different phase function.

In addition, the absorption may be different in the two layers; in this case we have a constraint which is the known value of the spherical albedo and we have to adjust the albedos for single scattering of both layers and the optical thickness of the upper layer to keep the exact value of the spherical albedo.

We have tried such models with two homogeneous layers; the results will be discussed in Section 4.

3. Method of computation

Fig. 1 shows the geometry of the problem: O is the center of the planet, T the sub-spacecraft point projected at the center of the planetary disc, S the subsolar point, and V the phase angle. Let ψ and ξ be the latitude and the longitude of the point of observation M, which in projection on the disc is defined by the rectangular coordinates (x,y). The directions of incidence and reflection at point M are respectively characterized by the azimuths θ, ϕ, and by $\mu_0=\cos\theta_0$ and $\mu=\cos\theta$, where θ_0 and θ are the angles with OM of the Venus-Sun OS and Venus-spacecraft OT directions ($\theta_0>0$).

The diameter defined by ST will be called the optical equator [in this paper] and the perpendicular axis PP′, the optical line of poles. They correspond to the sym-

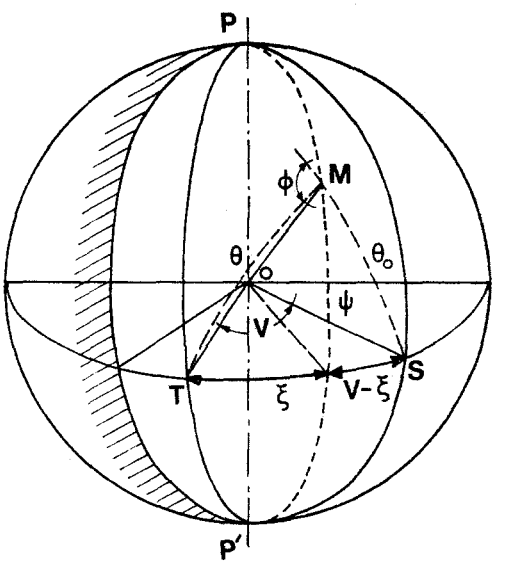

FIG. 1. Geometry of the problem.

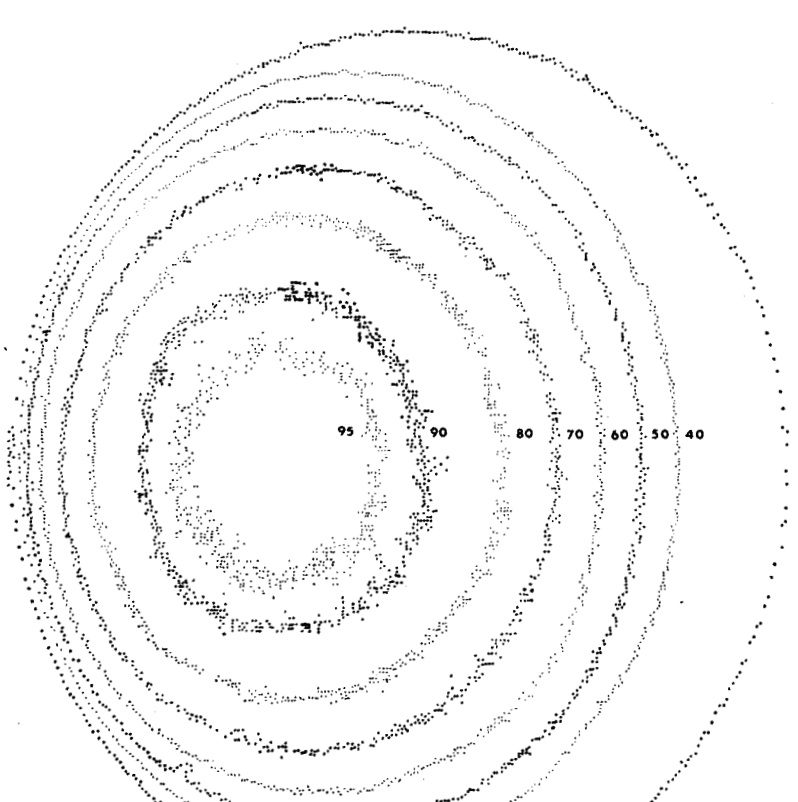

FIG. 2. Isophots of Venus deduced from measurements with the orange filter (F.D.S. No. 72-246).

metry of the optical problem for a homogeneous atmosphere, but they may differ from the real equator and line of poles of the planet.

The radiance $I(\tau;\mu,\phi)$ at an optical depth τ and in the direction (μ,ϕ) is given by the equation of transfer

$$\mu\frac{\partial I(\tau;\mu,\phi)}{\partial\tau}=I(\tau;\mu,\phi)-\frac{\omega_0(\tau)}{4}p(\tau;\mu,\phi,\mu_0,0)Fe^{-\tau/\mu_0}$$

$$-\frac{\omega_0(\tau)}{4\pi}\int_0^{2\pi}\int_{-1}^{+1}p(\tau;\mu,\phi,\mu',\phi')I(\tau;\mu',\phi')d\mu'd\phi', \quad (1)$$

with

$$I(0;\mu<0,\phi)=0,$$

plus boundary condition at ground level. (2)

In the two-layer model we have another condition—the continuity at the boundary level between the layers. The incident solar flux per unit area on a plane perpendicular to the sun beam direction $(\mu_0,0)$ is πF.

The equation of transfer is solved by the method of spherical harmonics (Guillemot, 1967; Deuze *et al.*, 1973) which gives the solution in the form

$$I(\tau;\mu,\phi)=\sum_{s=0}^{L}\cos s\phi\sum_{i=s}^{L}P_s^i(\mu)A_s^i(\tau). \quad (3)$$

The computations are made for $\mu_0=0.01$, 0.05 step 0.05 to 0.7, step 0.025 to 0.975, and step 0.005 to 0.990 and 0.999. So that, even for small phase angles, there are sufficient points to obtain an accurate distribution of the scattered light over the disc. For a given ellipse $\mu_0=\cos\psi\cos(\xi-V)=$constant, projected upon the apparent Venus disc, $I(0,\mu\phi)$ may easily be computed for as many points as necessary by (3), with

$$\left.\begin{aligned}\mu&=\cos\psi\cos\xi\\ \cos\phi&=(\mu\mu_0-\cos V)/[(1-\mu^2)(1-\mu_0^2)]^{\frac{1}{2}}\end{aligned}\right\}. \quad (4)$$

The computations have been made for an effective wavelength which has been chosen at 0.36, 0.46 and 0.58 μm, respectively, for the three filters.

It may appear necessary in refined studies to make computations for a series of wavelengths for each filter

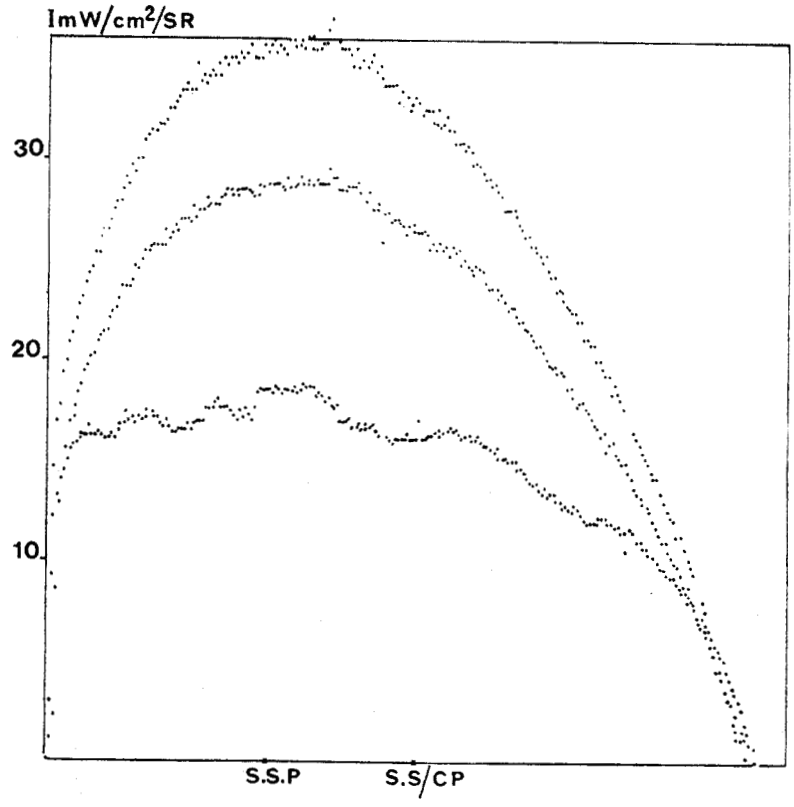

FIG. 3. Experimental equatorial radiance distributions in orange (upper curve), blue (middle curve) and UV (lower curve): S.S.P., subsolar point; S.S./C.P., subspacecraft point.

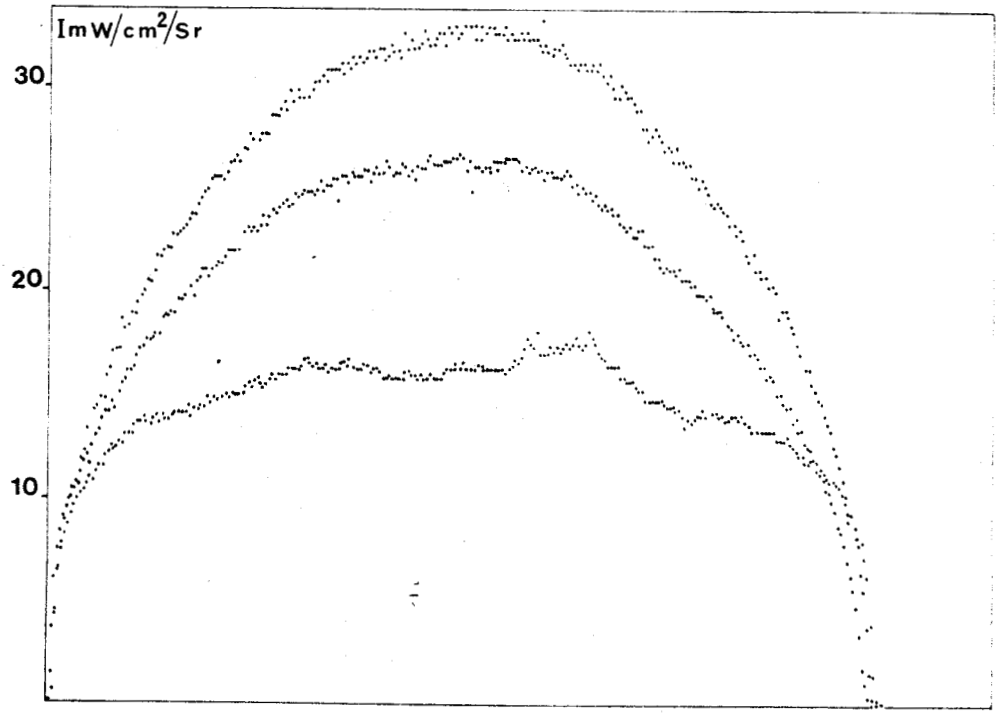

FIG. 4. As in Fig. 3, except for the pole-to-pole line.

and then to integrate over the bandwidth of the filter; the corresponding correction, which is expected to be small, will be evaluated in a future study.

The incident solar flux has been given its integrated value from 0.2 to 0.7 μm, i.e.,

$$\pi F = \int_{0.2}^{0.7} E_\lambda d\lambda,$$

where E_λ is the solar spectral irradiance (W cm^{-2} μm^{-1}) at the mean distance Sun-Venus. This rather arbitrary choice has been made in order to render our results comparable to the experimental results on an absolute scale.

4. Results

a. *Experimental results*

The pictures of Mariner 10 we have worked on are as follows:

Type of photograph*	No.	Filter	Day	Time (GMT)	Spacecraft to Venus distance (km)
FDS	72 230	Blue	043	17/25/20	5 011 865
FDS	72 246	Orange	043	17/36/32	5 017 589
FDS	72 266	UV	043	17/50/32	5 024 854

* The television system resolution is 4.5 arcsec (=2.2 TV lines).

The phase angle for these three pictures is 23.35° and its variation across the disc is negligible (<0.05°).

When multiplied by a given factor the printed numbers on the photographs give the radiance (W cm^{-2} sr^{-1}) normalized to the integrated solar radiance from 0.2 to 0.7 μm.

The results to be presented have not been corrected for distortion, nor for the aspect ratio.

The optical distortions are small in the orange picture, as can be seen from the regular spacing of the grid points on the Venus disc shown on Fig. 2, an isophot map for this color. On the blue and the ultraviolet pictures, Venus is located in the upper right corner, and there are big aberrations. So we have only investigated, for a first analysis, the radiance distributions along the optical equator and the pole-to-pole line. These two cross sections are given in Figs. 3 and 4, respectively, for the three color filters. On all figures S.S.P. is the subsolar point and S.S./C.P. the sub-spacecraft point. A horizontally homogeneous model is certainly not sufficient to explain the irregularities, which appear even in the orange picture; in ultraviolet the dark and clear areas must evidently be due to horizontal inhomogeneities. This is more obvious in Fig. 5, where the radiance distributions for the three colors have been drawn along the line going from the sub-spacecraft point to the two optical poles of Venus. Asymmetries

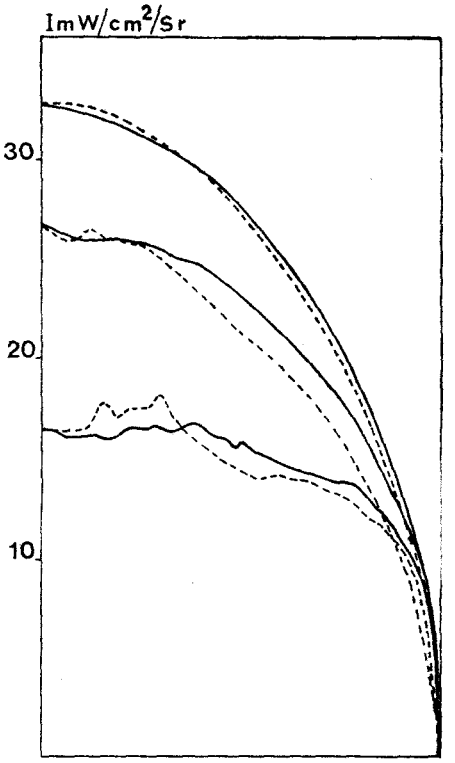

FIG. 5. Experimental radiance distributions along the sub-spacecraft point to north pole line (solid) and the sub-spacecraft point to south pole line (dashed) for orange (upper curve), blue (middle curve) and UV (lower curve).

between the two hemispheres appear clearly, and a correlation between the three colors seems to exist, although correcting for the optical distortion may change quantitatively the results for blue and ultraviolet light. Nevertheless, except for such small local anomalies, the global radiance pattern is regular for orange and blue light (see Figs. 2, 3 and 4), and we can hope that a homogeneous model will fit these results, to a first approximation.

b. *Basic model*

The theoretical radiance distributions have been computed for the basic model given in Section 2a, with a single scattering albedo ω_0 deduced from the spherical albedo of Venus, as given in Table 1. Since the Mariner 10 data are absolute radiances, the comparisons have been made on absolute scales. Figs. 6–11 give these comparisons, along the pole-to-pole line and the equator, for the three effective wavelengths considered. Qualitatively, the results are coherent; in particular, the global flattening of the curves, with decreasing wavelength, is retrieved. But there remain large discrepancies between the experimental and theoretical curves. These discrepancies are certainly partly due to the inaccuracies in the spherical albedo and in the Mariner 10 calibra-

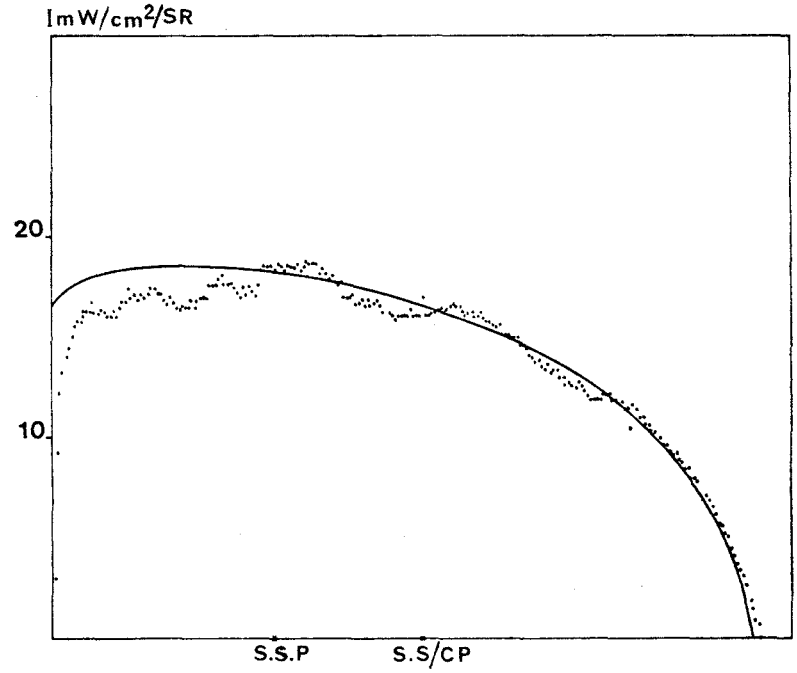

FIG. 6. Equatorial radiance distribution for UV: Mariner 10 results (dots) and theoretical results for a homogeneous model (solid curve). Absolute scales.

tion, and a more refined analysis will be made, taking these errors into account. Nevertheless, neither a different assumed ω_0, nor a modification of the calibration factor could give good agreement especially near the limb and the poles of the planet. As an example, for the orange wavelength for which the homogeneity is the best, the theoretical results have been computed for three assumed values of the spherical albedo A in the range of its acceptable values: 0.92, 0.8 and 0.843; that is, $\omega_0=0.9996$, 0.9972 and 0.9984, respectively. For $A=0.843$, the disagreement near the limb is particularly clear. Fig. 12 gives a magnified picture of this zone.[2] The same qualitative features are obtained for blue and ultraviolet wavelengths.

[2] Data which are corrected from aberrations are available to us since this first study and the same features are obtained.

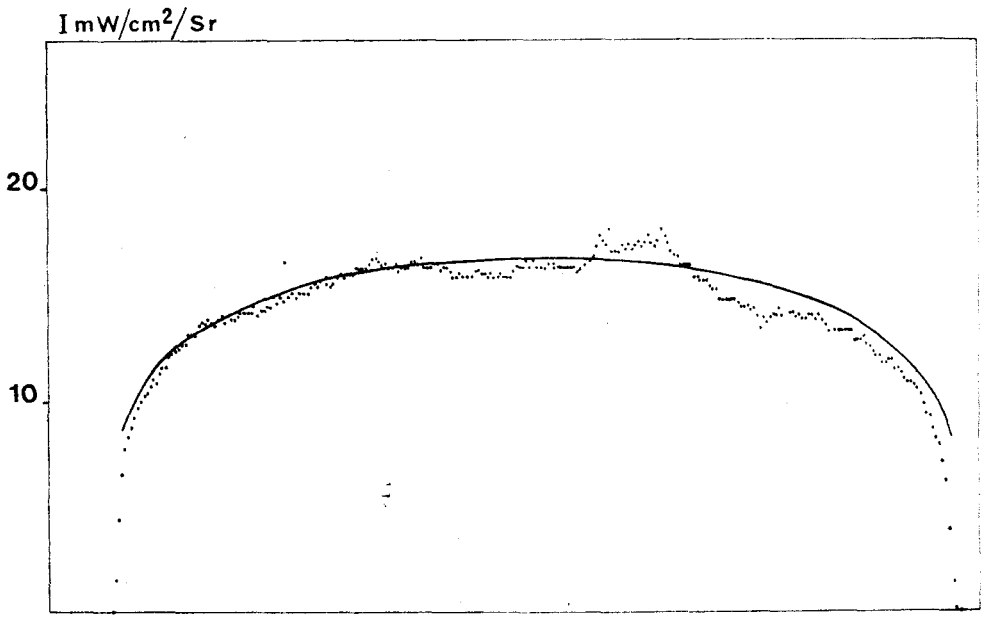

FIG. 7. As in Fig. 6 except for the pole-to-pole line.

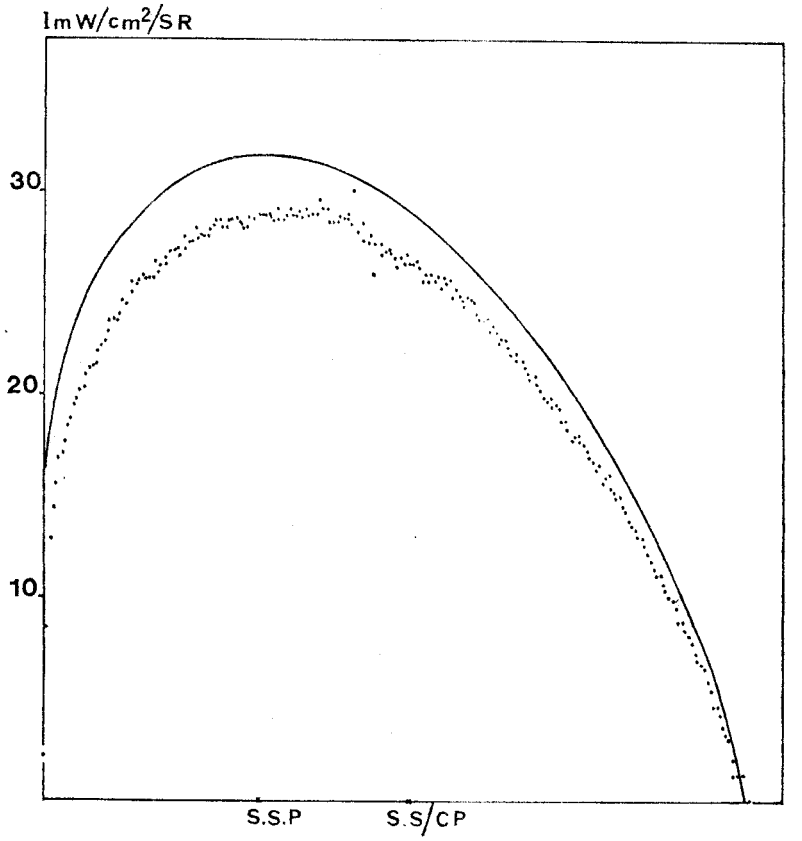

FIG. 8. As in Fig. 6 except for blue.

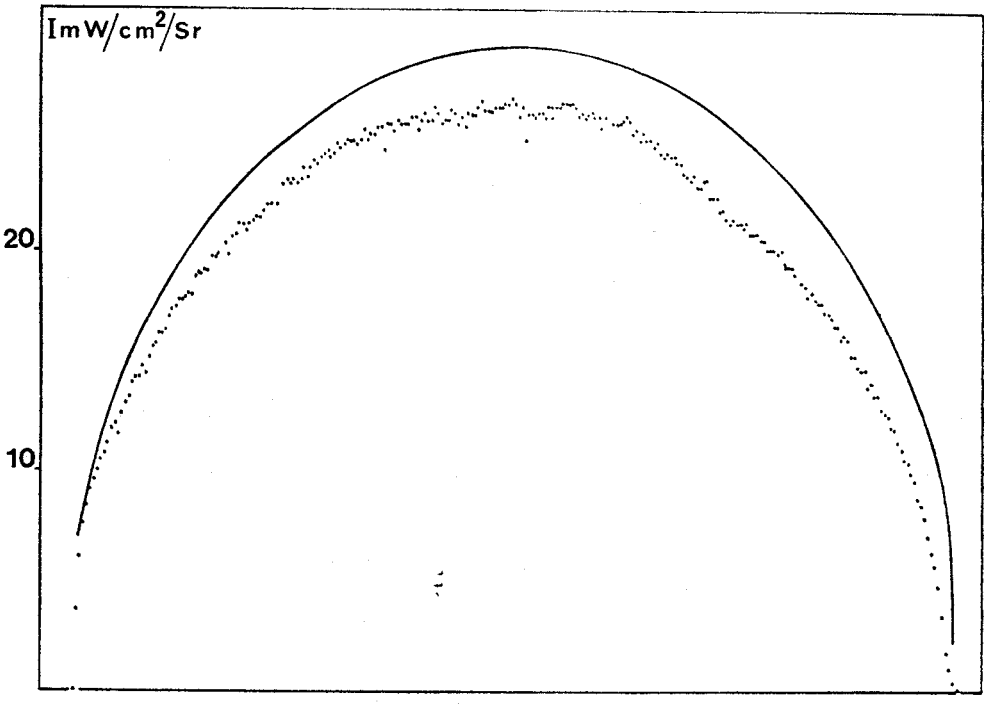

FIG. 9. As in Fig. 7 except for blue.

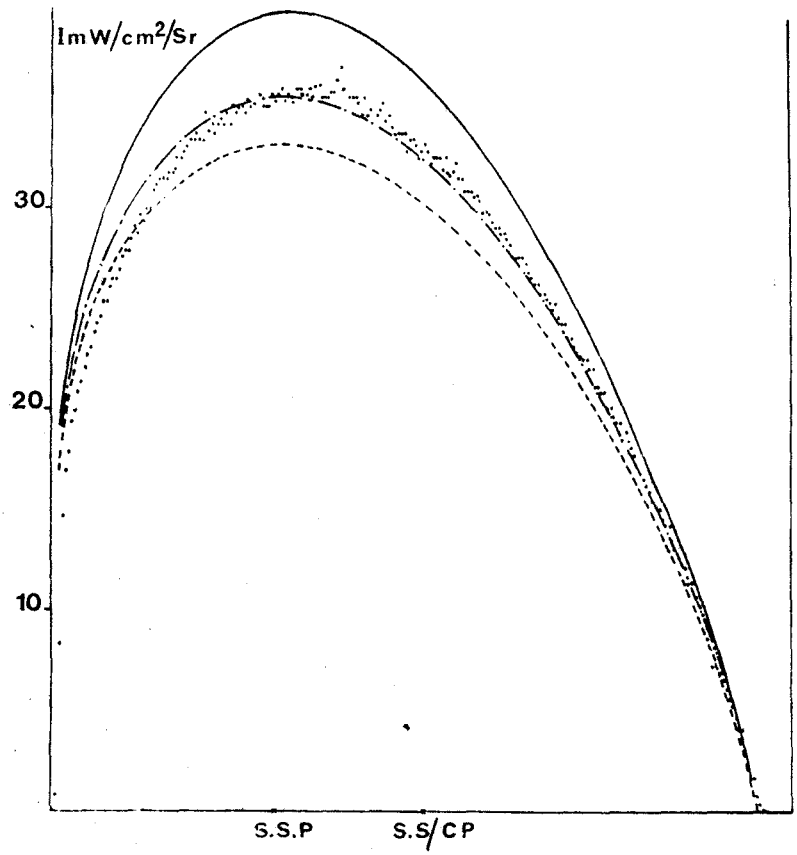

FIG. 10. Equatorial radiance distribution for orange. Mariner 10 results (dots) and theoretical results for a homogeneous model: $A=0.92$ (solid), $A=0.843$ (dot-dashed), $A=0.8$ (dashed).

It may be thought that this feature is meaningless, and is only due to the necessity of using spherical geometry for the points near the limb. However we see (Fig. 12), that the disagreement between the experimental and the theoretical results appears for points where incidence and emergence are far from grazing ($\theta \approx 37$; $\theta_0 \approx 13°$), and it seems doubtful that sphericity effects could appear for such conditions. More precisely, for the assumed model and for normal incidence and emergence, the mean optical path of an emerging photon is of the order of 100 (Fouquart, 1973); with oblique emergence and incidence such a value is certainly an upper limit. For the Venus clouds, the currently assumed photon mean free path is of the order of 1 km so that we cannot obtain at a point M light corresponding to point of incidence farther than 100 km from M, and the corresponding variations of μ and μ_0 when taking into account the sphericity are absolutely negligible.

In conclusion, although the need for spherical geometry may deserve a special study, it seems very unlikely that even the gross features observed in orange and blue light can be explained by a homogeneous model consistent with the polarization measurements.

c. Two-cloud models

The preceding results lead us to investigate two-cloud models, even for visible light. With the multiplicity of the parameters, we shall probably be able to work out a model to fit any results we want, and here the first problem is rather to put forward the possibilities of the analysis, rather than to try to obtain a definitive solution. We have to keep, for the upper cloud, the basic model (Section 2a) deduced from the polarization measurements, and to keep for the lower cloud a large optical thickness ($\tau_1 \to \infty$). We then have, at each point, four unknowns: the optical depth τ_1 of the upper cloud, the single scattering albedos ω_0 and ω_0' for the two clouds, and the phase function $p'(\theta)$ for the lower cloud.

This last parameter is the worst. Various kinds of particles have been proposed for Venus, but we have no idea of the size distributions nor of the shape of these particles. Fortunately, it seems possible to evade this question for our purpose. Let us assume that the two clouds have nearly equal reflectivities. Then, with a two-layer model, the upper cloud will receive at its lower boundary the same flux as in the homogeneous

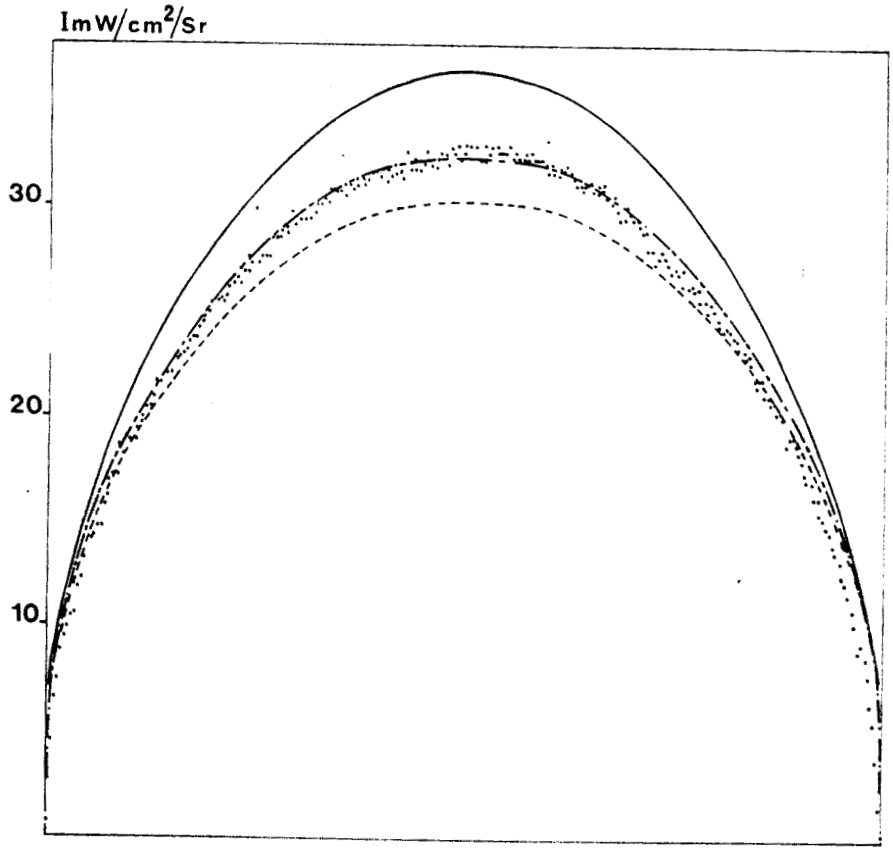

FIG. 11. As in Fig. 10 except for the pole-to-pole line.

case; only the spatial distribution of this upgoing radiation will be modified, due to substituting $p'(\theta)$ for $p(\theta)$ in the lower layer. Then we shall get the upper limit of the possible modification in the observed radiance distribution, due to $p'(\theta)$, by computing these distributions, again for homogeneous models, but for

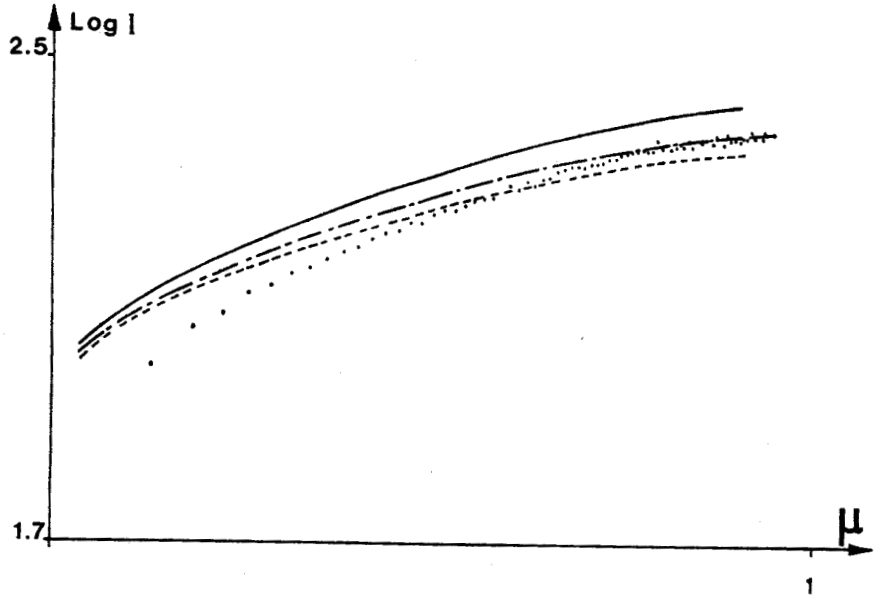

FIG. 12. Magnified view of the discrepancies near the limb, for orange. Same notation as in Fig. 10.

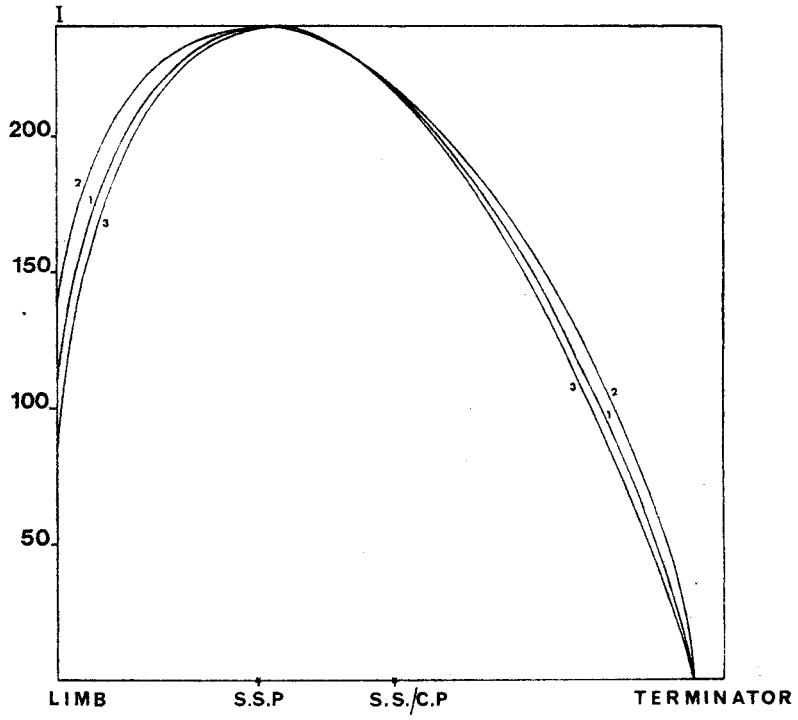

FIG. 13. Theoretical equatorial radiance distributions, for orange, with homogeneous models (arbitrary units).

Curve (1): basic model ($\bar{r}=0.85\ \mu$m; $m=1.44$)
Curve (2): Rayleigh scattering
Curve (3): terrestrial cloud ($\bar{r}=4\ \mu$m; $m=1.33$).

scattering laws other than the one given in Section 2a; this means that we assume the upper layer to be negligibly thin. Fig. 13 shows such results, along the optical equator, for $\lambda=0.58\ \mu$m. Two extreme cases are compared with the preceding basic model (curve 1): Rayleigh scattering (curve 2) and scattering by a terrestrial cumulus cloud ($\bar{r}=4\ \mu$m; $m=1.33$) (curve 3). These results could *a priori* suggest an explanation for the observed discrepancies near the limb; we could assume that in this part of the Venus disc the mean

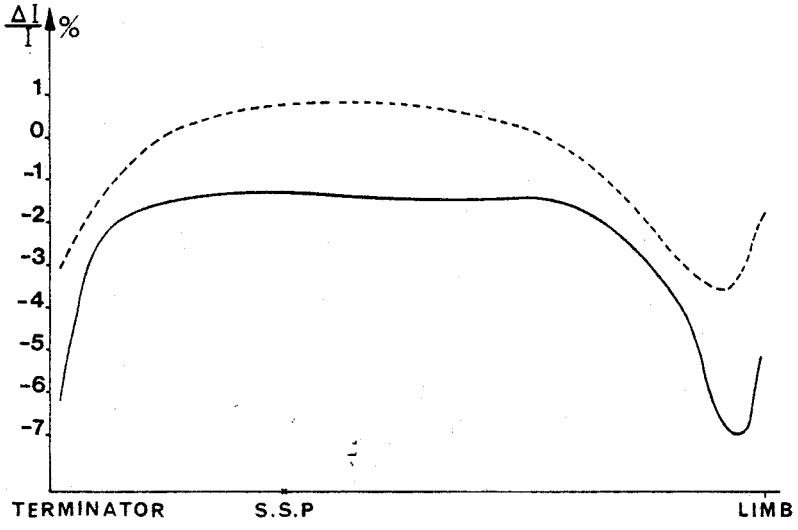

FIG. 14. Equatorial radiance distributions for blue showing the relative discrepancies between the basic model and a two-layer one. Upper layer: $\omega_0=0.9967$, $\tau_1=0.5$ (solid), $\tau_1=1$ (dashed); lower layer: isotropic upward radiance, $\rho=0.77$.

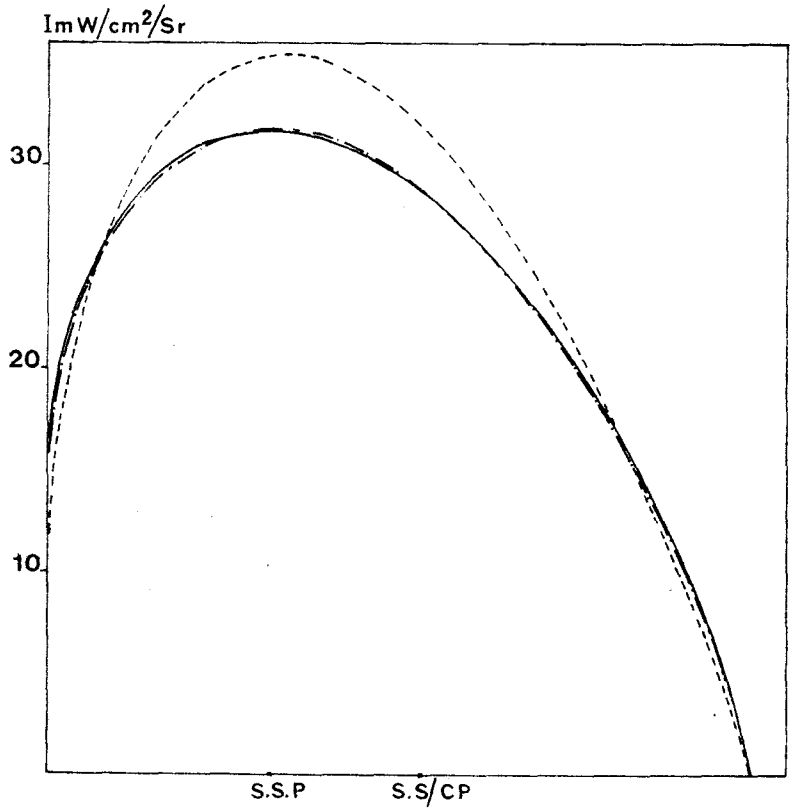

FIG. 15. Equatorial radiance distributions for blue. Theoretical results for a homogeneous model (solid), for an upper conservative layer ($\tau_1=1$, $\omega_0=1$) above an absorbing lower layer ($\rho=0.76$) (dot-dashed), and for an upper absorbing layer ($\tau_1=1$, $\omega_0=0.9322$) above a perfectly reflecting lower layer ($\rho=1$) (dashed).

optical depth of the upper cloud becomes smaller and smaller above a lower cloud with bigger scattering particles, but with a nearly equal reflectivity. Nevertheless, this explanation seems doubtful, because the small discrepancies which are observed (Fig. 13) will probably be eliminated when we superpose above the lower cloud, the thin but not negligible layer of the basic model, which is necessary to explain the observed polarized light. Actually we do not know the minimum optical thickness this upper cloud must have, but $\tau_1 \approx 1$ seems a plausible order of magnitude. We have compared (Fig. 14) the radiance distributions along the equator, obtained with an upper cloud of uniform optical thickness $\tau=0.5$ and 1, above a lower cloud of the same reflectivity integrated on a hemisphere, but giving an isotropic upgoing radiance according to a Lambert law. Even for such an extreme modification of the upward radiation received at the bottom of the upper cloud, for $\tau_1=1$ the results of the basic model are practically retrieved within 1%.

Therefore, the scattering function $p'(\theta)$ of the lower layer is not at all important for a first analysis, for our purpose and we may merely substitute for this lower cloud a fictitious medium which gives an isotropic upward radiance, and which has the reflectivity $\rho(\lambda)$ of the real lower cloud. The validity of such a simplification will have to be verified *a posteriori*, and a more refined study will be necessary if the obtained values for τ_1 are too small in some parts of the Venus disc.

We have seen that the radiance distribution corresponding to a homogeneous model will, in the case of a two-layer model, be modified chiefly because of the difference in the reflectivities of the two clouds. The very accurate measurements made by Mariner 10 have shown that the blue and orange wavelengths are already sensitive to these differences. In principle, it then seems possible to extract, from these absolute data, an approximate value for the optical thickness $\tau_1(M)$, the single scattering albedo $\omega_0(\lambda)$ of the upper cloud, and the reflectivity $\rho(\lambda)$ of the lower one, for the three effective wavelengths and for different points M on the Venus disc. [If a scattering model is assumed for the lower cloud, its single scattering albedo $\omega_0'(\lambda)$ will be deduced from $\rho(\lambda)$. Indeed, if we can get n observed points M with different values for $\tau_1(M)$, we shall get $3n$ equations with $n+6$ unknowns since $\tau_1(M)$ is nearly independent of the wavelength]. Whether such a system will prove to be well conditioned and to have a solution is quite another matter, for until now we have only investigated the general features of the problem. For

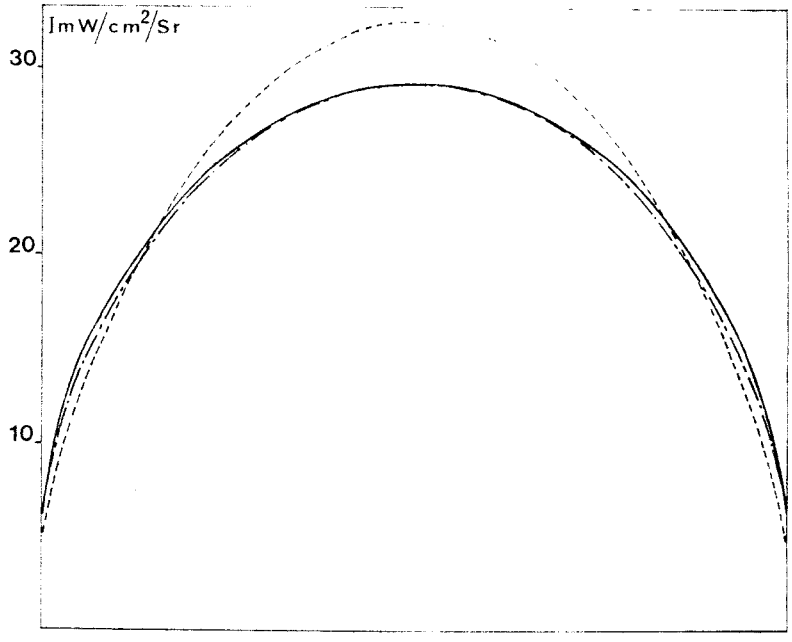

FIG. 16. As in Fig. 15 except for the pole-to-pole line.

the blue light ($\lambda=0.46\,\mu$m), we have computed the theoretical radiance distributions, assuming a uniform optical thickness $\tau_1=1$ for the upper cloud. Two extreme cases have been considered: (i) $\omega_0=1$, $\rho=0.76$ and (ii) $\omega_0=0.9322$, $\rho=1$; that is, respectively, a perfectly conservative upper layer or a lower one, the reflectivity or the single scattering albedo of the other layer being adjusted to restore the measured spherical albedo A. The results are compared in Figs. 15 and 16 to those obtained with the homogeneous model. For the case of an upper conservative cloud [a plausible hypothesis, if it is assumed that H_2SO_4 is its mean constituent (Hansen and Hovenier, 1974; Young, 1973)], the relative radiance is nearly the same as for the basic model. For this small phase angle the outgoing light comes mostly from the lower cloud, the reflectivity of which is not greatly modified by the presence of an upper cloud, because of the constraint of A. With the contrary hypothesis [case (ii)], the modifications are important. The global magnification of the reflected flux comes from the large increase of the mean cloud reflectivity ($\rho=1$). We may notice that such an effect could correspond to the feature of the Venus phase curve, as measured by Knuckles *et al.*, which seems difficult to fit with a homogeneous model (Arking and Potter, 1968). In addition, for case (ii), the variations of the radiance distribution could explain quantitatively the observed experimental disagreement. Nevertheless, the high values obtained for the radiance could be incompatible with the tolerable inaccuracy in the Mariner 10 calibration factors and in A.

5. Conclusion

The mean features observed in blue and orange light cannot be explained by a single homogeneous cloud, consistent with the polarization measurements.

For a first analysis of the Mariner 10 data with a two-cloud model, it seems possible to escape the difficult problem of chosing a scattering model for the lower cloud. Then we can hope to extract from these data some knowledge of the variations of the optical thickness of the upper cloud, and of the respective reflectivities of the two layers. Such an analysis will be undertaken. A previous knowledge of the aberration defects and of the tolerable errors in the calibration factors will be necessary if we are to make such a study.

Acknowledgments. It is a pleasure to acknowledge the kind support of the Mariner 10 Team, of the Jet Propulsion Laboratory, and especially of Dr. E. Danielson, who made the data analyzed here available to us.

REFERENCES

Arking, A., and J. Potter, 1968: The phase curve of Venus and the nature of its clouds *J. Atmos. Sci.*, **25**, 617–628.

Bigourd, C., J. L. Deuze, C. Devaux, M. Herman and J. Lenoble, 1973: Interprétation théorique de la répartition de luminance sur le disque de Venus. Presented at Copernicus Symposium on the Exploration of the Planetary System, Torun.

——, C. Devaux, M. Herman and J. Lenoble, 1975: Photometry of Venus II. Theoretical brightness distribution over the disc. *Icarus* (in press).

Deuze, J. L., C. Devaux and M. Herman, 1973: Utilisation de la méthode des harmoniques sphériques dans les calculs de transfert radiatif. Extension au cas des couches diffusantes d'absorption variable. *Nouv. Rev. d'Opt.*, 4, 307–314.

Devaux, C., M. Herman and J. Lenoble, 1974: Mariner 10 mission. Interpretation of the photometric measurements of Venus. Progress Report No. 1, Lab. Opt. Atmos.

——, and ——, 1975: Venus: Cloud optical depth and surface albedo from Venera 8. *Icarus*, 24, 19–27.

Dollfus, A., C. Boyer, H. Camichel, M. Auriere, E. Bowell and J. Nikander, 1975: Photometry of Venus: I Observations of the brightness distribution over the disc. *Icarus* (in press).

Fouquart, Y., 1973: Profondeur de pénétration et formation des raies dans une atmosphère diffusante. Presented at Copernicus Symposium on the Exploration of the Planetary System, Torun.

Guillemot, J. C., 1967: Contribution à l'étude du transfert de rayonnement dans les nuages par la méthode des harmoniques sphériques. *Rev. d'Opt.*, 6, 281–308.

Hansen, J. E., and A. Arking, 1971: Clouds of Venus: Evidence for their nature. *Science*, 171, 669–672.

——, and J. W. Hovenier, 1974: Interpretation of the polarization of Venus. *J. Atmos. Sci.*, 31, 1137–1160.

Irvine, W. M., 1968: Monochromatic phase curves and albedos for Venus. *J. Atmos. Sci.*, 25, 610–616.

Knuckles, C. F., M. F. Sinton and W. M. Sinton, 1961: UBV photometry of Venus. *Lowell Obs. Bull.*, No. 115, 4 pp.

Young, A. T., 1973: Are the clouds of Venus sulfuric acid? *Icarus*, 18, 564–582.

Article N°4. Submitted to ICARUS (May 1977).

TITLE:

PHOTOMETRY OF VENUS III : Interpretation of Brightness Distributions over the Disk.

by: M.Herman, C.Devaux and A.Dollfus

M.Herman and C.Devaux: Laboratoire d'Optique Atmosphérique.
Université des Sciences et Techniques de LilleI
B.P. 36 59650 Villeneuve d'Ascq France.

A.Dollfus : Laboratoire de Physique du Système Solaire
Observatoire de Paris-Meudon Section Astrophysique
92 190 Meudon. France.

Number of manuscript pages: 24
Number of figures : 26
Number of tables : 2

PROPOSED RUNNING HEAD

Analysis of Isophote Maps of Venus

Proofs should be directed to:

Maurice Herman

Laboratoire d'Optique Atmosphérique

Batiment P.5.

Université de Lille I

B.P. 36

59 650 Villeneuve d'Ascq France.

ABSTRACT

A series of solar brightness distributions observed over the Venus disk at several wavelengths is analysed. A single absorption mechanism is assumed, the main localization of which is varied within the clouds, in different models. An attempt is made to retrieve the whole of the observations from one or more of the models. Models in which the absorption is highly localized give a better fit with the ultra-violet observations, although better measurements are awaited for, before a definite conclusion may be drawn. Isophote maps in visible light disagree with the theoretical predictions of all the models, suggesting that a second absorption mechanism (perhaps the ground) ought to be called for in this spectral region.

INTRODUCTION

The characteristics of the upper atmospheric aerosols of Venus are now precisely known (Hansen and Arking, 1971; Hansen and Hovenier, 1974). These aerosols are probably constituted of hydrated sulfuric acid (Sill, 1972; Young, 1973). However the way in which solar radiation is absorbed on Venus, and the precise atmospheric levels in which the solar energy is deposited are still unknown. This question is particularly relevant to the sulfuric acid hypothesis, as this constituent is transparent in the spectral interval which corresponds to the weakest Venusian reflectivity (0.3 - 0.5 μm.).

A detailed analysis of the light rediffused at different wavelengths might be informative with respect to this problem. Let us consider an absorption mechanism more or less localized in the cloudy layer and for which the efficiency varies with wavelength. Its relative influence upon the intensity rediffused by different points on the disk should vary according to the level of the layer in which the mechanism is localized.

It is for this purpose that the radiance repartitions observed on Venus, as presented by Dollfus et al., 1975 (Paper I), were compared to theoretical distributions calculated for different models, according to the procedure described by Brogniez et al., 1975 (Paper II).

The work essentially deals with a series of photographs taken nearly simultaneously at several wavelengths from 0.585 μm. to 0.327 μm., and showing the apparition of the classical ultraviolet dark markings. This analysis attemps to determine wether a single absorption mechanism can explain the whole of these observations, and wether it is possible to deduce a general localization of the level of the layer where the absorption takes place.

EXPERIMENTAL DATA

Figures 7a to 7f reproduce the isophote maps of Venus, from Paper I, which were observed 31 July 1969. Table I sums up the corresponding data; the photometric technique utilised was described in Paper I;

In figure 1, the most recent estimation of the spherical albedo of Venus (Travis, 1974) is compared to that which would be due only to molecular scattering, if the planet were totally devoid of aerosols and presented no ground reflectivity. Shortwards of about 0.45 μm., it is clear that nearly all absorption takes place in an absorbant located at quite high altitudes. At 0.52 μm., it is no longer certain that the ground plays no role, and it could constitute a second absorption mechanism. At 0.585 μm., all absorption could be attributed to the ground if the cloud cover were conservative; its average optical thickness would then be about 50.

In this first analysis however, in order to limit the free parameters as much as possible, and to conserve the significant character of the results, we will suppose that the influence of the ground is negligible at all wavelengths, and that all of the absorption is due to a single type of absorbant. Only the altitude of this absorbant will be adjustable. It is only if these hypothesis are unable to explain the observations that the variable influence of the ground or the coexistence of different absorbants will be called into consideration in more complicated models.

CLOUD MODELS

In order to localize the absorbant, our reference level will be the aerosol layer which the polarized light comes from. Its component particles are well known, and its average altitude is known to be about 70 km., at $\tau = 1$; thus the role of molecular scattering will be no greater than a few percent in the spectral interval investigated (Hansen and Hovenier, 1974).

We will consider three possible extreme absorption distributions relative to this scattering layer. Figure 2 schematically depicts these models.

In model I, we will suppose that all of the absorption is localized above the clouds; this means that a purely absorbant aerosol, for exemple, is situated at a minimum altitude of about 70 kilometers. It will be assumed that the optical thickness of

the conservative medium found under this absorber is great at all wavelengths.

The nature of the aerosols below 70 km. is entirely uncertain. But it has been shown (cf. PaperII) that light scattered by a stratified medium depends upon the phase function of the first scattering layer encountered (thus the one where the polarized light is formed), and hardly at all upon those of the lower cloud layers, which intervene only by their reflectivity ρ(thus $\rho = 1$, in the hypothesis of this model)

Thus, we here will have a purely absorbant layer with an optical thickness τ_a which is arbitrarily variable on the disk, and which overlies a thick, conservative,homogeneous cloud, having the characteristics of the reference layer probed by polarization. The radiance distribution depends only weakly upon the phase function, and the small Rayleigh component of this layer, and its phase function variations with wavelength will be disregarded; the invariant phase function of the scattering cloud will be that of spherical particles with refractive index and granulometry:

(1) $m = 1.44$; $n(r) = n_o\, r^{12} \exp(-12r/r_m)$; $r_m = 0.83$ µm.

(Hansen and Hovenier, 1974), calculated for the wavelength $\lambda = 0.585$ µm.

In model II, it will be assumed that all the absorption takes place in one or several lower cloud layers found under the conservative reference haze. The properties of these lower layers will be assumed to be constant over the whole planet, and they will be characterised by their reflectivity ρ_λ at a given wavelength. The only horizontal variant will be the optical thickness of the overlying haze. The phase function defined in (1) will be conserved for this haze. It hereagain seems justifiable to neglect molecular scattering. The conservative haze, in this model, can only have a fairly small average optical thickness $<\tau_1>$; In order that the spherical albedo decreases to 0.5 at about 0.3 µm., $<\tau_1>$ should be no greater than a maximum of 4. It therefore can be hoped that the characteristics of the top of the haze remain valid for such a small thickness, and that the molecular scattering for the whole layer not exceed a few percent. The optical thickness at a point will thus correspond only to aerosols and will hardly vary at all with wavelength.

In model III , the absorption will be distributed within the haze itself. The albedo for single scattering ω_o will thus be supposed independent of optical depth for a given point on the disk, and only horizontal variations of this parameter will be foreseen. For the same reasons given above, the scattering law (1) will be retained, and it will simply be supposed that the optical thickness of this cloud is infinite.

Plane geometry will be used: it will be admitted that the medium is stratified at all points, and that the horizontal variations of its parameters remain negligible for a photon mean free path. The calculations will be made with the spherical harmonics method.

ANALYTIC METHOD

One of the photographs from the observed series (figures 7a to 7f) will be chosen, which corresponds to wavelength λ_o. For any point M of the disk, $\tau_a(M,\lambda_o)$, or $\tau_l(M)$ for a defined ρ_{λ_o}, or $\omega_o(M,\lambda_o)$ will be adjusted in calculations, to reconstruct the radiance distribution observed at λ_o. Starting from these initial solutions, the radiance distributions which should be observed for other wavelengths of the series will then be computed for each of the three models.

The relative measurements of figures 7a to 7f are normalised to 100 for the maximum. As the radiance variations in function of adjustable parameters are not linear in any of the models, we must employ absolute radiances. This will be done through the use of the magnitude $m_\lambda(\alpha)$ of the planet.

In table II, column 2, are found the mean $m_\lambda(\alpha)$ values interpolated from the phase curves of Irvine (1968), for

the relevant wavelengths and phase angle. The reduced magnitudes given by Irvine can be written

$$(2) \qquad m_\lambda(\alpha) = m_\odot - 2.5 \log\left[\frac{\pi R^2}{2}(1+\cos\alpha)\right] - 2.5 \log\left[\frac{1}{S}\iint_S I(M,\lambda)\,dS\right]$$

where $m_\odot$ is the reduced visual solar magnitude, R the radius of Venus, S the apparent fraction of the disk, and $I(M,\lambda)$ the absolute radiance for a point M on the disk, normalised to a solar flux of unity. The values of the integral $\frac{1}{S}\iint_S I(M,\lambda)dS$, deduced from (2), are found in table II, column 3. The estimation used here for m_0 is that of Johnson (1965): $m_\odot = -26.75$.

It thus is the absolute radiance repartition $I(M,\lambda_o)$ which will be restored by the calculation, by adjusting the variable parameter of the model. In model II a given radiance can correspond to a whole interval of values of ρ_{λ_o}, which are associated with appropriate thicknesses $\tau_1(M)$. A family of solutions is obtained. For the moment, we will keep only the extreme distributions $\tau_1^{max}(M)$ and $\tau_1^{min}(M)$, which correspond respectively to the minimum $\rho_{\lambda_o}^{min}$ and maximum $\rho_{\lambda_o}^{max}$ reflectivity values which can simultaneously be suitable for all points on the disk.

If another wavelength is now considered, the absorption of the medium will vary, and for the varius models, the following simple transformations will occur:

(3) I : $\tau_a(M,\lambda_o) \rightarrow \tau_a(M,\lambda_1)$ where $\tau_a(M,\lambda_1) = A(\lambda_1).\tau_a(M,\lambda_o)$

(4) II : $\tau_1(M);\rho_{\lambda_o} \rightarrow \tau_1(M);\rho_{\lambda_1}$

(5) III : $\omega_o(M,\lambda_o) \rightarrow \omega_o(M,\lambda_1)$ where $\dfrac{\omega_o(M,\lambda_1)}{1-\omega_o(M,\lambda_1)} = B(\lambda_1)\dfrac{\omega_o(M,\lambda_o)}{1-\omega_o(M,\lambda_o)}$

The constants $A(\lambda_1)$, ρ_{λ_1} and $B(\lambda_1)$ are independent of the point considered. Eq. (3) simply conveys the fact that $\tau_a(M,\lambda)$ is in the form $f(\lambda).g(M)$, where $g(M)$ is proportional to the quantity of absorber in M, and where $f(\lambda)$ represents the spectral variation of the absorption coefficient. The transformation law (5) is more restrictive. It implies that, the absorption in model III is due to a purely absorbant constituant mixed with conservative particles of sulfuric acid. For these components, let b be the absorption coefficient and k the scattering coefficient. Since the variations of k with wavelength are neglected, and as the mixing ratio is supposed independent of altitude, we will have for a given point on the disk

$$\frac{1-\omega_o(M,\lambda)}{\omega_o(M,\lambda)} = \frac{b}{k} = f(\lambda).g(M),$$

where $f(\lambda)$ will here also represent the spectral variation of the absorption coefficient, and $g(M)$ will be proportional to the mixing ratio of the two components.

Relations (3), (4) and (5) thus permit calculations starting from the initial solutions $\tau_a(M,\lambda_o)$, $\tau_1(M)$ or $\omega_o(M,\lambda_o)$, which give the absolute radiance $I(M,\lambda_1)$ in function of a single adjustable parameter. $A(\lambda_1)$, ρ_{λ_1} or $B(\lambda_1)$ is then varied, so that when carried over to eq. (2), the resulting radiances $I(M,\lambda_1)$ give the observed magnitude $m_{\lambda_1}(\alpha)$. The isophote maps corresponding to this concurrence will be compared to the observations.

Before applying this method to the measurements, the following points should be noted:

a) Measurements of figures 7a to 7f are not deconvoluted from the effects due to the atmospheric turbulence and the apparatus. The blurring of the images limits the choice of the reference wavelength. The ideal would be to start from one extremity of the spectral interval explored, in order that the domain of variation in which the different models can be differentiated might be as large as possible. But in the present case, we take as λ_o the average wavelength 0.379 μm., in order to minimize the propagation of initial errors upon $I(M,\lambda_o)$.

b) In order to determine $\tau_a(M,\lambda_o)$, $\tau_1(M)$ or $\omega_o(M,\lambda_o)$ from $I(M,\lambda_o)$, the localization of a given point M (longitude and latitude) should be known with good precision. To superimpose the theoretical contour of the apparent disk of Venus upon the experimental maps, the two following criteria were selected.
(i) the theoretical terminator is placed as parallel as possible to the experimental isophote 20; the lowest radiance levels are

effectively those which are the least distorted by dissymmetries. (ii) the theoretical limb is placed on the experimental isophote 45 near the radiance maximum (or maximums); this choice results from a summary analysis of photographs deterioration (cf. Annex). These two criteria finally lead to a fairly precise positioning.

c)Radiances near the limb not being usable, calculations are limited to the central part of the disk, the useful radius being about 4/5 of the planet radius. At a given wavelength λ_1, the theoretical radiances $I(M,\lambda_1)$ must be adjusted in order to restore the planet magnitude. The integral which appears in eq. (2) can be evaluated only for the usable surface S' instead the entire surface S of the apparent disk. We will assume that the flux backscattered by S and S' evolve in approximately the same way with wavelength for all models, so that

$$\frac{\iint_S I(M,\lambda_1)\,dS}{\iint_{S'} I(M,\lambda_1)\,dS'} = \frac{\iint_S I(M,\lambda_o)\,dS}{\iint_{S'} I(M,\lambda_o)\,dS'}$$

Almost all error will thus be found to be concentrated in the evaluation of this term from the reference photograph. It is evaluated as being of about 5 percent. The limitation of the data to the usable surface S' should lead to only a systematic overestimation or underestimation of the magnitudes, the spectral variations of which should however be well respected.

RESULTS

The initial distributions $\tau_a(M,\lambda_o)$, $\tau_1(M)$ and $\omega_o(M,\lambda_o)$ obtained at 0.379 µm., are found in figures 3, 4 and 5 respectively. Figure 4 presents the $\tau_1(M)$ distribution corresponding to the average solution obtained; it appears that the extreme solutions τ_1^{max} and τ_1^{min} are very close, the optical thickness at the center of the disk varying only from about 2.5 to 3.5 . The thicknesses greater than τ_1^{max} imply an initial reflectivity $\rho_{\lambda_o}^{min}$ so weak that it would no longer be possible to find the decrease in magnitude when approching 0.3 µm. . Optical thicknesses of less than τ_1^{min}, entailing a reflectivity higher than $\rho_{\lambda_o}^{max}$, tend to give a radiance distribution which is too homogeneous, and it becomes impossible to restore the observed dissymmetries.

The great fragility of this model thus appears. It can be wondered whether, with deconvoluted photographs where radiance dissymetries would be more pronounced, or with observations corresponding to exceptionally inhomogeneous conditions (cf. Paper I), this model might be invalidated at this stage.

The obtention of high optical thicknesses at the terminator and poles seems to retroactively contradict certain hypothesis of this model; as it seems hasardous to extrapolate the characteristics of the top of the haze for such great optical thicknesses, a sizeable part of them could correspond to molecular scattering and depend upon wavelength. This point is of no importance; for such large values of $\tau_1(M)$, backscattered radiance

becomes fairly insensitive to variations of τ_1 and ρ_λ. Results obtained simply indicate that the terminator and poles regions, in model II, should be covered by a thick conservative layer, for which the precise τ_1 values obtained are only indicative.

The different models then can be extrapolated to the other wavelengths of the series. Table II gives the values of constants $A(\lambda)$, ρ_λ and $B(\lambda)$ needed for these extrapolations.

The calculation of different theoretical distributions $I(M,\lambda)$ shows first that models I and III lead to practically indistinguishable results in the useful part of the disk, in the whole spectral interval explored. For model II appreciable differences do not appear between the previsions deduced from the initial extreme solutions $(\tau_1^{max}, \rho_{\lambda_o}^{min})$ and $(\tau_1^{min}, \rho_{\lambda_o}^{max})$. It here shall be necessary to be content with the comparison of experimental maps with the merged results of models I and III on one hand, and with the results of the average model II on the other.

These different results are reported in figures 6a to 6f, and 8a to 8f, in the order of increasing values of magnitude, from left to right. The upper series corresponds to models I and III, the lower one to model II. The experimental maps, figures 7a to 7f, are placed between them, facing theoretical maps corresponding to the same magnitude. One theoretical

map was drawn, which corresponds to the wavelength interval 0.39-0.43 μm., for which measures are not available, but where the relative evolutions of the different models are interesting.

Model II implies an increase of the dissymetries in the ultra-violet region which is clearly greater than that observed. The observations thus seem much better restituted by models I and III in which there is a high localization of the absorption.

In the transitory region 0.39-0.43 μm., a differenciation of models again seems possible, the contrasts disappearing more rapidly in model II than in models I and III. Observations in this region unfortunately are not available; the photograph at 0.430 μm. in Paper I was taken 24 hours after the rest of the series, and could not be used quantitatively.

Lastly in the visible, the previsions of the three models become nearly identical. Whatever the localization of the absorbant may be, the models predict an almost total disparition of its influence. All these results, however, seem unreconcilable with observations. Furthermore exceptional conditions occur (Paper I gives exemples of such observations) for which large inhomogeneities in the isophotes are recorded at 0.585 μm..

DISCUSSION

The first result of our comparison, which leads to the localization of the ultra-violet absorption over or within the upper haze layer, must be considered with precaution. This conclusion is founded essentially upon the hypothesis that image deterioration be uniform within the series of dissymetries considered. The rigorous taking into account of apparatus and atmospheric effects would be indispensable before a definitive conclusion could be reached.

The second result shows that it is not possible to correlate the visible and ultra-violet observations in the hypothesis of a single absorption mechanism. This result seems more certain. From the terminator to the subsolar point, there is a regular decrease in observed radiance, if compared to calculated previsions. The same phenomena is also found in two others observations presented in Paper I (Photographs from 22/II/1945, $\alpha = 101°,9$; and from 23/III/1948, $\alpha = 75°,5$). The radiance distributions, presented here again in figures 9 and 10, seem very uniform; nevertheless, they clearly deviate from the theoretical repartitions calculated for an uniform and conservative layer of model (1), which are reproduced on the same figures; such repartitions nearly coincide with the preceeding results deduced from the ultra-violet contrasts. A deficit of light is once more noted towards the subsolar point. The same conclusions were arrived at in the analysis of

results from Mariner 10 (Devaux et al., 1974).

In his analysis of the ultra-violet contrasts on Venus, Travis (1976) arrived at the same general conclusion as to the need to invoke at least two distinct major sources of absorption to explain the whole of the observed features. However the need for a second absorption mechanism here derives only from the detailed analysis of the isophote maps in yellow light, not from the contrast curves which wash out such detailed information. As an exemple, contrast curves have been plotted in figure 11, for a mid-latitude point, from the theoretical results corresponding to our models. It seems that the typical features of the contrast curves observed may be restituted with models with a single absorption mechanism.

If model III were valid the simplest interpretation of this yellow discrepancy would be to suppose that the cloud layer thickness decreases regularly from the terminator to the subsolar point. This light deficit in the vicinity of the subsolar point would then be attributed to the influence of the dark ground which could appear as a result of the decreasing absorption and molecular scattering, in visible light. Such two parameters models have not been investigated here; typically, optical depths

of about 15 at the subsolar point could explain the observed radiance decreasing.

Aside from image deterioration, our results are still blemished by the initial incertitude of $m_{\lambda_o}(\alpha)$. The analysis was resumed for two series of values of the integral $\iint_S I(M,\lambda)dS/S$ which respectively were 8 percent greater than, and 8 percent less than those of the data in table II. For the lesser series the values of $\tau_a(M,\lambda_o)$, $\tau_l(M)$ and $\omega_o(M,\lambda_o)$ obviously are slightly modified, but the main results remain qualitatively unchanged. For the series of greater values on the contrary, it becomes impossible to restitute the original radiance distribution in any of the models. The absolute radiances obtained, already towards the center of the disk, correspond to an almost non-existant absorption, and the relative increase of the radiance towards the terminator and the poles can no longer be assessed. Probably, such high radiance values are overestimation, as they correspond to the simultaneous selection of the maximum relative incertitude announced by Irvine (1968), and to the lowest evaluation of the visual solar magnitude.

CONCLUSION

The type of analysis presented here seems capable of contributing positive information about the cloud structure of Venus, but in order to distinguish models I and III from model II,

photometry with about a 5 percent relative precision is necessary.

Although these initial results are in favor of a localization of the absorption high in the atmosphere, a definite conclusion must await the results of more accurate observations, completed by the recording of the apparatus function. Such observations are planed. The spectral region 0.39 - 0.43 μm. seems rather favorable for this type of analysis, because of its greater experimental convenience than the ultra-violet region.

If models I and III should prevail, their differenciation seems to be at the limit of the possibilities of the method, as would be a very precise determination of the conservative optical thickness, if model II should prevail.

Perhaps the most significant result stemming from this work is that a hypothesis assuming a single absorption mechanism for the entire spectral interval explored is incapable of reconstituting observations as a whole. It thus seems that the anomalies observed in yellow light (and sometimes very contrasted; see Paper I) correspond to an absorption source which is different from that which appears in ultra-violet. Although the ground may appear to be a likely second source of absorption, the question necessitate more careful consideration.

ANNEX

The exact positionning of the theoretical isophote maps upon the experimental ones is crucial. Particularly important is the precise localization of the theoretical limb.

Taking into account the nearly translationnal character of the symetry of the radiance distributions observed in the vicinity of the equator for visible light, it will be assumed in a crude approximation that the problem here is unidimensional.

If the real equatorial radiance distribution $I(x)$ was a step function, it is clear that the limb ought to be placed upon the isophote 50. The difficulty lies in the determination of the experimental values $I'(x_1)$ and $I'(x_2)$ which are measured with the real radiance distribution, respectively at the point where the radiance is maximum and at the limb.

Theoretical equatorial radiance distributions $I(x)$ have been computed for a cloud cover assumed to be thick, horizontally homogeneous, with the scattering law (1). The single scattering albedo was adjusted so that the spherical albedo in visible light was obtained. The phase angles 67°,3 75°,5 and 101°,9 where choosen, for days where homogeneous conditions seemed to prevail on Venus.

The exact apparatus function $g(x)$ being unknown, three arbitrary functions have been tried. The results are independant of the assumed apparatus function, and will be given for one of them:

$$g(x) = C \left[\frac{\sin(\pi x/x_o)}{\pi x/x_o} \right]^2$$

The theoretical distributions I(x) have been convoluted with this function, the parameter x_o being adjusted, in each case, until the obtained distribution

$$I'(x) = \int_{-\infty}^{+\infty} g(x-y)\ I(y)\ dy$$

fit the observed equatorial radiance distribution in the vicinity of the limb.

Figure 12 shows the normalised equatorial distribution $I'(x)/I'(x_1)$ obtained for the phase angle 101°,9. For $15.5 \leq x_o \leq 18.5$, there is a good restitution of the observed radiance profile near the limb, and the corresponding values $I'(x_1)$ and $I'(x_2)/I'(x_1)$ are nearly constant (0.95 and 0.54 respectively). But it must be noted that the equatorial distributionswhich can fit the observed onesnear the limb disagree with them in the central part of the disk.

The same conclusions appear for the two other phase angles, with different values for $I'(x_1)$ and $I'(x_2)/I'(x_1)$. The values $I'(x_1)$ has been taken into account for the various maps drawn in this paper. The results obtained from this crude analysis in yellow light have been used for the other wavelengths of the series, for which the same study was not resumed.

REFERENCES

BROGNIEZ C., DEVAUX C., HERMAN M., LENOBLE J. - Photometry of Venus II: Theoretical brightness distribution over the disk- Icarus, 1975, 26, 73-84.

DEVAUX C., HERMAN M., LENOBLE J. - Interpretation of the photometric measurements of Venus by Mariner 10- J1. Atm. Sc., 1975, 32, 6, 1177-1189.

DOLLFUS A., CAMICHEL H., BOYER C., AURIERE M., BOWELL E., NIKANDER J. -Photometry of Venus I: Observation of the brightness distribution over the disk.- Icarus, 1975, 26, 53-72.

HANSEN J. E., ARKING A. - Clouds of Venus: Evidence for their nature. Science, 171, 669-672.

HANSEN J.E., HOVENIER J.W. - Interpretation of the polarization of Venus - J1. Atm. Sc., 1974, 31, 1137-1160.

IRVINE W.M. - Monochromatic phase curves and albedos for Venus- J1. Atm. Sc., 1968, 25, 610-616.

SILL G.T. - Sulfuric acid in the Venus clouds- Comm. Lunar Planet. Lab., 1972, 171,91-198.

TRAVIS L.D.- On the origin of the ultraviolet contrasts of Venus- Jl; Atm. Sc., 1975, 32, 1190-1200.

YOUNG A.T.- Are the clouds of Venus of sulfuric acid?- Icarus, 1973, 18, 564-582.

TABLE I

Plates of Venus for which isophotes are derived.

Date	Time (UT)	α (deg)	λ (μm.)	Observatory	Observer	Fig. n°
31 Jul. 69	04h18	-67°.3	0.327	Pic du Midi	Fryer	7a
31 Jul. 69	04h08	-67°.3	0.354	Pic du Midi	Fryer	7b
31 Jul. 69	04h03	-67°.3	0.379	Pic du Midi	Fryer	7c
31 Jul. 69	03h52	-67°.3	0.520	Pic du Midi	Fryer	7e
31 Jul. 69	03h45	-67°.3	0.585	Pic du Midi	Fryer	7f

TABLE II

Data used for models.

λ (μm.)	$m_\lambda(\alpha)$	$\frac{1}{S}\iint_S I(M,\lambda)dS$	$A(\lambda)$	ρ_λ	$B(\lambda)$
0.327	-2.790	0.070	1.5	0.18	0.46
0.354	-2.895	0.078	1.3	0.27	0.60
0.379	-3.045	0.085	1.0	0.39	1.0
0.412	-3.185	0.100	0.70	0.53	2.0
0.520	-3.390	0.120	0.30	0.69	8.0
0.585	-3.535	0.140	0.25	0.85	10.8

FIGURE CAPTIONS

Figure 1: Spherical albedo for Venus. Full line: from Travis, 1975. Dashed line: with pure Rayleigh scattering.

Figure 2: Theoretical models.

Figure 3: Optical depth $\tau_a(M)$ of the upper absorbing layer. Model I, $\lambda_o = 0.379$ µm..

Figure 4: Optical depth $\tau_1(M)$ of the upper conservative layer. Model II,

Figure 5: Single scattering albedo $\omega_o(M)$ of the cloud. Model III, $\lambda_o = 0.379$ µm..

Figures 6a to 8f:

6a to 6f: theoretical results with models I and III.

7a to 7f: experimental results, from Dollfus and al. 1975.

8a to 8f: theoretical results with model II.

a to f: wavelengths 0.327, 0.354, 0.379, 0.412, 0.520, 0.585 µm.

Figure 9: Isophote maps. $\alpha = 101°.9$. Full lines: experimental results (22 Feb. 45, 18h47, λ=0.585 µm., Camichel H., Pic du Midi). Dashed lines: theoretical results with a homogeneous and thick cloud; scattering law: eq. (1).

Figure 10: Same as Figure 9, at $\alpha = 75°.5$ (23 Mar. 48, 18h27, $\lambda = 0.585$ µm., Camichel H., Pic du Midi).

Figure 11: Contrast curves $(\bar{I} - I_{0.585})/I_{0.585}$, deduced from the calculations, with models I and III and with model II.

Figure 12: Normalized equatorial radiance distributions near the limb

limb. $\alpha = 101°.9$. Dots: experimental results. Theoretical profiles with x_o=12.5 (dashed line, x_o=23.5 (dot-dashed line) and with $15.5 \; x_o \; 18.5$ (shaded area).

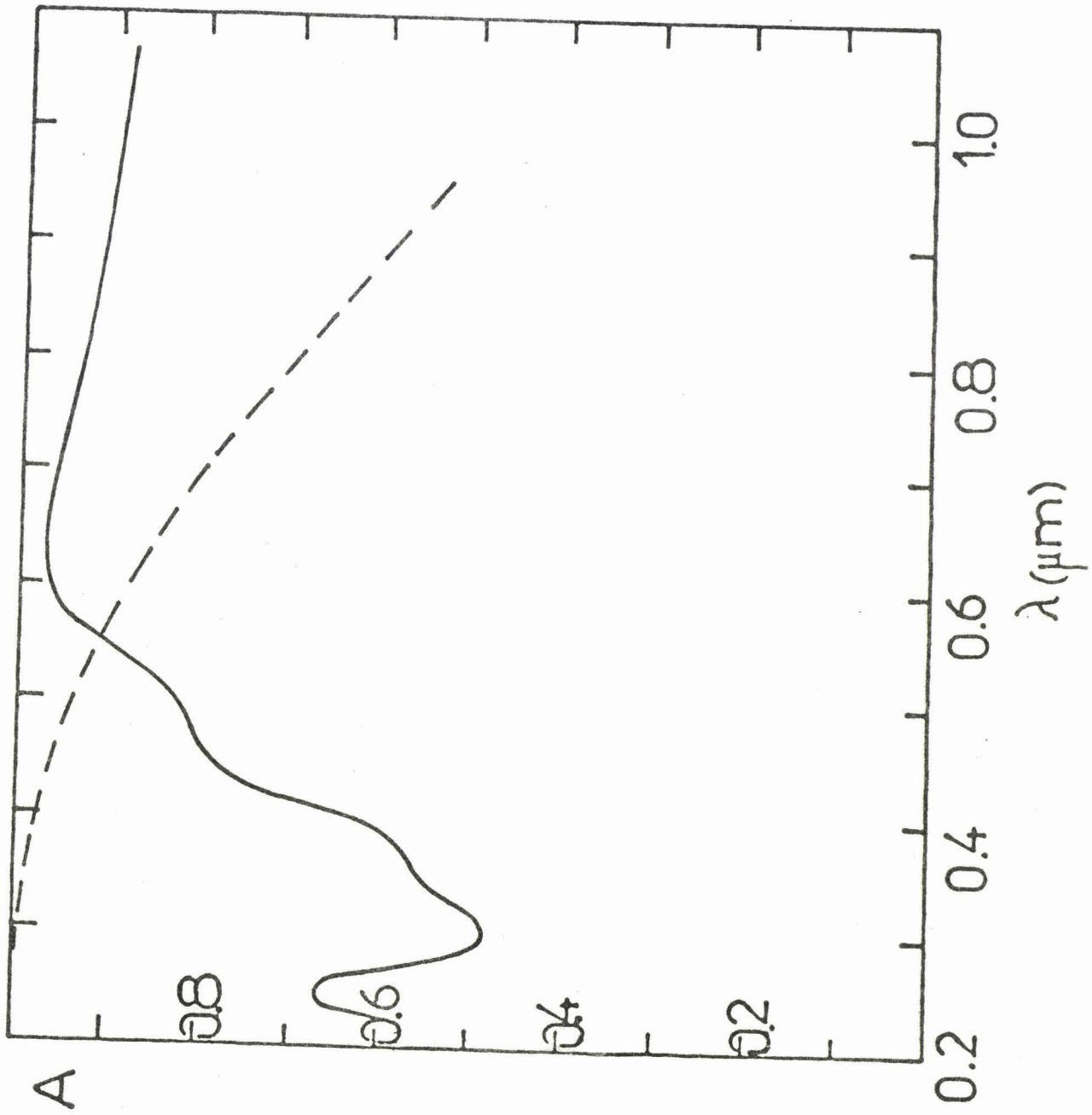

fig 1

fig 2

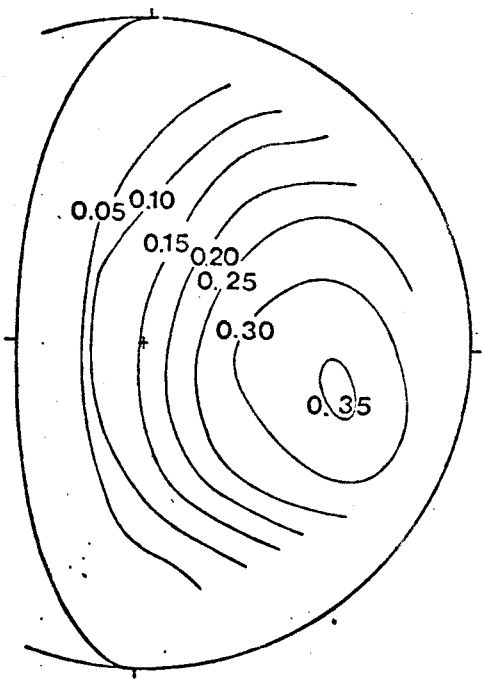

Fig 3

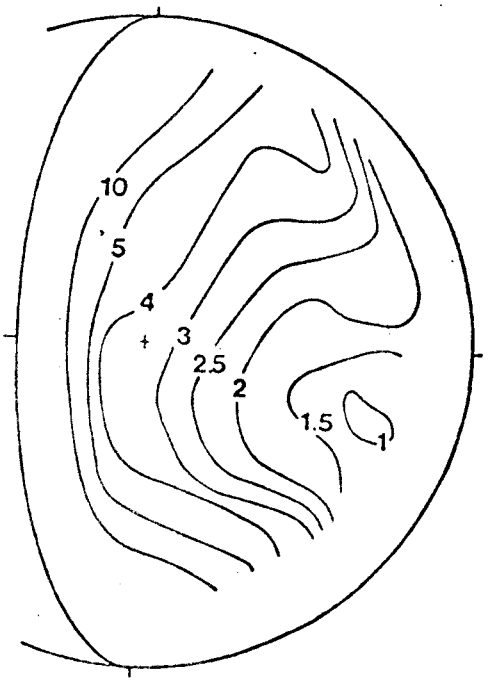

Fig 4

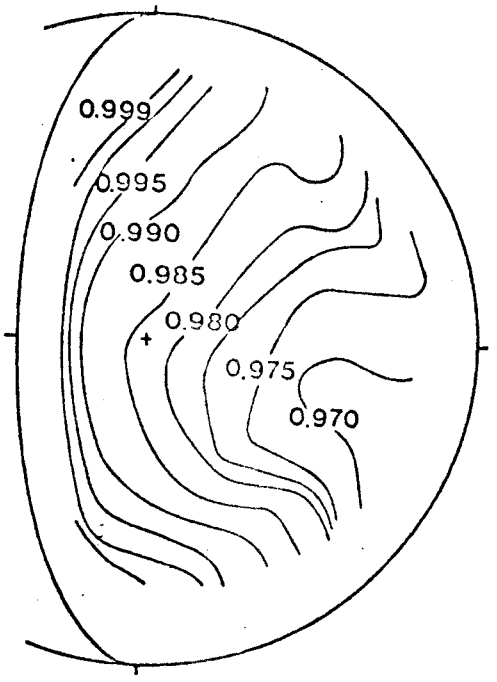

Fig 5

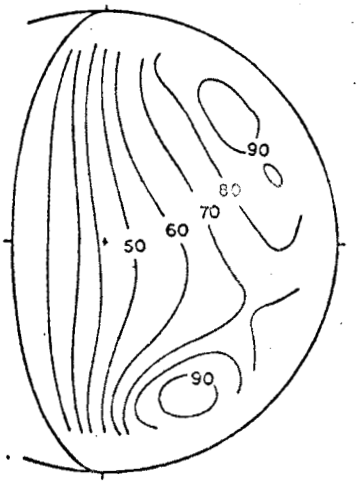

Figure 6a

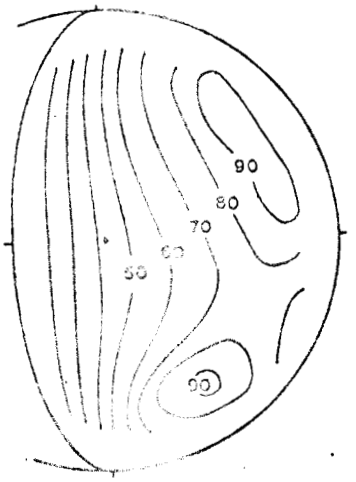

Figure 6b

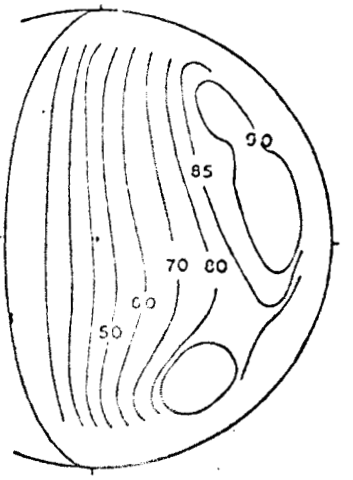

Figure 6c

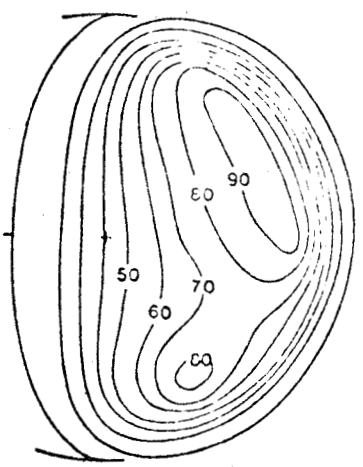

Figure 7a

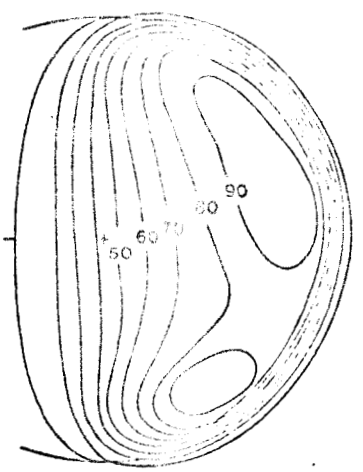

Figure 7b

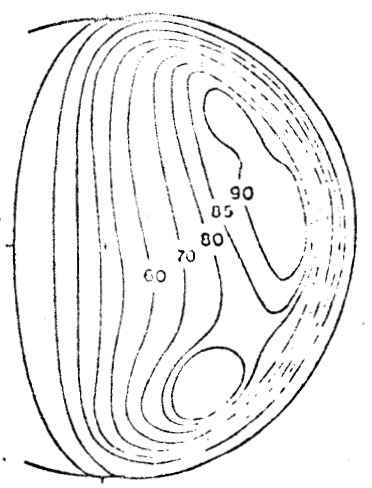

Figure 7c

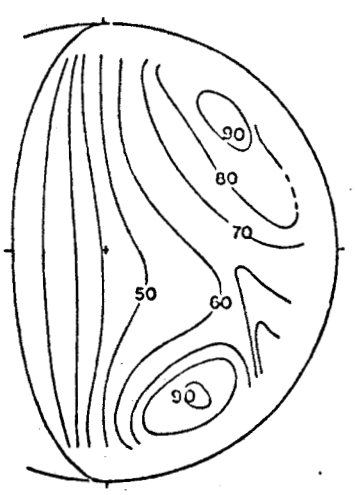

Figure 8a

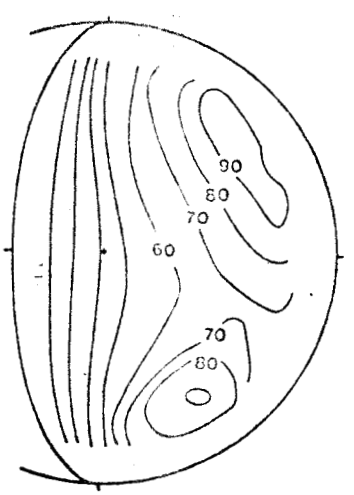

Figure 8b

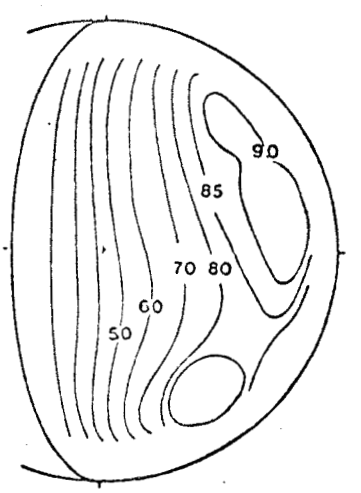

Figure 8c

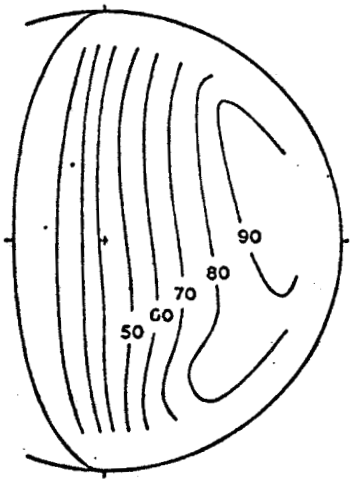

Figure 6d

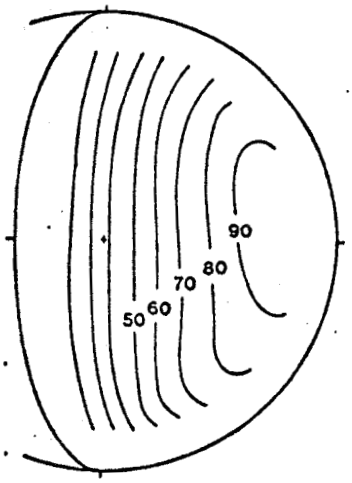

Figure 6e

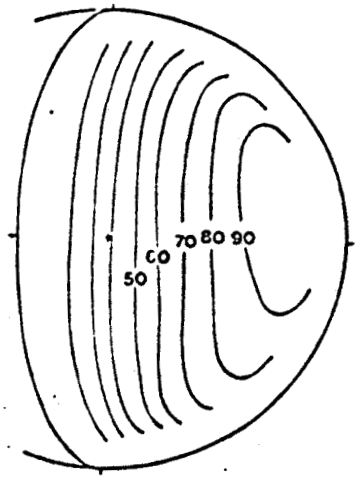

Figure 6f

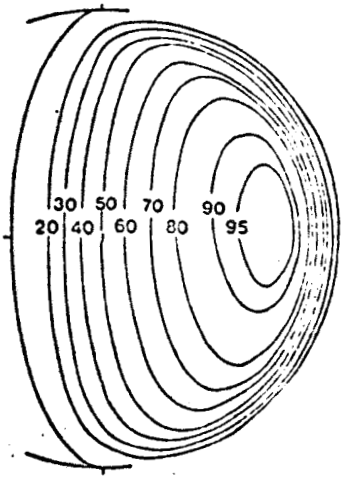

Figure 7e

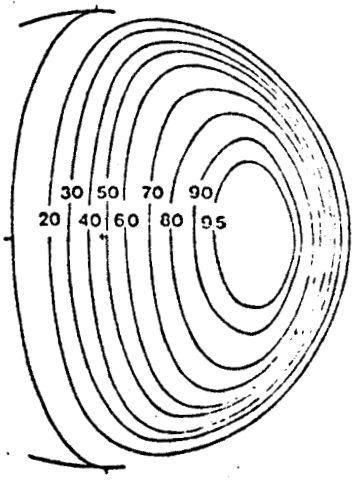

Figure 7f

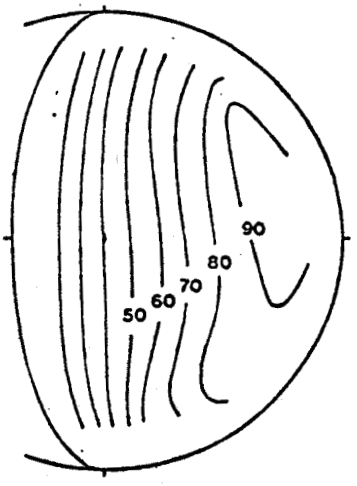

Figure 8d

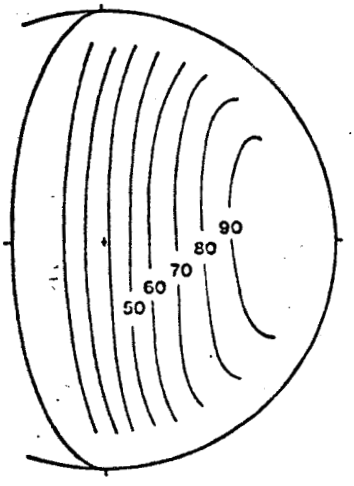

Figure 8e

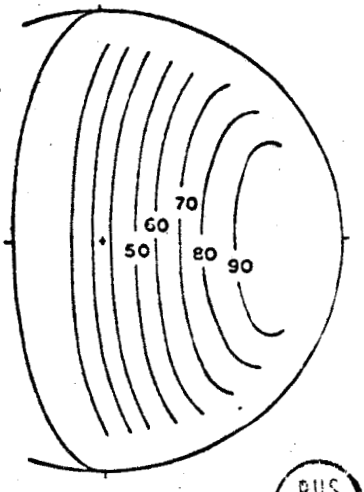

Figure 8f

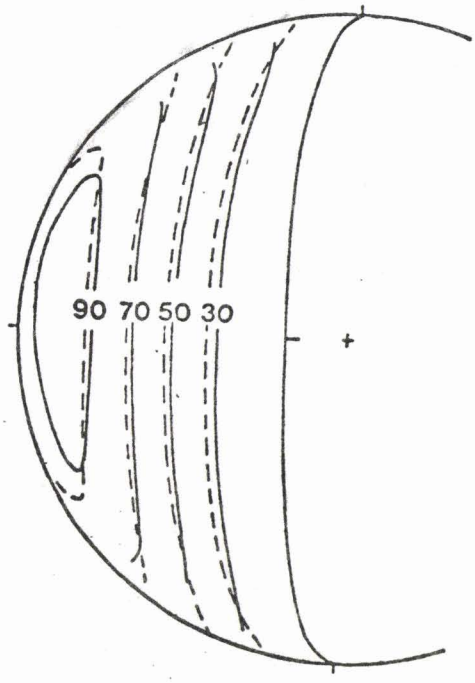

Figure 9

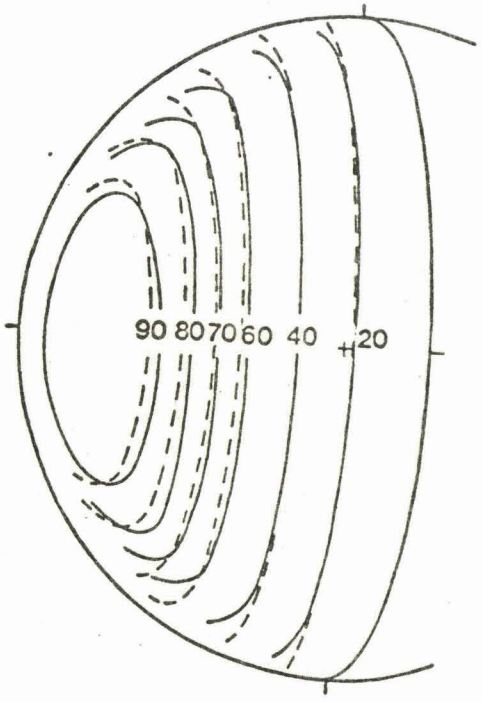

Figure 10

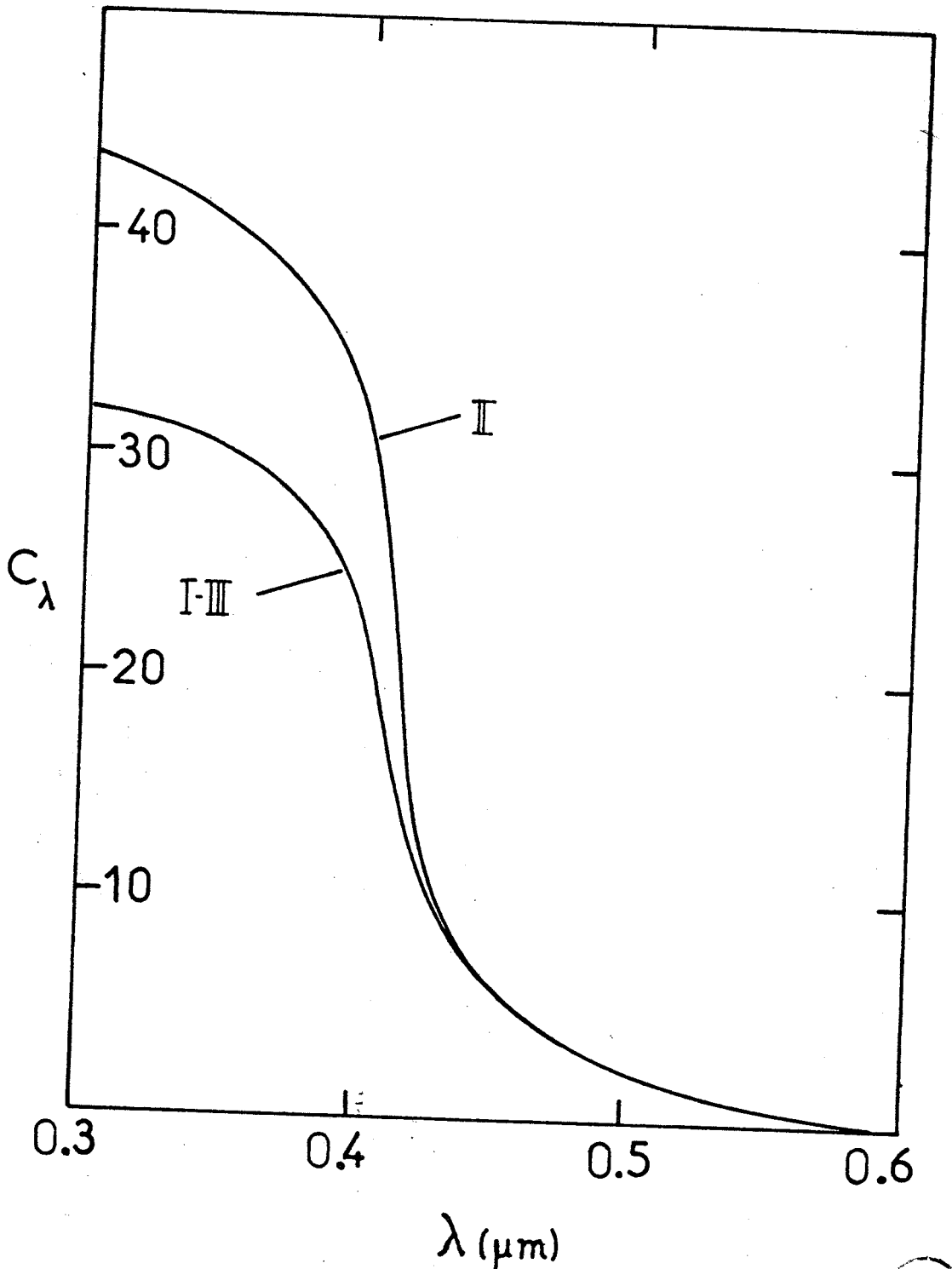

fig 11

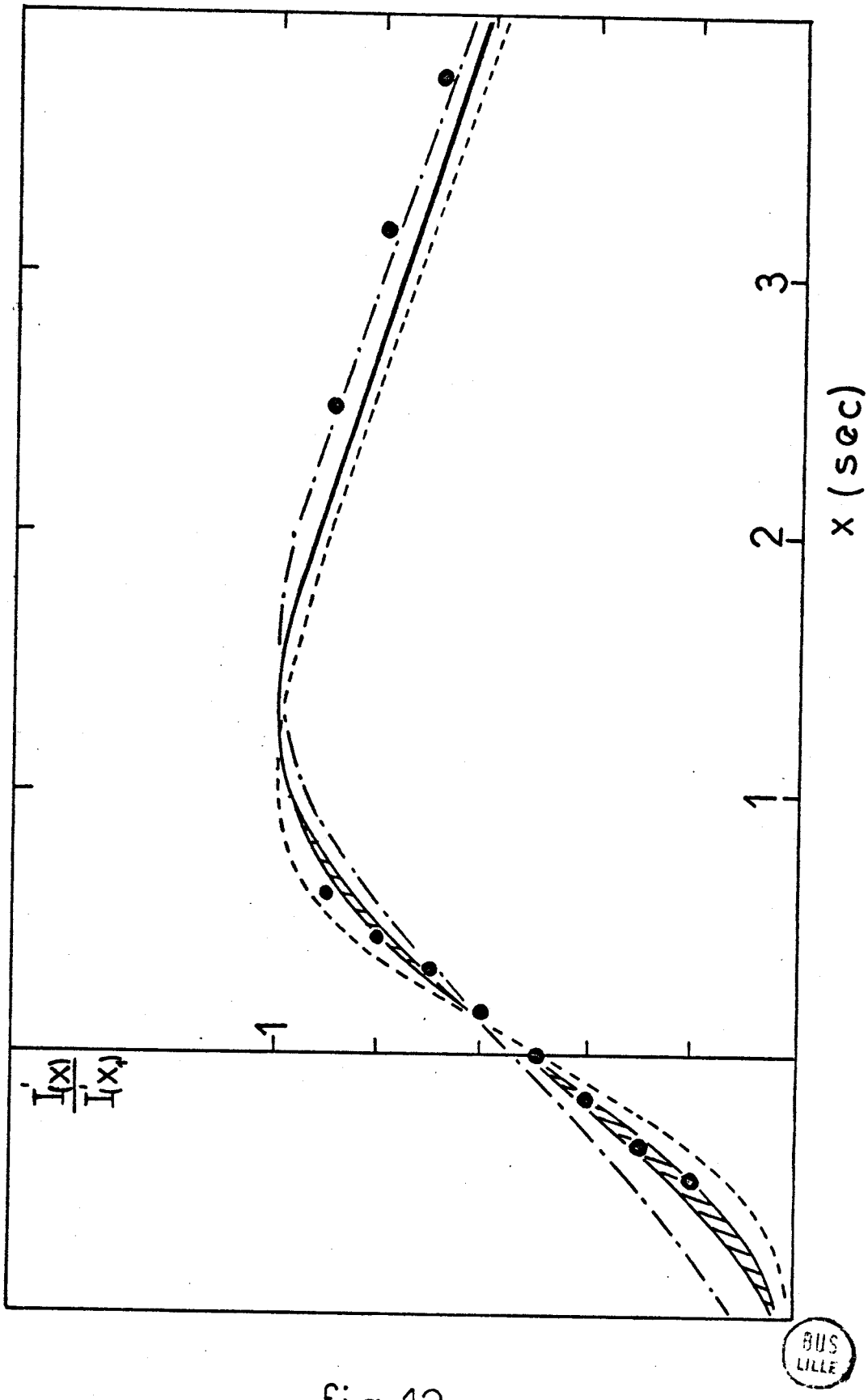

fig 12

CONCLUSION

Les diverses améliorations apportées à l'analyse et à la programmation de la méthode des Harmoniques Sphériques nous ont finalement procuré un outil très performant.

Ayant permis de tester très largement une méthode analytique approchée de calcul de flux et d'albédo sphériques, la méthode des Harmoniques Sphériques, de par sa rapidité et sa structure en blocs très poussée, s'est avérée particulièrement bien adaptée à l'étude du rayonnement rétrodiffusé par les atmosphères planétaires, étude qui nécessite la détermination complète du champ de rayonnement pour de nombreux cas de modèles diffusants.

Cette première analyse détaillée du rayonnement solaire rediffusé par Vénus, a permis de dégager des simplifications intéressantes et s'est révélée capable d'apporter des informations positives sur la structure nuageuse de cette planète. L'impossibilité de concilier les observations visibles et ultra-violettes, dans l'hypothèse d'un mécanisme d'absorption unique, suggère autour de 0,6 µm une influence possible du sol localisée au voisinage du point subsolaire. Une telle éventualité que les sondages de Vénéra 9 et 10 semblent confirmer, revaloriserait considérablement les études photométriques dans le cas de la planète de Vénus.

En ce qui concerne une localisation haute pour l'absorption responsable de la faible réflectivité de Vénus en ultra-violet, ce résultat moins certain nécessite des observations similaires mais, plus variées et plus précises. Vénus devant se présenter dans de bonnes conditions d'observation au cours de l'été 1977, une campagne d'observation a été projetée. Les objectifs de cette campagne ont pu être précisées à partir de cette première étude et on peut espérer en collaboration avec les expérimentateurs de Meudon et du Pic du Midi que la précision nécessaire (de l'ordre de 5%) sur la photométrie sera atteinte et permettra une conclusion définitive.

L'éventualité de l'influence du sol sur les anomalies observées en lumière jaune est un problème qui semble également à la portée des observations terrestres. L'évolution des réseaux d'isophotes dans cette gamme Spectrale devrait en effet permettre de confirmer ou d'infirmer son rôle en jouant sur l'effet de masque variable de la diffusion Rayleigh. Les contrastes observés en lumière jaune étant généralement beaucoup plus faibles qu'en U.V, à moins de rencontrer des conditions d'exceptionnelle inhomogénéité, leur analyse devra néanmoins attendre qu'une photométrie très précise soit accessible.

Dans l'immédiat, l'expérience acquise au cours de cette étude des clichés télescopiques a rendu envisageable une analyse similaire sur les clichés à très haute résolution transmis par Mariner 10 et ce travail est actuellement en cours.

Parallèlement à l'analyse photométrique l'étude de la polarisation détaillée sur le disque a été développée au Laboratoire (DEUZE, 1974) et fait actuellement l'objet du travail de recherche de R.SANTER (1977). La campagne d'observation prévue cet été devrait permettre d'obtenir des mesures simultanées (photométrie au Pic du Midi et polarisation à Meudon). Il sera alors intéressant de confronter les conclusions obtenues par ces deux méthodes d'analyse.

REFERENCES

ARKING,A.,and POTTER,J.(1968). The Phase Curve of Venus and the Nature of its Clouds.J.Atm.Sci,25,617-628.

AVDUEVSKY,V.S.,MAROV,M.Ya.,MOSHKIN,B.E., and EKONOMOV,A.P.(1973). Venera8: Measurements of solar illumination through the atmosphere. J.Atm.Sci,30,1215-1218.

BELTON,M.,HUNTEN,D.M., and GOODY,R.M.(1968). The atmosphere of Venus and Mars. Gordon and branch;New-York.

BOYER,C.,GUERIN,P.(1966). Mise en evidence directe ,par la photographie d'une rotation rétrograde de Vénus en 4 jours. C.R.Acad.Sci. Paris,263,253-255.

BROGNIEZ,C.BIGOURD.(1975). Calcul approché des flux radiatifs en milieu diffusant.Application aux mesures de Venera 8.Thèse 3ème Cycle Université de Lille.

BROGNIEZ,C.BIGOURD.,DEVAUX,C., and HERMAN,M.(à paraitre) Methode du noyau exponentiel.

CANOSA,J.,and PENAFIEL,H.R.(1973). A direct solution of the Radiative Transfer: Application to the Rayleigh and Mie Atmospheres. Jl.Quant.Spectrosc.Radiat.Transfer,13,21-39.

CHANDRASEKHAR,S.(1950). Radiative transfer.Oxford University Press.

COFFEEN,D.L., and GEHRELS,T.(1969). Wavelength dependence of polarisation. XV.Observations of Venus.Astron.J,74,433-445.

DAVE,J.V.(1974). A direct solution of the Sphérical Harmonics approximation to the transfer équation for a plane-parallel,non homogeneous atmosphère. Available from National.Techn.Inform.Service(Springfield).

DAVISON,B. (1958). Neutron Transport Theory. University Press Oxford.

DEUZE,J.L. (1971). Extension de la méthode des harmoniques Sphériques au calcul de la luminance polarisée diffuse et au cas d'une couche d'absorption variable. Rapport D.E.A. Lille.

DEUZE,J.L.,DEVAUX,C.,HERMAN,M. (1973). Utilisation de la Méthode des Harmoniques Sphériques dans les calculs de transfert radiatif.Extension au cas de couches diffusantes d'absorption variable. Nouvelle Revue Optique,4,307-314.

DEUZE,J.L. (1974). Etude de la polarisation du rayonnement par les milieux diffusants.Application à la polarisation localisée de Vénus. Thèse 3emeCycle,Université de Lille.

DEUZE,J.L.,DEVAUX,c.,and HERMAN,M. (1975). Adaptation de la Methode des Harmoniques Sphériques aux calculs de lumière diffuse polarisée. Remarques sur la formation du rayonnement rediffusé par les atmosphères optiquement denses. Nouvelle Revue d'Optique,6,103-111.

DEVAUX,C.,FOUQUART,Y.,HERMAN,M., et LENOBLE,J. (1973). Comparaison de diverses méthodes de résolution de l'équation de transfert du rayonnement dans un milieu diffusant. J.Q.S.R.T,13,1421-1431.

DEVAUX,C., and HERMAN,M. (1975). Venus: Cloud optical depth and surface albedo from Venera 8. Icarus,24,19-27.

DOLLFUS,A. (1966). Contribution au Colloque Caltech.JPL. sur la lune et les planetes:Vénus. Jet Propulsion Laboratory Tech.Memo N°33-266, 187-202.

DOLLFUS,A., and COFFEEN,D.L. (1970). Polarization of Venus.I.Disk observations. Astron.Astrophys,8,251-266.

DOLLFUS,A.,CAMICHEL,H.,BOYER,C.,AURIERE,M.,BOWELL,E., and NIKANDER,J. (1975). Photometry of Venus.I. Observations of the Brightness Distribution over the Disk. Icarus,26,53-72.

FEIGELSON,E.M., et al.(1973). The interpretation of the measurements of illumination by the automatic interplanetary station Venera 8. Presented at the Copernicus Symposium IV. I.A.U. Symposium 65, Torun, Poland.

FOUQUART,Y.(1975). Contribution à l'étude des spectres réfléchis par les atmosphères planétaires diffusantes. Application à Vénus. Thèse d'Etat,Université de Lille.

FYMAT,A.L., and LENOBLE,J.(1972). Absorption profile of a planetary atmosphere: a proposal for a scattering independent determination Appl.Optics,11,2249.

FYMAT,A.L., and KALABA,R.E.(1972). Inverse Multiple Scattering Theory: Minimization Search Method of Solution with Application to Venus' Atmosphere. Proceedings of the Internat.Radiation Symposium, Sendai,Japan.

GASTINEL,N.(1966). Analyse Numérique Linéaire. Enseignement des Sciences (Hermann).

GRAY,E.L.,COULSON,K.L.(1964). Molecular optical thickness of low density models of the atmosphere of Mars. General Electric Space Sciences Laboratory,R.64.SD21.

GRIGGS,M.(1968). Aircraft measurements of albedo and absorption of stratus clouds,and surface albedo. J.Appl.Meteorology,7,1012-1017.

GUILLEMOT,J.C.(1966). Contribution à l'étude du transfert du rayonnement dans les nuages par la methode des harmoniques spheriques. Thèse D^{r} Ingénieur,Université de Lille.

HANSEN,J.E.,(1969). Radiative transfer by doubling very thin layers. Astrophys.J1,155,565-573.

HANSEN,J.E., and ARKING,A.(1971). Clouds of Venus: Evidence for their nature. Science,171,669-672.

HANSEN,J.E., and HOVENIER,J.W.(1974) . Interpretation of the polarization of Venus. J.Atm.Sci.,31,1137-1160.

HERMAN,M.(1968). Contribution à l'étude du transfert radiatif dans un milieu diffusant et absorbant. Thèse d'Etat,Université de Lille.

HERMAN,M.,BIGOURD,C.,DEVAUX,C.(1973). Rapport Interne. Laboratoire d'Optique atmospherique.Université des sciences et techniques.U.E.R. Physique Fondamentale.

HORAK,H.G.(1950). Diffuse reflection by planetary atmospheres. Astrophys.J1,112,445-463.

IRVINE,W.M.(1968). Monochromatic phase curves and albedos for Venus. J.Atm.Sci,25,610-616.

JEANS,J.H.(1917). Monthly Notices Roy.Astron.Soc.,78,28.

KOURGANOFF,V.(1952). Basic Methods in Transfer Problems. Clarendon Press,Oxford.

LACIS,A.A.,HANSEN,J.E.(1974). Atmosphere of Venus: Implications of Venera 8 Sunlight Measurements. Science,184,979-981.

LENOBLE,J.(1954). Contribution à l'étude du rayonnement solaire ,de sa diffusion dans l'atmosphere et de sa pénétration dans la mer. Ann.Geophys,10,117-146,187-225.

LENOBLE,J.(1961 a). Application de la méthode des Harmoniques Sphériques au cas de la Diffusion Anisotrope. C.R.Ac.Sc,252,2087-2089.

LENOBLE,J.(1961b). Application de la méthode des Harmoniques Sphériques à l'étude de l'état de Polarisation du Rayonnement Diffus. C.R.Ac.Sc,252,3562-3564.

LENOBLE,J.(1970). Importance de la polarisation dans le rayonnement diffusé par une atmosphère planétaire. J.Quant.Spectrosc.Radiat.Transfer,10,533-556.

LOUKACHEVITCH,N.L.,MAROV,M.Ya.,FEIGELSON,E.M.(1973).Interpretation des mesures d'éclairement effectuées par la station interplanétaire automatique Venera 8 .Acad.Sci.U.R.S.S.Moscou.Preprint N°63.

LYOT,B.(1929). Recherches sur la polarisation de la lumière des planètes et de quelques substances terrestres. Ann.Observ.Paris(Meudon),8,161.

MARENGO,J.(1967). Application numérique de la méthode des Harmoniques sphériques.Etude de milieux diffusants et absorbants pour le cas d'une diffusion anisotrope Thèse D^{r} Ingénieur,Université de Lille.

MAROV,M.Ya.(1972). Venus: A perspective at the beginning of planetary exploration. Icarus,16,415.

MARSHAK,R.E.(1947). Note on the spherical harmonic method as applied to the Milne problem for a sphere. Phys.Rev,71,443.

POTTER,J.(1970). The Delta function approximation in radiative transfer theory. J.Atm.Sci.,27,943.

POUZET,P.(1964). Publications du Laboratoire de Calcul de la Faculté des Sciences de Lille.

SANTER,R.(1977). Contribution à l'étude de la Polarisation du Rayonnement Solaire Diffusé par Vénus. Thèse 3eme Cycle,Université de Lille.

SILL,G.T.(1972). Sulfuric Acid in the Venus Clouds. Comm.Lunar.Planet. Lab.,N°171,191-198.

SOBOLEV,V.V.(1964). Investigation of the Venusian Atmosphere. Soviet. Astron.- AJ,8,71-75.

TITARCHOUK,L.G.(1973). Proprietés optiques de la basse atmosphère de Vénus.Interprétation des résultats obtenus par la sonde Venera 8. Acad.Sci.U.R.S.S.Moscou.(Trad.CNES).

van de HULST,H.C.,GROSSMANN,K.(1968). The atmosphere of Venus and Mars. Gordon and Branch.New-York.

WANG,L.(1972). Anisotropic nonconservative scattering in a semi-infinite medium. Astrophys.Jl,174,671-678.

YOUNG,A.T.(1973). Are the clouds of Venus sulfuric acid? Icarus,18,564-582.